Oxidative Dehydrogenation of Ethane to Ethylene over Supported Vanadia and Ni-Nb-M-O Mixed Metal Oxide Catalysts

Dissertation

zur

Erlangung des akademischen Grades

doctor rerum naturalium (Dr. rer. nat.)

der Mathematisch-Naturwissenschaftlichen Fakultät

der Universität Rostock

vorgelegt von

M.Sc. Ailing Qiao

geboren am 18.03.1982 in Shandong, China

Rostock: 22. 10. 2013

Name: Ailing Qiao

Defense date: 18th February 2014 at 15:00 hr (Tuesday)

Defense place: Paul Walden Hörsaal, Universität Rostock

Thesis title: Oxidative Dehydrogenation of Ethane to Ethylene over Supported Vanadia and Ni-Nb-M-O Mixed Metal Oxide Catalysts

Referees

1. Dr. habil. Andreas Martin

      Leibniz Institute for Catalysis

      University Rostock

      Albert Einstein Str. 29a

      18059, Rostock

      Germany

2. Prof. Udo Kragl

      Institut für Chemie,

      University Rostock

      Albert Einstein Str. 3a

      18059, Rostock

      Germany

Datum der Einreichung: 25. Oktober 2013

Datum der Verteidigung: 18. Februar 2014

Declaration

I hereby declare that the work described in this thesis entitled, "Oxidative Dehydrogenation of Ethane to Ethylene over Supported Vanadia and Ni-Nb-M-O Mixed Metal Oxides Catalysts" is original work undertaken by myself to receive the doctoral degree, at Leibniz Institute for Catalysis, Rostock, Germany under the guidance of my supervisor Dr. habil. Andreas Martin (Head of Department "Heterogeneous Catalytic Processes") and Dr. V.N. Kalevaru (Group leader).

I further declare that either wholly or in part of this thesis have been submitted for the award of any other degree or qualification in any other university, institute or college of advanced education.

Rostock, 22.10.2013

Ailing Qiao

Acknowledgements

The voyage of three-year´s Ph.D. study at LIKAT has been proved to be a unique learning experience for me, both on the professional level and in the personal aspect. I am sincerely grateful to many people who accompanied with me during this challenging and exciting Ph.D. period.

First, I would like to express my sincere appreciation to my supervisor Dr. habil Andreas Martin for his continuous support and supervision throughout my Ph.D. studies.

春夜喜雨	Delighting in Rain on a Spring Night
---杜甫	---Du Fu (translated by Rendan O´Kane)
好雨知时节，	A good rain knows its season,
当春乃发生。	It waits until the spring to fall.
随风潜入夜，	It drifts in on the wind, steals in by night,
润物细无声。	Its fine drops drench, yet make no sound at all.

This Chinese ancient poem makes me associate with Dr. Martin. His rigorous scholarship, immense and extensive knowledge, meticulous scientific attitude and improving work style, which I can feel from the project discussion and manuscript correction, deeply influence and inspire me unobtrusively and imperceptibly. This influence is just like the way of spring rain to the world and that´s really beneficial for my future career. Additionally, during the three years' study I met many problems and difficulties; Dr. Martin is always generous to help me. Because of his valuable support, my Ph.D. work can be continued and finished successfully. He has truly provided cause for a lifetime of thanks.

Special thanks are due to Dr. N.V. Kalevaru for guiding me in my Ph.D. study process and numerous valuable discussions and suggestions about the research based on his excellent research skills and scientific experiences. I also appreciate his patient explanations on my doubts about work and many writing skills on manuscript. Without his reading and providing corrections to my work, the Ph.D. cannot be fully completed.

Ailing Qiao

Abstract

Ethylene is one of the most important petrochemically derived monomers that is used as a feedstock for the production of a variety of commercially useful chemical products such as plastics, fibres, resins, polymers, packaging materials and so on. Global consumption of ethylene is reported to be over 130 MMT in 2012, which is expected to reach 155 MMT by 2015. These numbers clearly demonstrate the commercial importance of ethylene in the global market. At present, ethylene is commercially produced mainly via steam cracking of naphtha and ethane feedstocks, which is an endothermic process operating at high temperatures (700-900 °C) consuming a lot of energy and also possess some thermodynamic limitations. In addition, CO, H_2, CH_4, C_2H_2, C_{3+} compounds are formed as by products during such process, which in turn lead to difficulties in their separation and purification. However, the addition of an oxidant such as O_2 to the reaction mixture allows performing exothermic oxidative dehydrogenation (ODH) seeming to be one of the more attractive alternative routes for the production of ethylene in one step. Because this ODH approach is an exothermic reaction and can be operated at relatively low temperatures (300-600 °C) thus requiring less energy input compared with the traditional production routes mentioned above. In addition, the presence of oxidant (e.g. O_2) in the feed gas certainly suppresses the coke formation to a large extent and thereby improves the long-term stability.

A wide of range of catalytic materials have been evaluated as potential catalysts for the ODHE. A multicomponent MoVTeNbO mixed oxide system with an optimum Mo-V-Te-Nb formulation of 1: 0.15: 0.16: 0.17 is reported to give an ethane conversion higher than 80% with a selectivity to ethylene above 80% at 350-400 °C and atmospheric pressure. The most intensively studied catalysts are supported early-transition metal oxides, i.e., mainly V and Mo oxides due to their ability to provide lattice oxygen for hydrogen abstraction from alkanes and finally yielding desired alkenes via Mars-van Krevelen redox mechanism. The catalytic activity and selectivity of supported vanadia catalysts are significantly affected by the nature of supports because of their different physico-chemical properties like thermal stability, acid-base properties, porosity (surface areas), active phase-support interactions, oxygen storage capacity, reducibility and so on. More recently, NiO based catalysts have also received considerable research attention due to their unique ability of

exhibiting high reactivity at relatively low temperatures (300-450 °C) and thereby enhanced selectivity of olefins as well.

In view of this, this thesis is mainly aimed at preparation, characterization, and catalytic testing of five different series of catalysts for the ODHE. Different types of vanadia based catalysts using various catalyst carriers such as V_2O_5/Nb_2O_5, $V_2O_5/Al-x$ and V_2O_5/TiO_2 and additionally Ni-Nb based ones, for instance promoted Ni-Nb-M-O (M=Cr, Mo, W) catalysts were prepared by impregnation and evaporation methods, respectively. All these catalysts were characterized by several physico-chemical techniques for better understanding of their properties. The catalytic performance of these solids was evaluated towards the ODHE in a fixed bed quartz reactor at 500-600 °C for supported vanadia samples and 300-450 °C for Ni-Nb-M-O catalysts. Special emphasis is devoted to gain deeper insights on the physico-chemical characteristics of the catalysts in relation to their activity/selectivity properties. Some highlights on the results obtained from every series are briefly described below.

For V_2O_5/Nb_2O_5 catalysts with varying V_2O_5 contents (5-20 wt%), it has been observed that the catalytic activity and selectivity are found to depend strongly on the nature of vanadium oxide species formed and the surface enrichment of vanadium in the near-surface-region. These two properties in turn strongly depend on the content of vanadium in the catalysts. At low V_2O_5 content ($\leqslant 10$ wt%), monomeric and oligomeric VO_x species were formed while more polymeric species were found (similar to bulk V_2O_5 sample) at higher loadings as shown by UV-vis-DRS studies. XPS revealed that pronounced enrichment of vanadium occurs in the near-surface-region in the samples with low vanadia contents. Among all, 10 wt% V_2O_5/Nb_2O_5 catalyst has displayed the superior performance (X = 28%, S = 38% at 600 °C) due to clear enrichment of vanadium in the near-surface-region and formation of optimum amount of monomeric/oligomeric VO_x species. Based on this result, 10 wt% V_2O_5 has been selected as an optimum loading and used in all further studies.

The investigations on exploring the nature of alumina support using 10 wt% V_2O_5 as an optimum loading (i.e. V_2O_5/Al_2O_3 series with five with different types of Al_2O_3 supports) revealed that the nature of the Al_2O_3 source showed a significant influence on the catalytic performance of the solids. Among all catalysts investigated, the high surface area γ-alumina based catalyst displayed the best performance in the ODHE

due to the high dispersion of VO_x species over the support surface. On the other hand, low surface area α-Al_2O_3 but also low surface area γ-Al_2O_3 supported catalysts exhibited high ethane conversion but low selectivity to ethylene because of the existence of bulky V_2O_5 particles. In addition, a recently described low-surface area ball-milled alumina containing a high amount of penta-coordinated Al sites was also included in this study. This special alumina supported V_2O_5 catalyst astonishingly displayed a quite good performance in the ODHE despite its small surface area. Such behaviour can be ascribed mainly to the presence of penta-coordinated Al surface sites acting as anchors for preferentially monomeric and low-oligomeric VO_x species leading to a prime dispersion.

In further studies, the effect of oxide support material (Nb_2O_5, TiO_2, Al_2O_3) on the activity and selectivity behavior of vanadia catalysts (10 wt% V_2O_5) was examined. The nature of the support has shown substantial influence on the catalytic performance in the ODHE reaction. This phenomenon could be attributed to the dispersion of VO_x species on the support, strength of metal-oxide and support interactions, acidity characteristics, reducible properties, nature of VO_x species formed etc. It has been noticed that Lewis acidity seems to play a key role on the performance. The best V_2O_5 catalyst supported on Al_2O_3 with highest surface area yield the highly dispersed monomeric vanadia species resulting in the superior catalytic performance in the ODHE reaction.

In addition, Ni-Nb-O based catalysts were further modified by three promoters, i.e. Cr, Mo, W (Ni: Nb: M atomic ratio of 1: 0.176: 0.1), that belong to the same group of elements but showing different d-characters. Compared with that of parent Ni-Nb-O solid, the promoted Ni-Nb-M-O (M: Cr, Mo, W) samples didn't show any changes in XRD patterns particularly in terms of crystalline behaviour and phase composition. However, considerable differences could be noticed concerning BET surface area data, reducibility, acidity characteristics as well as surface composition. Among the three auxiliaries used, Cr promoted Ni-Nb-Cr-O displayed relatively superior catalytic performance in the ODHE to ethylene, yielding in an ethane conversion of 26% and an ethylene selectivity of ca.65% at 420 °C. Ni-Nb-O and promoted Ni-Nb-M-O (M: Cr, Mo, W) catalysts were also further tested in the ODH of ethane in the presence of CO_2 with an intention to improve activity and/or selectivity. The introduction of CO_2 into the reactant feed mixture is found to improve the selectivity of ethylene

considerably but resulted in a marginal loss of activity. Among all, Ni-Nb-Cr-O solid revealed an ethylene selectivity of ca.85% at slightly less ethane conversion.

On the whole, it can be concluded that the content of vanadia, nature of support, type of VO_x species formed and their dispersion on the support surface, acidity characteristics, reducibility, surface compostion etc. are some of the key parameters that need to be controlled carefully to achieve enhanced performance of the catalysts

Zusammenfassung

Ethylen, eins der wichtigsten Monomere der Petrochemie, dient als Basischemikalie in der Herstellung einer Vielzahl von Produkten. Beispiele sind Kunststoffe, Fasern, Harze, Polymere, Verpackungsmaterialien und einige mehr. Der globale Verbrauch 2012 betrug 130 Megatonnen bei einem erwarteten Anstieg auf 155 Megatonnen bis 2015. Diese Zahlen verdeutlichen die wirtschaftliche Bedeutung von Ethylen im Weltmarkt. Hauptproduktionsweg ist derzeit das Steamcracken von Naphtha und Ethan. Ein thermodynamisch limitierter, energieintensiver, endothermer Prozess der bei Temperaturen von 700-900°C durchgeführt wird. Als Nebenprodukte entstehen CO, H_2, CH_4, C_2H_2 sowie C_{3+}-Verbindungen. Dies zieht Abtrenn- und Reinigungsschritte nach sich. Die Zumischung eines Oxidationsmittels (O_2) eröffnet als alternativen Reaktionsweg die exotherme oxidative Dehydrierung (ODH) von Ethan. Da es sich bei der ODH um eine exotherme Reaktion handelt, kann die Reaktion bei vergleichsweise niedrigen Temperaturen von 300 bis 600 °C durchgeführt werden. Im Vergleich mit herkömmlichen Herstellungsverfahren bedeutet das eine deutliche Energieeinsparung. Des Weiteren unterdrückt O_2 die Koksbildung und führt daher zu verbesserten Katalysatorstandzeiten.

Eine große Bandbreite verschiedener Materialien wurde als Katalysator in der ODH von Ethan (ODHE) getestet. Ein mehrkomponentiges MoVTeNbO-Mischoxidsystem (optimales Verhältnis 1: 0.15: 0.16: 0.17) führt zu Ethanumsätzen von mehr als 80% bei Selektivitäten zu Ethylen von über 80% bei 350-400°C und Atmosphärendruck. Besonderes Augenmerk richtete sich auf Trägerkatalysatoren früher Übergangsmetalloxide. Aufgrund ihrer Eigenschaft, in einem Mars-van Krevelen-Mechanismus, Gittersauerstoff zur H-Abstraktion aus Alkanen bereitzustellen fiel die Wahl hauptsächlich auf V und Mo-Oxide. Die katalytische Aktivität und Selektivität geträgerter Vanadiumoxid-Katalysatoren verändert sich für unterschiedliche Trägermaterialien signifikant. Merklichen Einfluss haben dabei unter anderem folgende Eigenschaften des Trägermaterials: thermische Stabilität, Zahl und Stärke saurer und basischer Zentren, Porosität (Oberfläche und Porenvolumen), elektronische Wechselwirkungen zwischen Träger und Aktivkomponente, Sauerstoffspeicherkapazität, Redoxpotential. Aktuell erfahren NiO-basierte Katalysatoren erhöhte Aufmerksamkeit. Hier werden hohe Aktivitäten bei vergleichsweise niedrigen Temperaturen von 300-450 °C und zugleich guten Olefin-

Selektivitäten berichtet. Zur Vermeidung der Totaloxidation von Ethan in Gegenwart von Sauerstoff wurde der Einsatz von Kohlendioxid als mildes Oxidationsmittel erwogen. Dieses Vorgehen verspricht neben einer Minderung der Totaloxidation auch höhere Selektivitäten. Der vielversprechende Effekt einer CO_2 Beimischung in der ODH von Alkanen ist literaturbekannt. Eine weitere Verbesserung der katalytischen Kenngrößen NiO-basierter Systeme durch CO_2 Beimischung ist nicht auszuschließen.

Vor diesem Hintergrund besteht die Aufgabenstellung dieser Arbeit in der Herstellung, Charakterisierung und katalytischen Austestung von fünf ODHE-Katalysator-Serien. Vanadiumoxidbasierte V_2O_5/Nb_2O_5, $V_2O_5/Al-x$, V_2O_5/TiO_2 sowie Ni-Nb basierte (promotierte Ni-Nb-M-O (M=Cr, Mo, W)) Katalysatoren wurden durch Imprägnierungs- und Einengungsverfahren hergestellt. Sämtliche Katalysatoren wurden durch mehrere physikalisch-chemische Methoden charakterisiert. Katalytische Tests wurden in Festbett-Quarzreaktoren bei 500-600°C (VO_x) bzw. 300-450°C (NiNb-M-O) durchgeführt. Eine Beimischung von CO_2 wurde für Ni-Nb-M-O Katalysatoren getestet. Besondere Beachtung wurde der detaillierten physikochemischen Charakterisierung der Katalysatoren zur Erlangung von Auussagen zu Struktur-Aktivitäts-Beziehungen beigemessen. Ausgewählte Ergebnisse der verschiedenen Testserien werden hier zusammengefasst.

V_2O_5/Nb_2O_5 Katalysatoren mit unterschiedlichem V_2O_5-Gehalt (5-20 wt%): Aktivität und Selektivität hängen stark von der Art der gebildeten Vanadiumoxid-Spezies und der Anreicherung von Vanadium in Oberflächennähe ab. Diese beiden Eigenschaften fußen ihrerseits auf dem Vanadiumgehalt der Katalysatoren. Unter allen Getesteten zeigte die Probe mit 10 wt% V_2O_5/Nb_2O_5 die beste katalytische Leistung (X = 28%, S = 38% bei 600 °C). Dies liegt in der Anreicherung von Vanadium in Oberflächennähe und der Bildung einer optimalen Menge an monomeren/oligomeren VO_x Spezies begründet. Ausgehend von diesem Ergebnis wurden alle folgenden Studien mit dieser Probe durchgeführt.

Die Natur des Al_2O_3-Trägers hatte ebenfalls einen großen Einfluss auf die katalytische Aktivität. Dies wurde anhand von Messungen an 10 wt% V_2O_5 auf 5 verschiedenen Al_2O_3 Trägern nachgewiesen. Unter allen untersuchten Katalysatoren zeigten die auf γ-Al_2O_3 basierten Festkörper die besten Ergebnisse aufgrund der hohen Dispersität des Vanadiumoxids. Andererseits zeigten Katalysatoren, die α-

Al$_2$O$_3$ und γ-Al$_2$O$_3$ niedriger Oberfläche nutzten, hohe Ethanumsätze, jedoch schlechte Ethylenselektivitäten aufgrund der nachweislich vorhandenen V$_2$O$_5$ Partikel. Außerdem wurde ein kürzlich beschriebenes, kugelgemahlenes Aluminiumoxid niedriger Oberfläche getestet. Erstaunlicherweise zeigte der entsprechend geträgerte V$_2$O$_5$-Katalysator eine sehr gute ODHE-Aktivität, trotz der kleinen spezifischen Oberfläche. Das Verhalten kann hauptsächlich den pentakoordinierten Aluminiumspezies an der Oberfläche zugeschrieben werden. Hier wird bevorzugt monomeres und niederoligomeres VO$_x$ gebunden. Dies führt zu hervorragender Dispersität.

Weitere Untersuchungen hatten insbesondere den Einfluss des oxidischen Trägers (Nb$_2$O$_5$, TiO$_2$, Al$_2$O$_3$) auf die Aktivität und Selektivität der Vanadiumoxidkatalysatoren (10 wt% V$_2$O$_5$) zum Gegenstand. Hier zeigte sich ein substanzieller Einfluss auf die katalytischen Kenngrößen der ODHE-Reaktion. Das Phänomen konnte der Dispersität verschiedener VO$_x$ Spezies auf dem Träger, der Stärke der Träger-Metalloxid-Wechselwirkungen, Säurestärken, Reduzierbarkeit etc. zugeschrieben werden. Es wurde erkennbar, dass die Lewis-Säurestärke eine Schlüsselrolle zu spielen scheint. Der beste V$_2$O$_5$ Katalysator geträgert auf oberflächenaktiviertem Al$_2$O$_3$ mit der höchsten spezifischen Oberfläche ergab hochdisperse monomere Vanadiumoxidspezies. Dies führte zu der besten katalytischen Aktivität.

Außserdem wurden Ni-Nb-O basierte Katalysatoren durch Promotoren modifiziert. Dazu wurden: Cr, Mo, W (Ni: Nb: M Molverhältnis von 1: 0.176: 0.1) eingesetzt. Die Promotoren gehören zur selben Elementgruppe, zeigen jedoch unterschiedlichen d-Charakter. Unter den 3 Auxiliaren zeigten die Cr-promotierten Ni-Nb-Cr-O die besten Eigenschaften. Es wurde ein Ethanumsatz von 26% und eine Ethylenselektivität von ca. 65% bei einer Temperatur von 420 °C erreicht. Ni-Nb-O und promotierte Ni-Nb-M-O (M: Cr, Mo, W) Katalysatoren wurden ebenfalls bezüglich ihrer ODHE-Aktivität in Anwesenheit von CO$_2$ getestet. Die Beimischung von Kohlendioxid führte zu verbesserten Selektivitäten für Ethylen bei marginalem Aktivitätsrückgang. Unter allen getesteten Katalysatoren zeigte Ni-Nb-Cr-O eine Ethylenselektivität von ca. 85% bei geringfügig niedrigerem Ethanumsatz.

List of Acronyms, Symbols and Units

ODH	Oxidative Dehydrogenation
ODHE	Oxidative Dehydrogenation of Ethane
i.e.	id est
e.g.	Exampli gratia
et al.	et alii
FID	Flame Ionization Detector
GC	Gas Chromatograph
BET	Brunauer-Emmett-Teller and their adsorption model
ICP-OES	Inductive Coupled Plasma Optical Emission Spectroscopy
TGA	Thermogravimetric Analysis
UV-Vis	Ultraviolet visible spectroscopy
XRD	X-ray Diffraction
XPS	X-ray Photoelectron Spectroscopy
TEM	Transmission Electron Microscopy
FTIR	Fourier Transform Infrared spectroscopy
Py-FTIR	Pyridine adsorbed FTIR
STEM	Scanning Transmission Electron Microscopy
EDXS	Energy Dispersive X-ray Spectroscopy
HAADF	High Angle Annular Dark Field
MFC	Mass Flow Controller
mm	millimeter
GHSV	Gas Hourly Space Velocity
τ	Contact time
BE	Binding Energy
FWHM	Full width at Half Maximum

Structure of the thesis

The thesis is separated into seven chapters.

Chapter 1 contains a general introduction on ethylene manufacture and application, the motivation and the objective of the current study, a comprehensive literature review on useful ODHE catalysts including the general introduction of vanadia and molybdena based catalysts, the Ni-Nb-M-O mixed metal oxide catalysts and their advantages in selective oxidation reaction, the motivation on a third metal dopant into Ni-Nb-O catalysts and an introduction of CO_2 admixture in the reaction feed.

Chapter 2 gives a summary on experimental issues including the solids preparation methods, basic characterization techniques, and the introduction about the reaction setup and evaluation of the catalysts for the oxidative dehydrogenation of ethane to ethylene.

Chapter 3 shows the catalytic data obtained by using Nb_2O_5 supported vanadia catalysts. The catalytic performance of those catalysts is evaluated with the help of BET-SA, ICP, UV-vis, XRD, XPS, FTIR, TEM in detail.

Chapter 4 deals with the catalytic data obtained from catalytic performance tests over different alumina supported vanadia catalysts. The catalytic performance of those catalysts is evaluated with the help of the methods mentioned above.

Chapter 5 compares the catalytic data obtained from different supported vanadia catalysts and their characterization using the techniques listed above.

Chapter 6 presents the catalytic data obtained by Ni-Nb-M-O mixed metal oxide catalysts with and without CO_2 admixture under the same reaction conditions (T, GHSV), along with the solid state characterization to show the correlation between the nature of catalysts and different catalytic performance.

Chapter 7 summarizes the results of the investigations and gives some conclusions and an outlook for future research on the oxidative dehydrogenation of ethane to ethylene.

Content

1.   Introduction and literature survey

This chapter contains a general introduction on the manufacture and application of ethylene, the motivation and the objective of the current study. Furthermore, a comprehensive literature review on useful ODHE catalysts including a general introduction on vanadia based catalysts, Ni-Nb-O mixed metal oxide catalysts and their advantages in selective oxidation reactions. Moreover, this chapter reports on the motivation of the incorporation of a third metal dopant into Ni-Nb-O catalysts and an introduction on the admixture of CO_2 to the reaction feed.
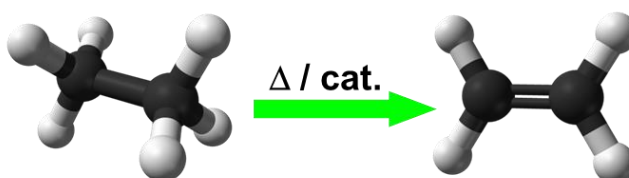
1.1 Ethylene - commercial manufacture, application, demand

Ethylene is one of the most important building blocks in the worldwide petrochemical industry (Fig. 1-1). About 80% of ethylene produced in the world is used for the manufacture of various commercially important chemicals such as vinyl acetate, vinyl chloride, ethylene oxide, ethyl benzene, linear higher olefins and so on [e.g.1]. It is also a key raw material for the production of numerous polymers such as synthetic lubricants, plasticisers, surfactants, detergents and so on. All these chemicals play an important role in our daily life.
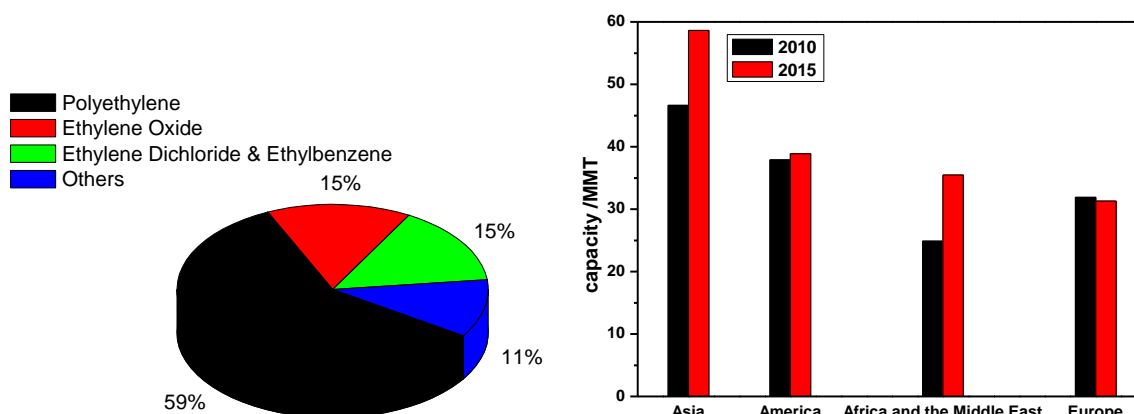
Fig. 1-1.   Ethylene capacities and main applications

USA is the highest exporter while China is the highest importer of ethylene. Although ethylene consumption growth dropped to around one per cent in 2012 as a result of the on-going economic problems around the world, the ethylene market is growing at a rate of ~3% per year [2, 3, 4]. In addition, one should also note that ethylene production and consumption is relatively less affected on the whole during global economic recession compared to other petrochemicals. In 2012, the worldwide ethylene consumption is estimated to be >130 MMT, which is expected to reach over 140 MMT by 2015. However, the worldwide ethylene production capacities from all units in 2012 are 150 MMT that would increase to 165 MMT by 2015. This means an operation rate of around 87% is recorded. Despite 1% decrease of global consumption in 2012 due to economic downturn in China, the global demand on the whole for ethylene is expected to grow by ~3% per year over a period of next five years. In other words, the global demand for ethylene would grow more or less at the same level as that of World GDP average growth rate (i.e. 3%). The largest Chinese market will continue to grow at a rate of 8-10% per year for next 5 years at least and

becomes the main driver in ethylene consumption, particularly polyethylene and ethylene glycol use in packaging, fibre and plastic industries (Fig. 1-1).

At present, the industrial methods for ethylene production are steam cracking of hydrocarbon feedstocks, with additional manufacture from fluid-catalytic-cracking (FCC) and catalytic dehydrogenation of paraffins [5], in general. These processes operate at temperatures between 500 and 900 °C, depending upon the raw materials, which consume a lot of energy and also possess some thermodynamic limitations [6]. In addition, CO, H_2, CH_4, C_2H, C_{3+} compounds are formed as by products during such processes, which in turn lead to difficulties in their separation and purification. It also limits the ethylene selectivity and favors carbon deposition on the active sites [7]. Furthermore, in thermal cracking at high temperatures (typically in the range of 450-750 °C) and pressures (up to 70 bar) large amounts of unwanted solid coke are formed [1]. Alternatively, steam cracking is also a large industrial process in which saturated hydrocarbons are broken down into smaller ones, often unsaturated hydrocarbons. It is the principal industrial method for the production of light olefins (e.g. ethylene and propylene). Similar to thermal cracking, the steam cracking also has some disadvantages such as (i) the reaction is highly endothermic depending upon the raw materials [1], (ii) coking problem is significant in the furnace and in the transfer line exchanger, (iii) deactivation of the catalyst and (iv) the more heavier the feedstock the more the formation of undesired products occurs [8]. Due to these problems, there is a real need to develop a new technology devoted to a more efficient ethylene production.

1.2 Oxidative dehydrogenation of ethane (ODHE)

The oxidative dehydrogenation (ODH) of alkanes to the corresponding olefins [e.g. 9, 10, 11] becomes to be an attractive route due to several advantages such as the use of cheap ethane or propane from natural gas sources. The addition of O_2 to the reaction mixture allows performing the exothermic ODH ($\Delta_R H$ = -105 kJ/mol ethane). So it can be operated at relatively low temperatures (350-600 °C) thus requiring less energy input compared with the traditional production routes mentioned above. The presence of oxygen also lowers the thermodynamic restrictions for dehydrogenation activity, reduces the coke formation to a large extent and thereby improves the long-term stability. In addition, the catalyst regeneration step (decoking)

is not necessary in the production process, because the catalyst regeneration occurs in situ by the presence of oxygen in the reactant feed itself. Thus, the ODHE over redox catalysts is an attractive alternative method to the current thermal / steam cracking processes for ethylene production [e.g.12, 13, 14].

In the ODHE, there are mainly three potential reactions (Fig.1-2), the selective ODH of ethane to desired ethylene (R. 1), total oxidation of ethane to CO_x (R. 2) and consecutive oxidation of ethylene to CO_x (R. 3). However, the formation of certain amounts of thermodynamically favoured products (e.g. CO_x and H_2O) cannot be excluded and hence the yield of ethylene achieved on most of the catalysts applied is still not very satisfactory. Therefore the key issue of ethylene production by the ODHE is linked to develop a catalytic system, which is capable to selectively convert ethane to ethylene and meanwhile prevent the ethane total oxidation and ethylene consecutive oxidation to CO_x.
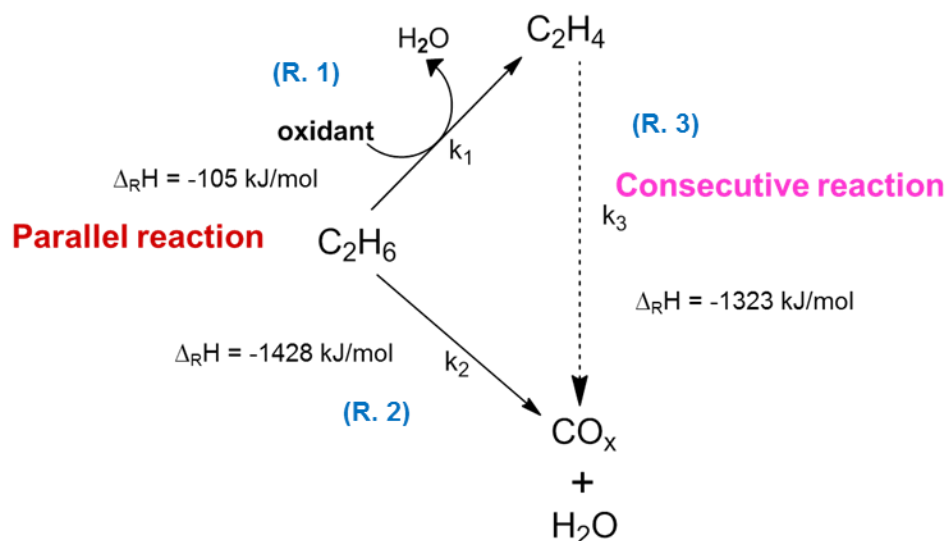
Fig. 1-2.   Main reaction paths running in the ODHE reaction

Literature survey reveals that a wide range of catalytic active materials have been studied as potential catalysts for the ODHE [4, 12, 13, 15, 16, 17]. In recent investigations, the most widely used catalysts for the ODH are supported early-transition metal oxides, i.e., mainly V and Mo oxides [18, 19, 20, 21]. López Nieto and co-workers have developed a multicomponent MoVTeNbO mixed oxide system with an optimum Mo-V-Te-Nb formulation of 1: 0.15: 0.16: 0.17 giving a selectivity to ethylene above 80%, ethane conversion is reported to be higher than 80% and about 75% ethylene yield at 350-400 °C and atmospheric pressure [22, 23]. Besides,

Heracleous and Lemonidou have reported on $NiNbO_x$ mixed oxides leading to an ethylene yield of 46% and 90% selectivity to ethylene at 400 °C [24]. Gaab et al. reported on ethylene yields up to 77% reached over molten alkali metal salts (Li, Na, and K chlorides) supported on Dy_2O_3/MgO [25]. The application of such chloride containing catalysts can also produce different Cl-containing by-products that might not jam subsequent vinyl chloride manufacture, for example. However, the work-up for other uses at industrial scale makes the process more expensive, unattractive, complex and also create environmental unfriendly issues.

Overall, the yield of ethylene obtained by the ODHE on most of the catalysts is not very satisfactory because of the weakly reactive of ethane, which could be attributed to the absence of lone electron pairs, empty orbitals, and polarity in their C-H bonds [26]. Currently, the ODHE is still under development and needs to breed more active catalyst system and optimized reaction conditions for its commercial implementation.

1.3 Supported vanadia catalysts in the ODHE

Supported catalysts represent the largest group of heterogeneous catalysts, in which small amounts of active materials, especially metals, are applied to another solids, the so-called supports. This kind of catalyst is of major economic importance, especially in refinery technology and the chemical industry. Supported catalysts are heterogeneous catalysts.

Supports such as SiO_2, Al_2O_3, Nb_2O_5 and so on, were initially considered as inert substance to provide a high surface area to carry the active metal oxide phase or to improve the mechanical strength of the catalyst material. Generally the catalytic activity and selectivity of supported catalyst are significantly affected by using of different supports because of their different physical and chemical properties like thermal stability, acid-base properties, different surface area, oxygen storage capacity and reducibility and so on. The effects of support oxide material properties on the activity and selectivity of supported metal oxide catalysts have been receiving more and more attentions since last decades [27, 28, 29, 30, 31, 32]. The interaction between surface metal oxide species with the oxide support called metal-support effect and/or strong metal-support interaction (SMSI) [29, 30], which strongly affect

the dispersion and morphology of the metal particles is probably due to various physical and chemical effects [27]:

- Electronic effects: electron transfer up to formation of chemical bonds
- Adhesive forces (van der Waals forces)
- Formation of reduced support species on the metal surface
- Formation of new phases at the boundary surface

Weckhuysen et al. have reported that among all different supported metal oxide catalysts 28% (expressed as a percentage of the total number of papers) are vanadia catalysts based on an extensive open literature search in the period 1967-2000 [29]. Supported vanadium oxide catalysts constitute a very important class of catalytic materials and have been extensively used in a large number of catalytic processes. Since they are well known to be active in the selective oxidation of alkanes and alkenes [33, 34, 35, 36], selective catalytic reduction of NOx with NH_3 [37, 38], oxidation of o-xylene to phthalic anhydride [39,40], decomposition of isopropylalcohol [41], total oxidation of benzene [42], ammoxidation of hydrocarbons and other organic substrates [43, 44], the oxidative dehydrogenation (ODH) of alkanes [21, 45, 46, 47, 48], as well as many other industrial processes.

The catalytic performance of supported vanadia catalyst is significantly determined by the variability in geometric and electronic structure of surface vanadium oxide species. For example, vanadia based catalysts have achieved an acceptably good ethylene selectivity in the ODHE that is mainly due to the ability of isolated/polymeric vanadia species to provide lattice oxygen for hydrogen removal from alkanes yielding alkenes via redox cycle (i.e. Mars-van Krevelen mechanism) [20, 49]. The deposition of vanadium oxide species on a support can result in several types of vanadium oxides [29, 32, 50, 51] including monovanadate and polyvanadate. At low vanadium oxide loading, the isomeric vanadia species are assumed to predominantly appear (Fig. 1-3a). VO_4 is the base unit in tetrahedrally coordinated structure consisting of a V=O double bond and three bridge V-O-sc (with sc the support cation) bonds linked to the support. With increasing the vanadium oxide loadings the dimeric or polymeric vanadia species are formed (Fig. 1-3b), which can be explained by the condensation of the monomeric species. The chains of vanadium ions building up a one-dimensional and then two-dimensional over-layer of supported vanadium oxides are developed with further rise of the vanadium oxide loadings until

the surface of the support is completely covered and a monolayer of vanadia species is formed (Fig. 1-3c). In addition to the monovanadate and polyvanadate, when the monolayer coverage is exceeded the formation of three-dimensional vanadium oxides V_2O_5 crystallites (Fig. 1-3d), and mixed metal oxide phases with the support, or a combination of the above-mentioned molecular structures can occur.
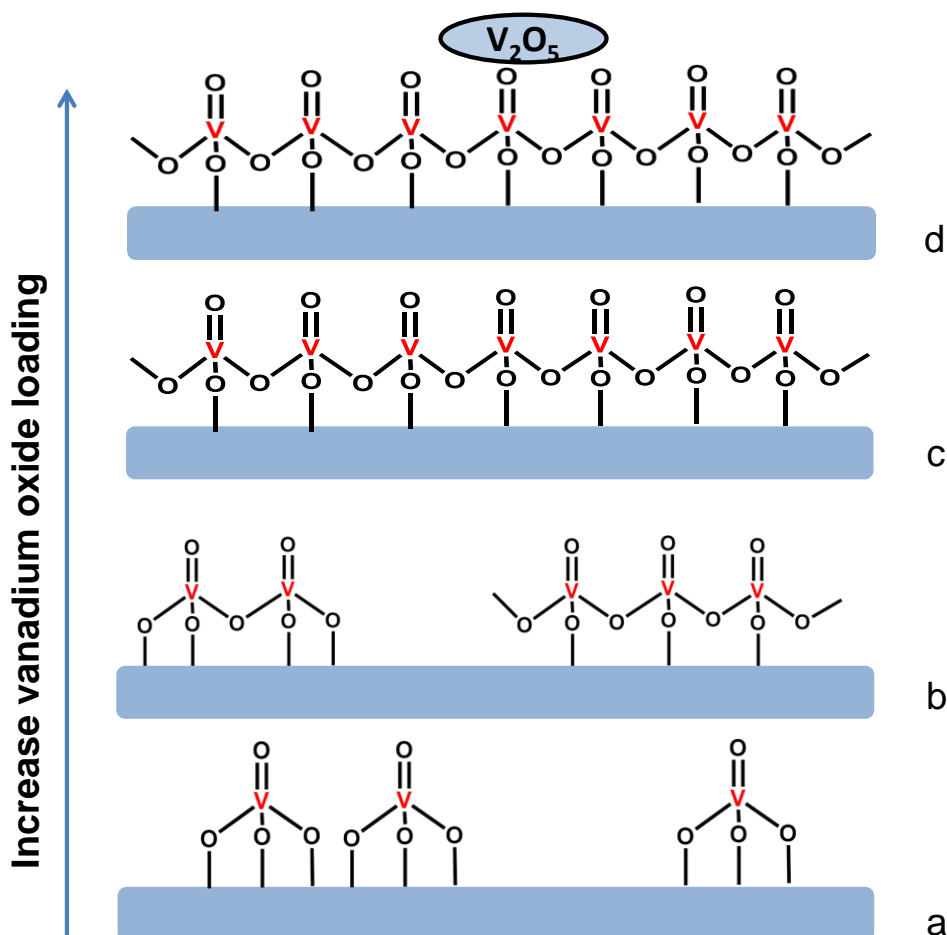
Fig. 1-3. **Schematic representation of the formation of surface vanadia species a) isolated vanadia species, b) dimeric/polymeric vanadia species, c) monolayer vanadia species, d) crystalline V_2O_5 particles above monolayer vanadia species**

However, the metal oxide-support effect is not well studied and therefore not well understood yet. Moreover the relationship between the structure of surface vanadia species and their catalytic activity for the ODHE is also not very clearly understood so far.

Many different oxide supports such as SiO_2, Al_2O_3, Nb_2O_5, TiO_2 were used for vanadia based catalysts in ODHE. Nb_2O_5 was firstly used as a support for V_2O_5 for the ODHE in our work [21], which was however mostly used as active component in

many cases of catalysts for the ODH. As shown by Viparelli et al. [52], the selectivity to propylene in the ODH of propane increased when niobium was associated to vanadium at low V/Nb ratios. The enhanced effect of Nb on the catalytic performance in the ODHE was also illustrated in a Cr-Al-Nb catalyst reported by Liu et al [53]. Nb_2O_5 supported V_2O_5 catalyst were also used in the selective oxidation of propylene to acrolein [32, 54] and vapour phase ammoxidation of toluene to benzonitrile [55].

TiO_2 supported catalysts were also commonly studied in the ODHE. Ciambelli et al. reported on TiO_2 supported vanadyl phosphate catalysts [56] for the ODHE and claimed that the reducibility and acidity of vanadium phosphate is strongly enhanced by deposition on TiO_2 with respect to the bulk phase. This TiO_2 supported catalysts are active and selective in the ODHE to ethylene in the temperature range of 450-550 °C. Heracleous et al. [20] revealed the TiO_2 supported V_2O_5 catalyst exhibit superior activity but inferior selectivity than the corresponding Al_2O_3 supported vanadia catalyst.

Alumina is the most wildly used support, which has been used extensively as adsorbent [e.g. 57], active catalyst [e.g. 58], catalyst support [e.g. 59] and also for numerous other applications in many industries. It occurs in various crystallographic modifications, among which the α- and γ-phases are the most important solids used in catalysis compared with the other six polymorphs of Al_2O_3 (i.e. σ, η, θ, κ, ρ, and χ phases). As earlier as 1963, Maciver et al. have reported that α- and γ-phases of Al_2O_3 possess characteristically distinct chemisorption properties [60] and the catalytic activity of the γ-phase of Al_2O_3 usually turns out to be higher than that of α-phase of the catalysts due to diverging characteristics such as acidic properties or BET surface area, for example. Moreover, γ-phase of Al_2O_3 is commonly used as catalyst support, which allows the dispersion of metal species like vanadium cations as vanadium oxide monolayer on its surface. As mentioned before, the catalytic activity of supported metal oxide catalysts could be significantly affected by the different properties of the support. Zhang et al. [61] have reported the application of various types of alumina supported nickel oxide catalysts for the ODHE reaction. The different physical properties of supports have shown a clear influence on the dispersion of nickel oxide over the support and thereby catalytic performance as well. More recently, Düvel et al. have presented a structurally disordered γ-Al_2O_3 with a

controllable amount of pentacoordinated Al sites [62], which was mechanically treated in a planetary mill to initiate the transformation of γ- into α- phase under ambient conditions. During such phase transformation, 5-fold coordinated Al^{3+} centres were created on the surface of γ-alumina, and these sites are expected to act as binding sites for active catalyst phases, for example the industrially important catalyst system Pt/γ-Al_2O_3 [63, 30]. Considering this issue of generation of penta-coordinated Al sites and their potential benefits of higher activity and selectivity, such alumina is also used in the present study as one of the supports for vanadia based catalysts in the ODHE reaction.

1.4 Ni-Nb-O mixed metal oxide catalysts in the ODHE

Most promising low temperature catalysts reported so far for the ODH of ethane to ethylene are based on multicomponent mixed oxides (e.g. MoVTeNbO) that work at 340-400 °C exhibiting about 75% ethylene yields [23]. Further modification to MoVTeNbO catalyst was carried out by Millet and co-workers [64,46] by addition of silica to the starting slurry during the preparation and changing the final heat treatment conditions [64]. The addition of silica increases the conversion without modifying the selectivity to ethylene and the final heat treatment decreases the ethane conversion but increases the ethylene selectivity [64]. Some research efforts have also been focussed on the application of Ni-based catalysts that also work at low temperatures for the ODH of short alkanes [65, 66, 67]. Schuurman et al. [66] investigated the ODHE over unsupported metal catalyst from group VIII at low temperature and revealed that unsupported Fe, Co and Ni gave interesting results. However, when temperature increased the selectivity towards ethylene remained nearly constant for nickel whilst ethylene selectivity decreased for Co and Fe, making Ni-based catalysts the most attractive candidate for the ODHE reaction. Supported NiO and promoted Ni-M-O catalysts were also intensively studied for the ODHE reaction. According to Zhang [68] there are two kinds of active oxygen species (the more active one and less active one) on the fresh Al_2O_3 supported NiO catalyst. However, only less active oxygen species exist on the treated NiO/Al_2O_3 catalyst, which can only convert ethane to ethylene. Zhang [69] also claimed that highly dispersed NiO on support prefers to convert ethane to ethylene and large crystal NiO on support prefers to convert ethane to carbon dioxide. Heracleous et al. [70]

reported that Nb promoted Ni-M-O/Al_2O_3 catalyst showed enhanced reactivity toward ethane by more than 50% while maintaining the high ethylene selectivity. Later on Heracleous and Lemonidou synthesized a series of Ni-M-O mixed metal oxides and tested them in the ODHE. They found that its selectivity can be significantly improved by the addition of another metal that can reduce the formation undesired electrophilic oxygen species on the surface being responsible for the total oxidation of ethane and consecutive oxidation of ethylene to carbon oxides both running in parallel. The best performance was reached by $Ni_{0.85}Nb_{0.15}O$ at 400 °C resulting in ca.45% ethylene yield under optimised conditions [24, 71]. The enhanced catalytic activity of NiO based catalysts with Nb dopant was related to the favourable ionic radii, valency and electron-donor properties of niobium cations filling the cationic vacancies and/or substituting nickel atoms in the NiO lattice, forming a Ni-Nb solid solution and a highly distorted Nb-rich amorphous phase and therefore reduce the structural defects in NiO resulting in high selectivity to ethylene [24, 71, 72, 73].

More recently, López Nieto's research group studied the ODHE to ethylene over Ni-Ce-O mixed oxide catalyst [12] and claimed enhanced activity. Such increase in the catalytic activity is attributed to the increased surface area by the addition of CeO_2, as well as the changes in the nature of Ni sites. They also explored W [13] and Sn [74] promoted NiO catalyst in the ODHE and concluded that the interaction of NiO particles with WO_x nanoparticles seems to be an important factor in the improvement of the selectivity to ethylene, probably blocking the active and nonselective sites of pure nickel oxide, similarly to Ni-Nb-O catalysts. While the highly improved catalytic behaviour of SnO_2-promoted NiO catalyst could be explained by several modifications such as a decrease in the crystal size and modification of surface Ni species, which favours a lower reducibility and/or a lower presence of electrophilic oxygen species. Comparing MoVTeNbO [22, 23] and Ni-Nb-O [4, 24, 71], both these catalyst systems work at low temperatures ($\leqslant$ 400 °C), but having some advantages and disadvantages. The first one gives superior performance, but it is a multi-component system involving rather complex synthesis procedures being guarded by various patents [75, 76]. Alternatively, Ni-Nb-O catalyst is somehow less active, but it is a simple system that can be easily prepared. Considering the simplicity of this Ni-Nb-O system, we are intended to further enhance its performance by the incorporation of some suitable redox promoters.

From previous investigations dealing with other oxidation reactions, we have observed that the promoters (for instance Cr, Mo, Fe etc.) clearly enhanced both the activity and selectivity of VPO catalysts [77, 78]. Based on earlier experience, we would like to extend such knowledge to the present ODHE reaction and apply some selected redox promoters (e.g. Cr, Mo, W) that are expected to show positive influence and thereby improve the catalytic properties of Ni-Nb-O system.

1.5 Introduction of CO_2 in the ODHE

So far the most commonly used oxidant in the ODH is oxygen. The thermodynamically favoured reaction of ethane total oxidation and consecutive oxidation of ethylene to carbon oxides might occur easily. However, carbon dioxide, as one of the greenhouse gases, has also been considered as a mild oxidant in recent times. The application of CO_2 in the ODH could be considered as another route for increasing selectivity and to avoid total oxidation. The promising effect of CO_2 in the ODHE was first reported by Wang et al. [79]. They reported the promoting effect of CO_2 in the ODH at T≤650 °C, CO_2 either formed during reaction or added to the system increases the selectivity for the desired hydrocarbon products during the ODHE over Li^+/MgO catalysts. The improved selectivities are attributed to the poisoning effect of CO_2 on the secondary reactions of alkyl radicals with the active centers on the surface of catalysts [79]. Nakagawa et al. tested various metal oxide catalysts in dehydrogenation of ethane to ethylene in the presence/absence of CO_2 [80] and found that gallium oxide is the most effective catalyst, giving 18.6% ethylene yield with a selectivity of 94.5% in the presence of CO_2 at 650 °C. The activity of this Ga_2O_3 catalyst in the presence of CO_2 was twice that in the absence of CO_2. Some other catalysts have also been proposed for the ODHE to ethylene with the presence of CO_2 [81, 82]. It was proved that CO_2 can enhance the dehydrogenation of ethane [83, 84, 85] and propane [86, 87], but the reaction temperature was mostly above 700 °C [88]. As mentioned earlier, NiO-based catalysts can be applied at low temperatures in the ODHE reaction, therefore the introduction of CO_2 into this reaction system could probably further improve the NiO-based catalyst performance. In addition, the ODH of alkanes carried out in the presence of CO_2 would be a more benign process for both the environment and economics if the catalysts are efficient enough to make the process commercially attractive.

1.6 Motivations and aims of the thesis

The main goal of the present study in general is to develop highly active and selective catalysts for the ODHE to ethylene. Based on this purpose, two different series of catalyst were studied, i.e. supported vanadia and promoted Ni-Nb-O-based catalysts.

Supported vanadia catalyst:

i) Apply Nb_2O_5 as a support for V_2O_5 catalysts, and evaluate the influence of V_2O_5 loading from 5-20 wt% on the catalytic performance of V_2O_5/Nb_2O_5 catalysts in the ODHE to ethylene.

ii) Investigate different types of alumina-support including α and γ alumina with different surface areas, as well as the ball milled γ-alumina on the catalytic performance of vanadia catalysts for the ODHE. For this aim vanadia content will be fixed at 10 wt%.

iii) Include TiO_2 as support for vanadia catalyst for further study the effects of support on the properties of vanadia catalysts, the formation of vanadia species, as well as their activity and selectivity ability in the ODHE.

iv) Discuss the effect of the nature of the support and the impact of vanadia species in the light of a detailed characterization of the physic-chemical properties of the catalysts by N_2 adsorption, ICP, TGA, XRD, XPS, TPR, FTIR, and TEM.

Ni-Nb-O based catalyst:

v) Further modify the parent Ni-Nb-O catalyst with different promoters (Me = Cr, Mo, W) aimed to enhance the activity for ethane conversion and selectivity in ethylene.

vi) Test the ODHE reaction in the absence and presence of O_2 / CO_2 in the reactant feed over Ni-Nb-O and promoted Ni-Nb-Me-O (Me = Cr, Mo, W) catalysts to check the effect of CO_2-admixture on the catalytic performance of Ni-Nb-O based catalysts in the ODHE.

vii) Interpret the different properties and catalytic performance among promoted Ni-Nb-Me-O and parent Ni-Nb-O catalyst with the aid of different characterization techniques i.e. BET-SA, ICP, XRD, TPR, Py-FTIR, XPS.

2. Experimental methods and equipment

This chapter gives a summary on several experimental issues including the solids preparation methods, basic characterization techniques, and the introduction of the reaction setup and the evaluation of the catalysts for the oxidative dehydrogenation of ethane to ethylene.

2.1 Methods of solid catalyst preparation

Depending on the structure and method of synthesis, solid catalyst can be divided into three main groups [89], i.e. carrier-free (bulk) catalyst, supported catalyst and coated catalyst. The preparation of solid catalysts consists of many physical and chemical steps. The conditions in each step have a decisive influence on the catalyst properties. For supported catalyst, once the active composition and support were determined the catalyst properties and activity strongly depends on every steps of the preparation process. Supported catalysts could be prepared via several methods, i.e. impregnation, ion-exchange, adsorption and deposition-precipitation [29, 90, 91, 92, 93, 94], endowing the catalyst with different physical and chemical properties such as surface area, pore volume, formation of different active species on the surface of support and so on.
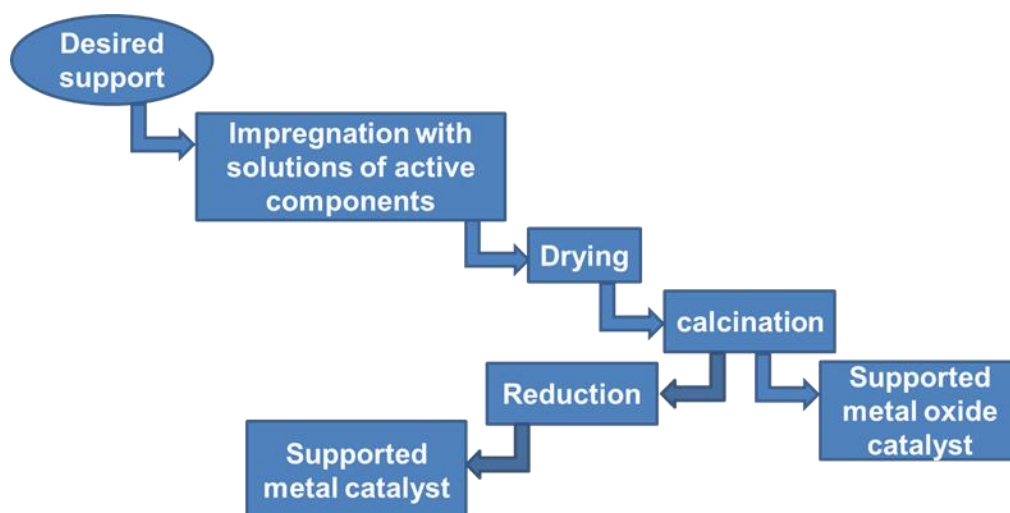
Scheme 2-1.   Manufacture of supported catalysts by impregnation method

With regard to the preparation of supported vanadium oxide catalysts, the most simple and widely used preparation technique is the impregnation method (Scheme 2-1). In this procedure, a certain volume of an aqueous or non-aqueous solution containing a vanadium precursor is contacted with an inorganic oxide support. Two main impregnation procedures can be distinguished, depending on the volume of solution: wet impregnation and incipient wetness impregnation. In wet impregnation the support is dipped into an excess amount of solution. Later on the excess amount of solvent is removed by a rota vapor under reduced pressure. In incipient wetness impregnation the support is contacted with the solution containing active phase precursor of appropriated concentration which is equal to the total known pore

volume of the support, or slightly less. This allows a precise control of the active phase composition on the support [29, 90].

The next step in the catalyst preparation process is very often a thermal treatment including generally drying and calcination steps [90, 91, 92], which is essential in all wet chemical processes. This leads to solvent-free materials and causes vanadia compounds anchored on the oxide support with the oxidation states of vanadia reaching their desired values. Moreover, in order to obtain desired surface area, pore structure, as well as different type active phase, the drying and calcination process should be well controlled by using suitable drying/calcination temperature, heating rate, atmosphere air and so on.

2.1.1 Preparation of V/Nb catalysts

A series of V_2O_5/Nb_2O_5 catalysts (V/Nb) with various V_2O_5 loadings (5 to 20 wt%) was prepared by the wet impregnation method. Required amounts of aqueous solutions containing ammonium metavanadate (99%, Alfa Aesar) and oxalic acid dihydrate (99%, Sigma-Aldrich) were prepared initially. Such solution was heated at 60 °C under continuous stirring for 80 min to ensure complete dissolution and good mixing. In every case, a fixed amount of oxalic acid dihydrate (NH_4VO_3: $(COOH)_2$ = 1: 1.5 mole ratio) was added to dissolve ammonium metavanadate easily and completely. Later on, this solution was impregnated onto the support, Nb_2O_5 (commercial sample supplied by CBMM, Brazil). The excess solvent was then removed under reduced pressure using a rota vapor, and the resulting solids were oven dried at 120 °C for 16 h. Finally, the oven dried samples were calcined at 600 °C for 6 h in air. The obtained catalysts were denoted as 5V/Nb-f, 10V/Nb-f, 15V/Nb-f and 20V/Nb-f, where the number 5 to 20 indicates the nominal proportion (wt%) of V_2O_5 in the catalyst. Additionally, pure V_2O_5 was prepared by calcining NH_4VO_3 at 600 °C for 6 h in air. All the catalysts were crushed and sieved to the desired fraction of 1.0 to 1.25 mm size and used for the activity tests. And the spent catalysts were denoted as 5V/Nb-s, 10V/Nb-s, 15V/Nb-s and 20V/Nb-s.
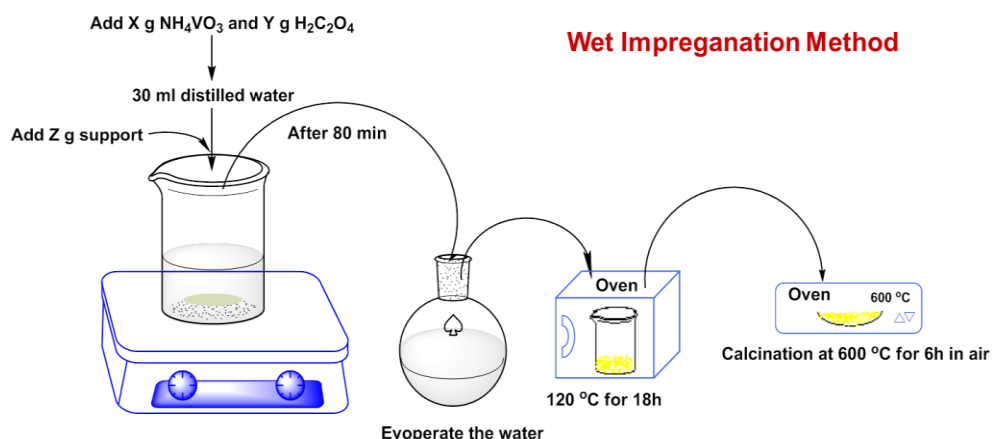
Scheme 2-2.   Schematic representation of preparation of V/Nb V/Al and V/Ti catalysts

2.1.2 Preparation of V/Al and V/Ti catalysts

The theoretical amount of vanadium pentoxide was fixed at 10 wt% irrespective the different type of alumina used.

Different types of Al_2O_3 supported V_2O_5 catalysts were prepared by wet impregnation technique (Scheme 2-2). NH_4VO_3 was used as a precursor for V_2O_5 and the content of V_2O_5 was fixed at 10 wt%. NH_4VO_3 was dissolved into deionized water together with oxalic acid at a mole ratio of NH_4VO_3: $(COOH)_2$ = 1: 1.5 under stirring at 60 °C to ensure complete dissolution and formation of a vanadium-containing solution. Five different types of alumina (samples denoted as Al-x with x = 1-5) with varying surface areas such as (1) high-energy ball milled γ-Al_2O_3 with an extraordinarily high amount of penta-coordinated Al sites prepared according to ref [62]. (BET-SA = 5.8 m^2/g), (2) α-Al_2O_3 (SASOL, Germany; BET-SA = 5.2 m^2/g), (3) γ-Al_2O_3 (Engelhard Italiana, S.p.A., BET-SA = 102 m^2/g), (4) γ-Al_2O_3 (CONDEA Chemie GmbH, Germany; BET-SA = 201 m^2/g) and (5) γ-Al_2O_3 (CONDEA Chemie GmbH, Germany; BET-SA = 294 m^2/g) were used as supports. Subsequently, the above described V-containing solution was impregnated on to these five different alumina supports. The samples were denoted as V/Al-x (x= 1-5), where x refers to the above stated source of alumina support. The excess solvent was then removed under reduced pressure using a rotavapor then oven dried at 120 °C overnight (samples denoted as V/Al-x-od). Finally all the samples were calcined at 600 °C in air for 6 h (samples denoted as V/Al-x-f). All the catalysts were crushed and sieved to the desired fraction of 1.0 to 1.25 mm size and used for the activity tests. Spent samples were denoted as V/Al-x-s.

The TiO$_2$ (Crenox GmbH, Germany) supported vanadia catalyst with 10 wt% theoretical amount of vanadium pentoxide was also prepared by wet impregnation technique (Scheme 2-2). The procedure was the same as that of V/Al-x catalyst. This catalyst was then crushed and sieved to the fraction of 1.0 to 1.25 mm size and evaluated in the ODHE tests. V/Ti-f V/Ti-od and V/Ti-s are represented to fresh oven dried and spent catalyst respectively.

2.1.3 Preparation of Ni-Nb-M-O (M: Cr, Mo, W) catalysts

A series of mixed Ni-Nb-M-O (M = Cr, Mo, W) catalysts, with constant Ni: Nb: M atomic ratio of 1: 0.176: 0.1 were prepared by using the evaporation method [4]. Doing so, aqueous solutions containing nickel nitrate hexahydrate (Alfa Aesar) and ammonium niobium oxalate (Aldrich) with different promoter sources such as i) chromium nitrate nonahydrate (Sigma-Aldrich) for Cr, ii) ammonium molybdate tetrahydrate (Alfa Aesar) for Mo, and iii) ammonium tungsten oxide pentahydrate (Alfa Aesar) as W source were mixed together in a desired proportion and heated at 70 °C under continuous stirring for 1 h to ensure complete dissolution and good mixing of the starting compounds. Then the solvent was gradually evaporated under reduced pressure using rota vapour, and the as-received solids were oven dried at 120 °C for 18 h, followed by calcination at 450 °C in synthetic air (20.5% O$_2$ in N$_2$) for 5 h. This series catalyst were also crushed and sieved to the fraction of 1.0 to 1.25 mm size and evaluated in the ODHE tests. The as-received solid were denoted Ni-Nb-M-O-f and Ni-Nb-M-O-s for fresh and spent catalysts respectively.
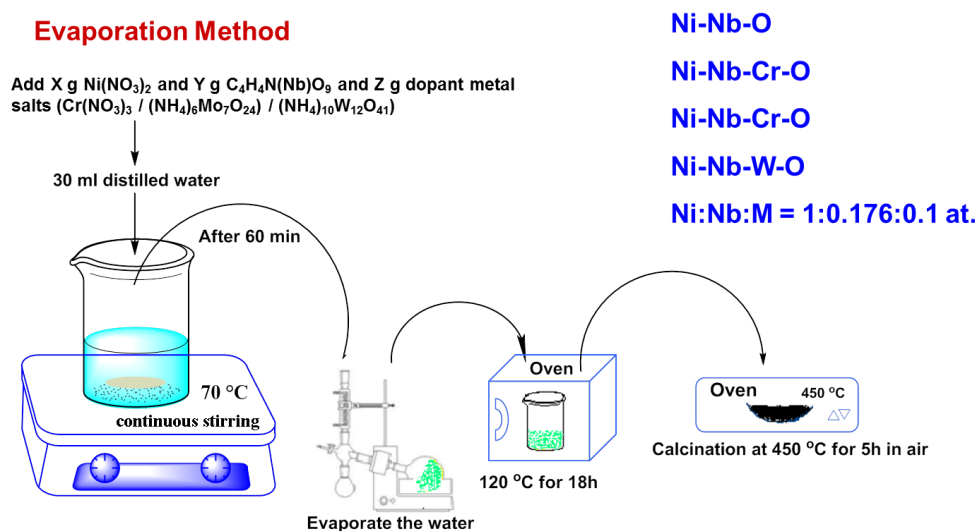
Scheme 2-2.   Schematic of preparation of Ni-Nb-M-O (M: Cr, Mo, W) catalysts

2.1.4 Catalysts prepared and tested in the ODHE

A list of all the catalysts prepared and tested in the ODHE is given in Table 2-1.

Table 2-1. Catalysts and denotation tested in the ODHE

Code	Catalyst Composition	Denotation
1	5 wt% V_2O_5 (s^a: Nb_2O_5)	5V/Nb
2	10 wt% V_2O_5 (s^a: Nb_2O_5)	10V/Nb
3	15 wt% V_2O_5 (s^a: Nb_2O_5)	15V/Nb
4	20 wt% V_2O_5 (s^a: Nb_2O_5)	20V/Nb
5	10 wt% V_2O_5 (s^a: Al_2O_3-1 high-energy ball milled γ-Al_2O_3)	V/Al-1
6	10 wt% V_2O_5 (s^a: Al_2O_3-2 α-Al_2O_3 SASOL, Germany)	V/Al-2
7	10 wt% V_2O_5 (s^a: Al_2O_3-3 γ-Al_2O_3 Engelhard Italiana, S.p.A.)	V/Al-3
8	10 wt% V_2O_5 (s^a: Al_2O_3-4 γ-Al_2O_3 CONDEA Chemie GmbH)	V/Al-4
9	10 wt% V_2O_5 (s^a: Al_2O_3-5 γ-Al_2O_3 (CONDEA Chemie GmbH)	V/Al-5
10	10 wt% V_2O_5 (s^a: TiO_2)	V/Ti
11	Ni: Nb = 1: 0.176 (atomic ratio)	Ni-Nb-O
12	Ni: Nb: Cr = 1: 0.176: 0.1 (atomic ratio)	Ni-Nb-Cr-O
13	Ni: Nb: Mo = 1: 0.176: 0.1 (atomic ratio)	Ni-Nb-Mo-O
14	Ni: Nb: W = 1: 0.176: 0.1 (atomic ratio)	Ni-Nb-W-O

[a]: support

2.2 Characterization of fresh and spent catalysts

Both the physical and the chemical structure properties of a catalyst must be known if relationships between the structure of the catalyst and activity, selectivity and lifetime have to be revealed. The physicochemical characteristics of all these catalysts (fresh and spent) presented above were studied by the following techniques. The catalytic performance test is included in this figure because it can be regarded as a kind of characterization with respect to catalytic activity and selectivity.

Vibrational spectroscopy
(FTIR)

Catalytic performance test
(ODHE)

Phase composition
(X-ray diffraction, Uv-Vis)

Texture
(N$_2$-adsorption)

Solid Catalyst

Surface characterization
(XPS, TEM)

Chemical composition
(ICP)

Thermal analysis
(TGA, TPR)
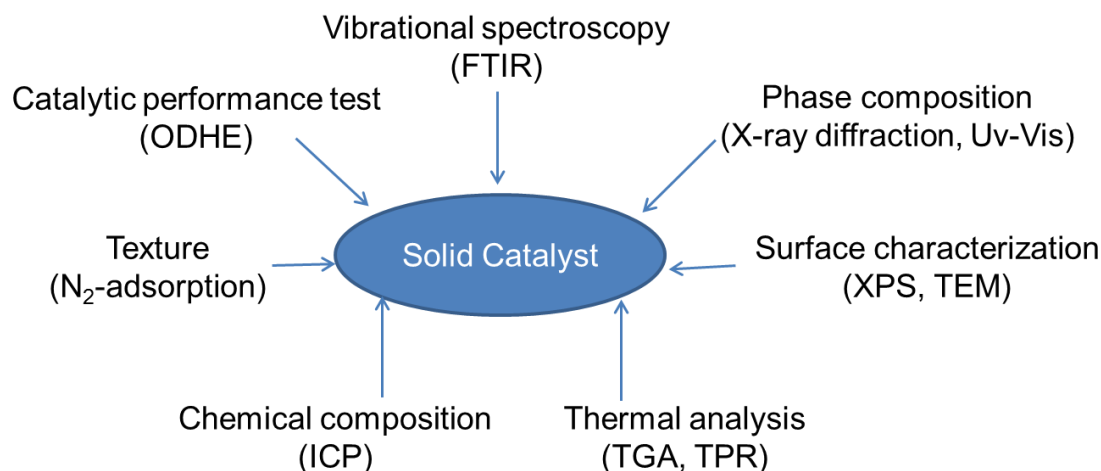
Scheme 2-4. Typical techniques for catalyst characterization

2.2.1 BET surface area and pore volume

The surface area measurement of catalyst reveals information on surface area pore size distribution and pore volume. This technique can be used to predict the efficiency of metal dispersion, porosity of catalyst as a method of assessing the efficiency of catalyst supports and promoters. In the present work the total surface areas and pore volume of the samples were determined by BET (Brunauer, Emmett and Teller) techniques using a NOVA 4200e device (Quantachrome Instruments) by N$_2$ adsorption at -196 °C. Prior to the measurement, the samples were evacuated for 2 h at 200 °C to remove physisorbed water.

2.2.2 Inductively coupled plasma optical emission spectroscopy (ICP-OES)

The elemental compositions were determined by ICP-OES using a Varian 715-ES ICP-emission spectrometer, which is a highly sensitive analytical technique for elemental determination and based on the principles of atomic emission. The samples were dissolved in a mixture of HF and aqua regia and then treated in a

microwave assisted sample preparation apparatus at 200 °C and 60 bar. Later on data analysis was performed on a TruSpec CHNS Micro analyzer (Leco).

2.2.3 Thermal gravimetric analysis (TGA)

Thermal gravimetric analysis (TGA) is a technique whereby the weight of a substance, in heated or cooled environment at a controlled rate, is recorded as a function of time or temperature. The TGA determinations were carried out on a TG apparatus NETZSCH STA 449F3. A stream of air at a flow rate of 25 mL/min was used as the reactive atmosphere. The samples weighed about 10 mg. The temperature was increased from 20 °C to 1000 °C at a rate of 5 K/min.

2.2.4 Temperature-programmed reduction (TPR)

Temperature programmed reduction (TPR) profiles were recorded in a range from r.t. to 900 °C at a heating rate of 10 K/min on a Micromeritics AC2920 instrument. Prior to TPR measurement, all the samples were pretreated under 5% O_2/He up to 450 °C with a rate at 20 K/min and kept at this temperature for 0.5 h then cool down to r.t. After this, 5% H_2/Ar was passed through the sample tube during the measurement and increase the temperature from r.t. to 900 °C with a rate at 10 K/min.

2.2.5 Pyridine Fourier transform infrared spectroscopy (Py-FTIR)

Pyridine was used as probe molecule to examine the surface acidity of the present samples. The pyridine adsorbed FTIR (Py-FTIR) measurements in transmission mode were performed on a Bruker Tensor 27 instrument equipped with a heatable and evacuable homemade reaction cell with CaF_2 windows connected to a gas-dosing and evacuation system. The sample powders were pressed into self-supporting wafers with a diameter of 20 mm and a weight of ca. 50 mg. Before pyridine adsorption, the samples were pre-treated by heating in synthetic air up to 400 °C for 10 min and then subsequent cooling to r.t. and evacuation. Pyridine was adsorbed at r.t. until saturation. Then the reaction cell was evacuated, and the pyridine adsorbate spectrum was recorded. The desorption of pyridine was followed by heating the sample in vacuum up to 400 °C and recording spectra every 50 °C. Generally, difference spectra were evaluated by subtracting the respective spectrum of the pre-treated sample from the adsorbate spectrum.

2.2.6 Ultraviolet–visible spectroscopy (UV-vis)

UV-vis diffuse reflectance spectroscopy (UV-vis-DRS) was mainly deployed to uncover vanadium coordination states of the present V/N catalysts using an AvaSpec 2048 fibre optic spectrometer (Avantes) equipped with an AvaLight-DHS light source and a reflection probe. UV-vis spectra were deconvoluted into Gaussian bands by GRAMS program (Galactic Industries Corporation).

2.2.7 X-ray diffraction (XRD)

The X-rays can penetrate deep into the materials and provide information about the bulk structure. XRD powder patterns at ambient conditions were recorded in transmission mode using Cu Kα radiation (λ = 1.5406 Å) in the 2θ range of 10-60° (step width: 0.25°, 25 sec per step) on a Stoe STADI P diffractometer, equipped with a linear Position Sensitive Detector (PSD). Processing and assignment of the powder diffraction patterns was done using the software WinXpow (Stoe) and the Powder Diffraction File (PDF) database of the International Centre of Diffraction Data (ICDD).

2.2.8 X-ray photoelectron spectroscopy (XPS)

X-ray photoelectron spectroscopy (XPS) is performed to gain information about the oxidation state, surface composition, as well as atomic ratios of the elements present in the near-surface-region of the catalysts due to shifts in the binding energies. XPS analysis was carried out using a VG ESCALAB 220iXL instrument with AlKα radiation (E = 1486.6 eV). The samples were fixed by using a double adhesive carbon tape on a stainless steel sample holder. The peaks were fitted by Gaussian-Lorentzian curves following a Shirley background subtraction.

### 2.2.9 Transmission electron microscopy (TEM)

Transmission electron microscopy (TEM) is useful for indicating the size of the supported metal crystallites in nm scale and it provides the information related to the morphology, composition and distribution. TEM measurements were performed using a JEM-ARM200F (JEOL) high-resolution electron microscope operated at a voltage of 200 kV, aberration-corrected by a CESCOR (CEOS) for the scanning transmission (STEM) applications. The microscope is equipped with a JED-2300 (JEOL) energy-dispersive X-ray-spectrometer (EDXS) for chemical analysis, which is operated with

spot size 6c and a 40 µm condenser aperture. Catalysts samples were deposited on a carbon coated grid (mesh 300) and transferred to the microscope.

2.3 Catalytic tests

All the catalysts prepared in this work were tested in the ODHE reaction using the same set up. Scheme 2-5 shows the flow diagram of the ODHE set up.
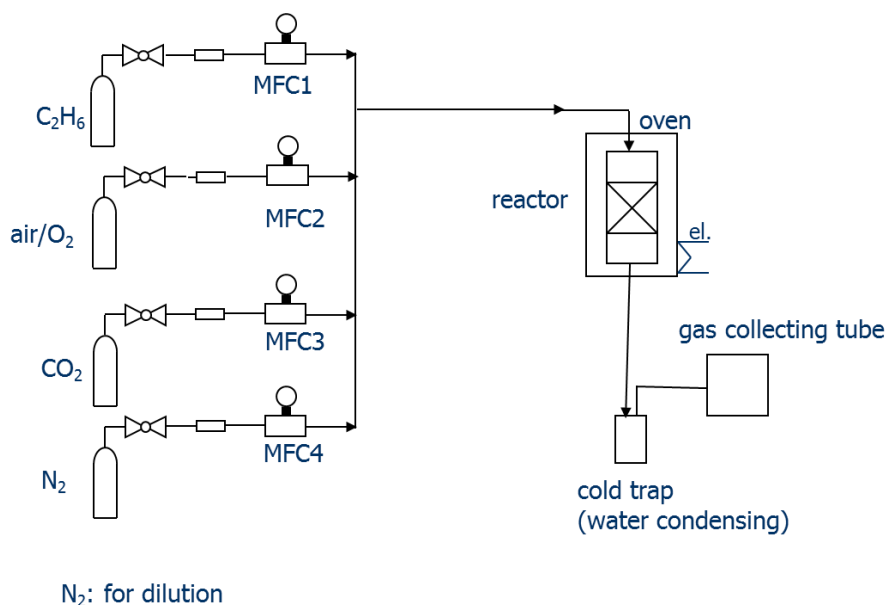
Scheme 2-5.   Flow diagram of the ODHE set up

2.3.1 Activity tests of different supported vanadia based catalysts

The activity measurements of the gas phase the ODHE over V/Nb, V/Al-x, V/Ti and catalysts were conducted in a fixed bed quartz reactor (i.d. 17 mm) at ambient pressure and at temperatures ranging from 500 to 600 °C. The reactant gases such as ethane (99%) and synthetic air (20.5% O_2 in N_2) used were supplied from the commercially available compressed gas cylinders (Air Liquide) and used without further purification. The flow rates of these gases were controlled using mass flow controllers. Two thermocouples were placed; one at the center of the oven to monitor the outside temperature of the reactor and the other at the middle of catalyst bed to indicate the temperature of the reaction. The reactor was filled with 1 g of catalyst particles (1-1.25 mm fraction) that were diluted with one equivalent (wt/wt) of quartz beads of the same size to achieve isothermal operation. The reactant feed was then introduced into the reactor and the reaction was performed, at a constant residence time of ~1.0 to 1.1 s and a gas hourly space velocity (GHSV) of ~3250 to 3545 h^{-1}.

For the determination of the activity of the catalysts as a function of temperature, the W/F ratio was kept constant at 0.92 g/cm$^3 \cdot$s^{-1}. The reactor off-gas composition containing mainly ethane and ethylene was analysed by off-line GC equipped with FID using CP-PoraBOND-Q column. The total oxidation products such as CO and CO_2 were estimated on-line using a non-dispersive infrared NGA 2000 gas analyser (Rosemount). The carbon balance was calculated based on ethane concentration at the inlet of the reactor.

2.3.2 Activity tests of Ni-Nb-O and Ni-Nb-M-O (M: Cr, Mo, W) catalysts

The activity measurements of Ni-Nb-M-O mixed metal oxide catalyst in gas phase ODHE were also conducted in the same reactor as V/Nb, V/Al-x and V/Ti catalysts. CO_2 was introduced into the reactant gas in order to study the effect of CO2-admixture on the performance of Ni-Nb-M-O catalysts in the ODHE. The reactant gases such as C_2H_6, O_2, CO_2 (with mole ratios of 1: 1.4-0: 2.1-0) and N_2 used as diluent to keep total flow at 3.9 l/h were supplied from commercially available compressed gas cylinders (Air Liquide) and used without further purification. The flow rates of these gases were set using mass flow controllers. The reactor was filled with 1.1 g of catalyst (sieve fraction of 1-1.25 mm) and equal amount (wt.) of quartz beads of the same size to achieve isothermal operation. The reactant feed was then introduced into the reactor in appropriate amounts by means of the mass flow controllers. The reaction was performed in the temperature range from 300 to 450 °C, at a residence time of ~1.0 to 1.1 s and a gas hourly space velocity of ~3250 to 3545 h^{-1} that depends upon the volume of catalyst for similar amount but the catalytic tests were carried out under identical conditions. For the determination of the activity of the catalysts as a function of temperature, the W/F ratio was kept constant at 1.02 g s/cm^3. The desired products and total oxidation product were also analyzed by off-line GC equipped with flame ionisation detector (FID) using a CP-PoraBOND-Q column and on-line using non-dispersive infrared analyser, respectively.

3. ODHE over V_2O_5/Nb_2O_5 catalysts

Chapter 3 shows the catalytic data obtained by using Nb_2O_5 supported vanadia catalysts. The catalytic performance of those catalysts is evaluated with the help of BET-SA, ICP, UV-vis, XRD, XPS, FTIR, TEM in detail.

$$C_2H_6 + 1/2\ O_2 \xrightarrow{V_2O_5/Nb_2O_5} C_2H_4 + H_2O$$
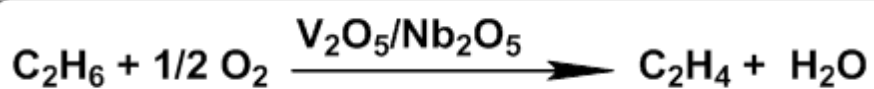
3.1 General studies on V_2O_5/Nb_2O_5 catalyst in the ODHE

V_2O_5/Nb_2O_5 catalysts with various V_2O_5 contents were prepared by impregnation and characterized by various techniques in detail. Oxidative dehydrogenation of ethane was carried out in a fixed bed quartz reactor at 500-600 °C. XPS analysis indicated a clear enrichment of vanadium on the near-surface-region and UV-vis diffuse reflectance spectroscopy revealed the nature of VO_x structures formed. It can be seen clearly from Fig. 3-1 that 10 wt% V_2O_5/Nb_2O_5 catalyst has displayed the superior performance (X = 28%, S = 38% at 600 °C) due to enrichment of vanadium in the near-surface-region and formation of optimum amount of monomeric/oligomeric VO_x species.
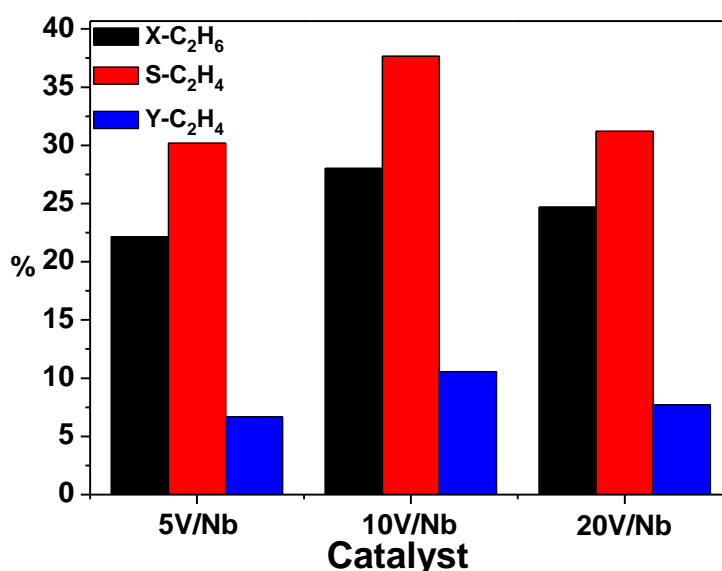

Fig. 3-1. Comparison of Nb_2O_5 supported V_2O_5 catalysts with various V_2O_5 loading

3.2 Characterization results of V/Nb catalysts

3.2.1 Texture data and catalyst composition

Surface areas, pore volumes and elemental analysis results of V_2O_5/Nb_2O_5 catalysts and both the pure oxides are presented in Table 3-1. The supplied niobia reveals a BET surface area of 21 m^2/g whereas the one of the homemade vanadia is much lower (6.3 m^2/g). It can be seen from the table that both the surface areas (18 to 4 m^2/g) and pore volumes (0.052 to 0.008 cm^3/g) of the V/Nb catalysts are observed to decrease continuously with increase in V_2O_5, as expected. This is mainly due to the formation of an increased proportion of various types of oxides of vanadium progressively blocking the access to the surface of the carrier. By

comparing the surface areas between fresh and spent samples, one can notice that the surface areas are not significantly altered in the spent solids compared to their corresponding fresh ones. Additionally, the contents of V$_2$O$_5$ estimated in all the catalysts from ICP are in good agreement with those of nominal values (Table 1).

Table 3-1

BET-surface areas and pore volumes of V$_2$O$_5$/Nb$_2$O$_5$ catalysts with different V$_2$O$_5$ loadings received from ICP

Cat. Code	BET-SA (m^2/g)		Pore volume (cm^3/g)		V$_2$O$_5$ (wt%)*	
	Fresh	Spent	Fresh	Spent	Fresh	Spent
5V/Nb	17.8	15.1	0.052	0.046	4.8	4.8
10V/Nb	16.8	16.7	0.053	0.086	9.6	10.2
15V/Nb	10.5	11.5	0.014	0.073	14.8	15.1
20V/Nb	4.1	6.2	0.008	0.010	20.1	20.2
V$_2$O$_5$	6.3	-	0.005	-	-	-
Nb$_2$O$_5$	21.0	-	0.021	-	-	-

* received from ICP-OES elemental analysis

3.2.2 X-ray diffraction

XRD patterns of fresh and spent V/Nb catalyst samples with varying V$_2$O$_5$ loadings are shown in Figs. 3-2a and b. It is clear from Fig. 3-2a that no XRD reflections corresponding to crystalline vanadium oxides are present in the solid with 5 wt% V$_2$O$_5$ loading. This result implies that the vanadia is finely dispersed on the support and may also be present in X-ray amorphous form up to this loading. However, weak reflections belonging to V$_2$O$_5$ crystallites can be seen from 10 wt% V$_2$O$_5$ loading onwards. As expected, the intensity of these reflections is increasing with increase in V$_2$O$_5$ content of the solids. Another notable observation is that the intensity of the reflections corresponding to Nb$_2$O$_5$ support is decreased gradually with increasing concentration of vanadia in the catalysts, probably due to a masking effect owing to the increased coverage of V-oxides on niobia with increase in the content of vanadia. Similar such effect was also observed earlier on V$_2$O$_5$/TiO$_2$ (anatase) catalysts [95]. Comparing the XRD patterns of fresh solids with those of spent ones (cf. Fig. 3-2b); no considerable differences could be noticed between them in terms of phase composition and crystallinity.
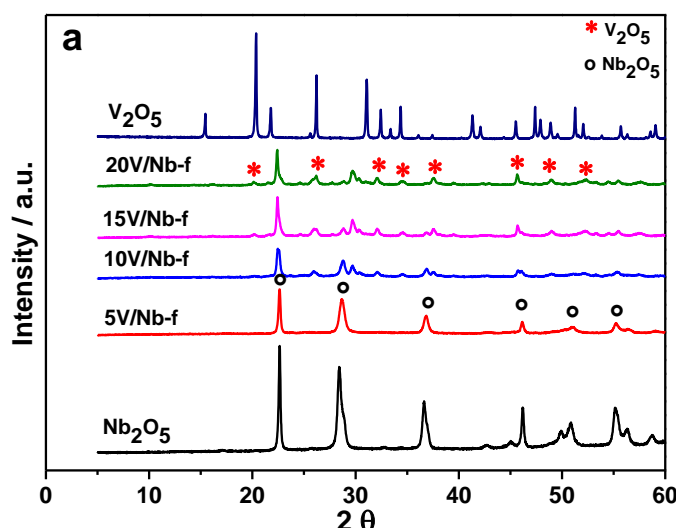
Fig. 3-2a. X-ray diffraction patterns of fresh V/Nb catalysts with varying V_2O_5 loadings (Nb_2O_5 and V_2O_5 patterns for comparison)
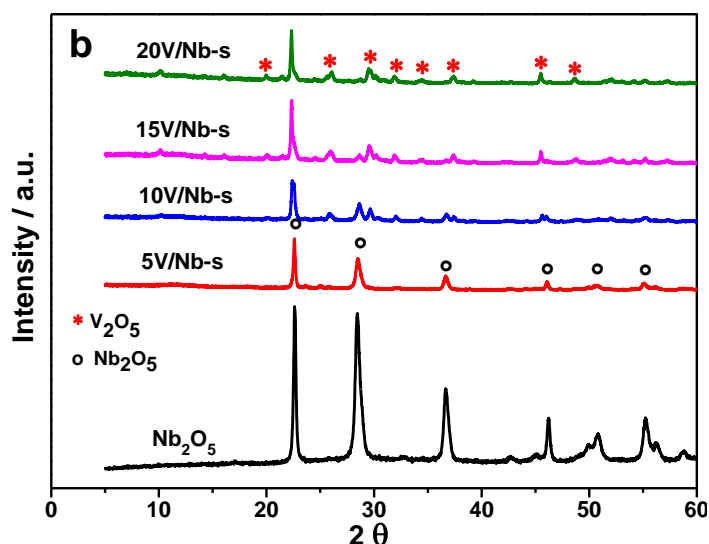

Fig. 3-2b. X-ray diffraction patterns of spent V/Nb catalysts with varying V_2O_5 loadings (Nb_2O_5 patterns for comparison)

3.2.3 UV-vis diffuse reflectance spectroscopy

UV-vis-DRS was used to elucidate the nature of various VO_x species in the present V/Nb catalysts. After high temperature calcination (600 °C) and with varying concentration of V_2O_5, different vanadium oxide species could be present in these catalysts in several VO_x structures such as isolated monomeric tetrahedral VO_4 species (O=V-(O-sup)$_3$) [96], one-dimensional polymeric surface species connected by V-O-V bonds in distorted tetrahedral coordination, two-dimensional polymeric species in octahedral coordination and bulk V_2O_5.

In general, UV-vis-DRS is a useful method to obtain information about the local geometry and bonding environment of the vanadium ions; with increasing coordination number a shift in the band position (oxygen to vanadium charge-transfer bands) to lower energy (higher wavelength) is expected [97, 98]. This technique also allows to distinguish tetrahedral and octahedral vanadium species. UV-vis spectra of the present V_2O_5/Nb_2O_5 fresh samples and the pure vanadia and niobia solids are illustrated in Fig. 3-3. The shape of 5V/Nb and 10V/Nb curves are similar, so as 15V/Nb and 20V/Nb. However, a red shift was observed with increasing V_2O_5 content. A visible shoulder appeared in particular in the higher loading catalysts (15V/Nb and 20V/Nb) at higher wavelength (>300 nm), which is due to the formation of higher concentration of oligomeric/polymeric VO_x species [99, 100]. To determine the structure of the vanadia species in more detail, the UV-vis spectra of all the samples have been deconvoluted. As a result, five bands (with Gaussian line shape) are obtained for each UV-vis spectrum of niobia supported vanadia samples (cf. Fig. 3-3). The three bands appeared in all the catalysts irrespective of V_2O_5 loading around 230, 250 and 280 nm are ascribed to isolated monomeric tetrahedral vanadium species [101]. The band at ca. 315 nm (cf. Fig. 3-3) is assigned to oligomeric distorted tetrahedral vanadium oxide species [97]. The intensity of this band is observed to increase with rise in V_2O_5 content. Additionally, a broad band at around 380 nm could be attributed to the aggregated vanadium entities in octahedral coordination. Two bands appeared above 400 nm only in case of pure V_2O_5, which are certainly due to the presence of bulk vanadium oxides. The comparison of the UV-vis spectra of all the catalysts clearly showed that the formation of oligomeric vanadium oxide species is increasing with rising vanadia content of the catalysts.

Unlike V_2O_5, the pure Nb_2O_5 shows all the bands (three bands) below 300 nm (see Fig. 3-3), which is in good agreement with those reported by Yan and Xue [102]. The appearance of bands below 300 nm (maximum intensity at 236 nm) might be due to formation of O-Nb_2O_5 (orthorhombic) phase [103], it can also be seen from the XRD pattern of Nb_2O_5, all peaks can be indexed to the orthorhombic Nb_2O_5 phase.
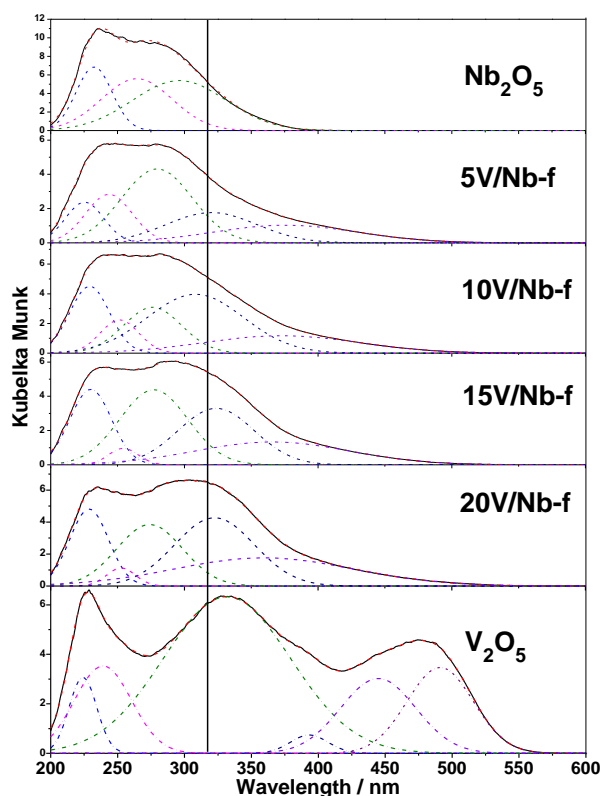
Fig. 3-3. **UV-vis-DR spectra of the fresh V/Nb catalysts with varying V₂O₅ loadings along with pure V₂O₅ and Nb₂O₅ (Measured: solid lines; Deconvoluted: dashed lines; vertical line at 315 nm points to oligomeric species peak maxima region)**

3.2.4 X-ray photoelectron spectroscopy

XPS analysis was performed to gain information about the oxidation state, surface composition as well as atomic ratios of the elements present in the near-surface-region of the catalysts due to shifts in the binding energies [104, 105, 106]. On the basis of the literature data [104, 107], the XPS V2p$_{3/2}$ peaks of the supported vanadia samples at 517.0 and 516.9 eV can be assigned to V^{5+} oxidation state considering the well-known variation of the binding energies of pentavalent vanadium in dependence of its environment. XP spectra of the present fresh and spent V₂O₅/Nb₂O₅ catalysts with varying V₂O₅ loadings are depicted in Figs.3-4a and b. XP spectra of all fresh solids show the presence of vanadium in +5 oxidation state. The value of Δ (i.e. the energy difference between the binding energy levels of O1s and that of V2p$_{3/2}$) also provides further indication that the vanadium is present in +5 oxidation state in all the fresh samples (cf. Table 3-2). In other words, the value of Δ remained almost constant at 12.7 eV irrespective of V₂O₅ content of the catalysts. Moreover, a shift in the binding energies with increasing V content towards higher

values could be observed, in particular for the spent samples (see Fig. 3-4b). A possible explanation could be given by different interactions between V and Nb. For the low V content of 5 wt%, this interaction should be more significant, e.g. the major part of V ions interacts with Nb ions, whereas for the higher loadings, the increased formation of oligomeric & polymeric VO_x species (V-O-V interactions) could be expected. However, no considerable shift in case of O1s peak is noticed particularly in the fresh samples with varying V_2O_5 contents (Fig. 3-4a). But such considerable shift towards higher binding energy value of O1s peak is observed with rise in vanadia content of the spent catalysts (Fig. 3-4b) indicating the formation of different types of oxygen species (probably some hydroxyl groups) in these spent solids by the influence of severe reaction conditions and reactant feed composition.
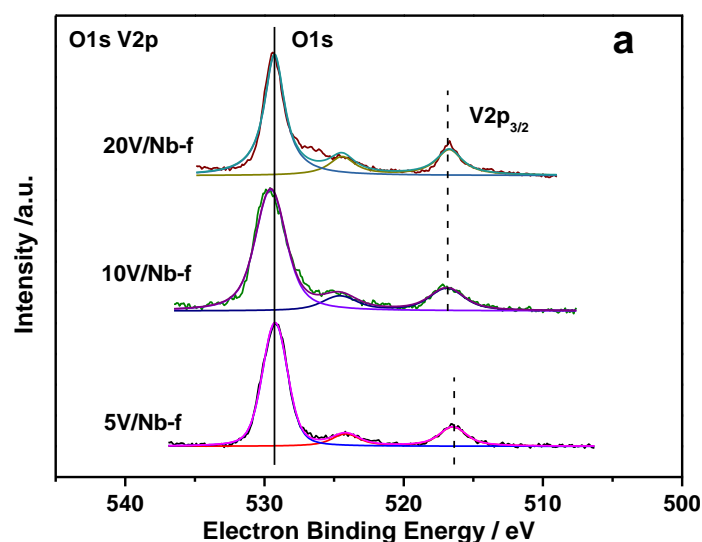

Fig. 3-4a. XP spectra of the fresh V/Nb catalysts with varying V_2O_5 loadings

Table 3-2

Result of XPS studies of V/Nb catalysts

Cat. Code	E O1s/eV	FWHM[1]	E V2p$_{3/2}$/eV	FWHM	Δ[2]
5V/Nb-f[3]	529.2	2.25	516.5	2.10	12.7
10V/Nb-f	529.6	2.81	516.9	2.45	12.7
20V/Nb-f	529.3	1.75	516.7	2.23	12.6
5V/Nb-s[4]	529.1	2.18	516.3	2.72	12.8
10V/Nb-s	529.7	1.80	517.0	2.18	12.7
20V/Nb-s	530.3	1.80	517.2	2.81	13.1

[1] FWHM is Full Width at Half Maximum; [2] Δ is the energy difference between O1s and V2p$_{3/2}$ peaks

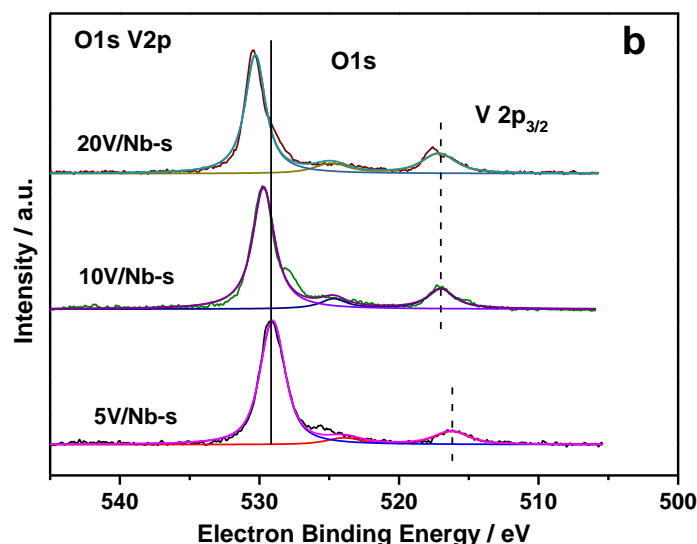[3] f—fresh catalyst, [4] s—spent catalyst

Fig. 3-4b.   XP-spectra of the spent V/Nb catalysts with varying V_2O_5 loadings

Fig. 3-5 compares the bulk (estimated by ICP) vs. near-surface (XPS) V/Nb ratios in both the fresh and spent solids. It is quite obvious from the figure that the V/Nb surface ratios of fresh samples are significantly higher than the corresponding bulk ratios showing a clear enrichment of vanadium in the near-surface-region independent on the V content. Such near-surface-region enrichment is much more pronounced in case of 5V/Nb and 10V/Nb catalysts compared to the highest loading catalyst (i.e. 20V/Nb). This is more likely due to the formation of different types of vanadium oxide species in these solids with varying V-contents as evidenced from UV-vis spectra. Such differences in the nature of near-surface VO_x species have shown clear impact on the catalytic performance. For instance, the amount of oligomeric VO_x species is somehow higher in 10 wt% than 5 wt% and hence this catalyst displayed superior catalytic performance as shown below. Coming to the highest loading (20V/Nb), this sample lacks pronounced surface enrichment of V and additionally it forms more polymeric type of VO_x species and is in the direction of bulk V_2O_5. In view of this, the 20V/Nb sample displayed inferior performance, which is however comparable to that of pure V_2O_5 (see below). It can also be seen clearly that both the V/Nb near-surface ratio and bulk ratio increased with increasing V_2O_5 loading, as expected.
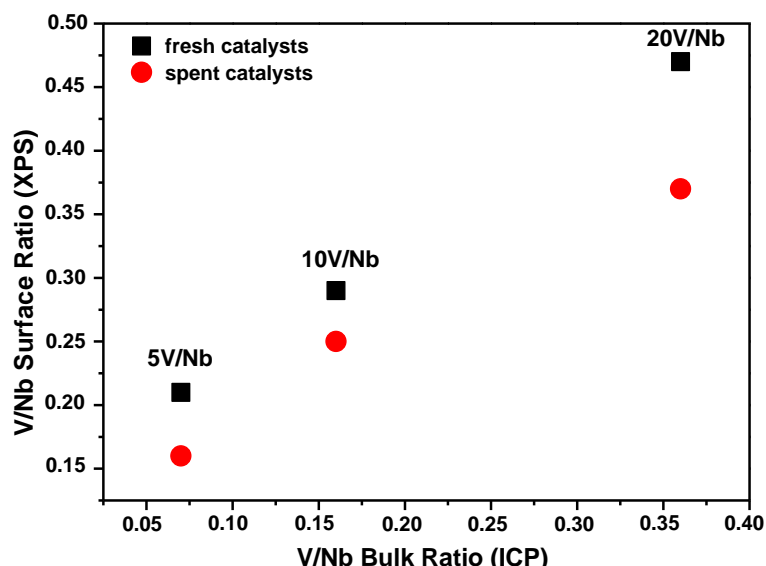
Fig. 3-5.   Comparison of bulk to near-surface-region V/Nb ratios for fresh and spent catalysts as a function of V$_2$O$_5$ loading

For the spent catalysts, the surface V/Nb ratios are slightly decreased compared to their corresponding fresh ones. Such decrease is more pronounced for the higher-loading catalyst. Possible reasons for this observation might be due to (i) the covering of a part of the V species by coke deposits, (ii) by the migration of V into the Nb support or (iii) the formation of larger three-dimensional polymeric VO$_x$ species. However, the formation of very low or almost no coke deposits in the spent catalysts was observed and hence we can exclude the first possibility of covering VO$_x$ species by coke. Especially, for the high V loading, the formation of bulk-like VO$_x$ species can be expected during time-on-stream. However, one should note that such decrease of V in the near-surface-region is not due to loss (leaching) of vanadium from the catalyst that is however evidenced from the ICP analysis of V-content in the spent solids. Careful observation of XPS and UV-vis-DRS results revealed that the near-surface enrichment of vanadium and the nature of VO$_x$ species formed in the catalysts play a key role on the catalytic performance.

3.3 Catalytic activity of V/Nb catalysts in the ODHE reaction

Figs. 3-6a and b depict the conversion of ethane and yield of ethylene as a function of V$_2$O$_5$ loading at three different reaction temperatures (500, 550 and 600 °C). Both the V$_2$O$_5$ loading and the reaction temperature have shown a strong influence on the conversion of ethane and yield of ethylene. The target product is ethylene while the by-products formed are only total oxidation products (i.e. CO$_x$).

With rise in reaction temperature, both the conversion of ethane and the yield of ethylene are commonly increased in every case irrespective of vanadia loading. As shown in Fig. 3-6a, the conversion of ethane has been increased with V$_2$O$_5$ loading up to 15 wt% and then decreased with further rise in V$_2$O$_5$ (cf. 20V/Nb). In other words, the conversion of ethane is increased from 22 to 31% and then decreased to 25%, when the comparison is made at the same reaction temperature of 600 °C. The behaviour of 20V/Nb solid is more or less comparable with that of pure V$_2$O$_5$ sample probably due to formation of similar type of VO$_x$ species in both the cases. The formation of different types of vanadia species that strongly depends on vanadia loading (cf. UV-vis results) seems to play a crucial role on the catalytic properties of the catalysts. In respect of the yield of ethylene (cf. Fig. 3-6b), it shows somewhat comparable tendency as that of conversion of ethane at all temperatures studied. The yield of ethylene progressively increased up to 10 wt% V$_2$O$_5$ loading, which remained at comparable level until 15 wt% V$_2$O$_5$ loading (despite increase in conversion at this loading) and then decreased considerably at higher V$_2$O$_5$ loadings. On the whole, the 10V/Nb catalyst at T = 600 °C displayed the best yield of 11% with no considerable coke formation after 9 hours-on-stream activity tests. Taking into account of UV-vis and XPS results, it can be explained that the enhanced performance of 10V/Nb solid is due to i) formation of higher amount of oligomeric distorted tetrahedral VO$_x$ species and ii) the presence of optimum amount of VO$_x$ species along with clear enrichment of vanadium in the near-surface-region.
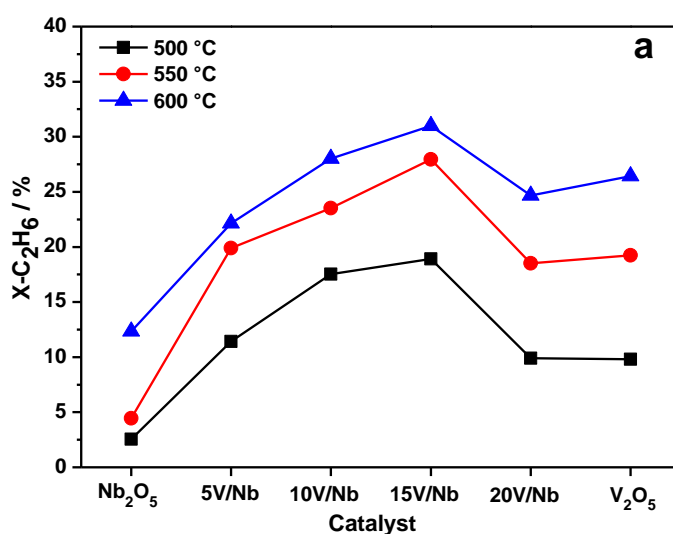

Fig. 3-6a. Influence of V$_2$O$_5$ loading on conversion of ethane (Reaction conditions: mole ratios: C$_2$H$_6$: O$_2$: N$_2$ = 1: 0.68: 2.65, GHSV = 3250 h^{-1}, 500-600 °C, τ = 1.1 s, cat.: 1 g)
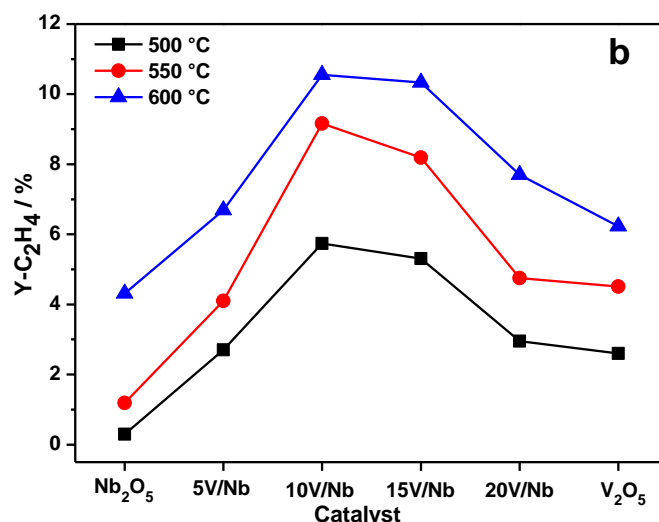
Fig. 3-6b. Influence of V$_2$O$_5$ loading on the yield of ethylene (Reaction conditions: mole ratios: C$_2$H$_6$: O$_2$: N$_2$ = 1: 0.68: 2.65, GHSV = 3250 h-1, 500-600 °C, τ = 1.1 s, cat.: 1 g)

As expected, pure Nb$_2$O$_5$ exhibited poor performance (X = 12% & Y = 4% at 600 °C), while the pure V$_2$O$_5$ also displayed relatively low conversion of ethane (22% at 600 °C) and low selectivity of ethylene (27%). The activity and selectivity of pure V$_2$O$_5$ is quite comparable with that of 20V/Nb catalyst (cf. Figs. 3-6a and b).

3.4 Summary and Conclusion

The catalytic activity and selectivity is found to depend strongly on the nature of vanadium oxide species and the surface enrichment of vanadium in the near-surface-region. These two properties in turn unquestionably depend on the content of vanadium in the catalysts. At low V$_2$O$_5$ loading (≤10 wt%), monomeric & oligomeric VO$_x$ species were formed while more polymeric species were found similar to bulk V$_2$O$_5$ sample at higher loadings as shown by UV-vis-DRS studies. XPS revealed that pronounced enrichment of vanadium occurs in the near-surface-region in the samples with low vanadia contents. Among all the catalysts, 10 wt% V$_2$O$_5$ on Nb$_2$O$_5$ has given the best catalytic performance with no considerable coke formation after 9 hours on-stream.

4. ODHE to ethylene over supported V_2O_5 catalysts: The effect of the nature of alumina support on the catalytic performance

Chapter 4 deals with the evaluation of the data obtained from catalytic performance tests over different alumina supported vanadia catalysts. The catalytic performance of those catalysts is discussed with respect to the results of several characterization methods such as N_2-physisorption, ICP, UV-vis, XRD, XPS, Py-FTIR, TEM in detail.
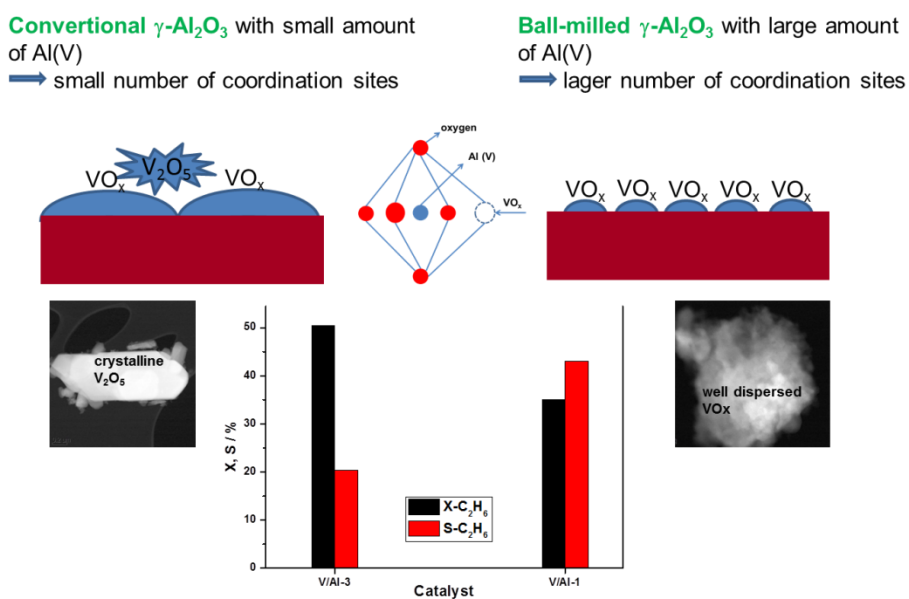
4.1 General studies on the effect of different types of Al_2O_3 supports on the properties of supported V_2O_5 catalysts

A series of V_2O_5/Al_2O_3 catalysts with fixed content of V_2O_5 (10 wt%) but different types of Al_2O_3 supports with varying surface areas were prepared by impregnation technique and tested for the oxidative dehydrogenation of ethane (ODHE) in a fixed bed quartz reactor in the temperature range from 500 to 600 °C. The nature of the Al_2O_3 source revealed a significant influence on the catalytic performance of the solids. Among all catalysts investigated, high surface area γ-alumina based catalyst showed the best performance in ODHE due to the high dispersion of vanadia species over the support surface. Otherwise, low surface area α-Al_2O_3 but also γ-Al_2O_3 supported catalysts exhibited high ethane conversion but low selectivity to ethylene because of the existence of bulky V_2O_5 particles. In addition, a recently described low-surface area alumina containing a high amount of penta-coordinated Al sites was included in the study. This special alumina supported V_2O_5 catalyst displayed a quite good performance in ODHE despite its small surface area. Such behaviour can be ascribed mainly to the presence of penta-coordinated Al surface sites acting as anchors for preferentially monomeric and low-oligomeric VO_x species leading to a prime dispersion.

4.2 Characterization of V_2O_5 catalysts supported on different type of Al_2O_3

4.2.1 BET-surface area and solid composition

Surface areas, vanadium contents and bulk as well as near-surface-region elemental analysis data of V/Al-x catalysts are presented in Table 4-1. Interestingly, the BET-SA of fresh V/Al-1-f is significantly increased compared to its parent pure support (i.e. from 5.8 to 18.3 m^2/g), while the surface area decreased in other cases. The increase in surface area of V/Al-1-f might be due to the reformation of a part of the γ-Al_2O_3 into the γ-AlO(OH) phase due to the contact with the water during the course of its preparation by wet impregnation method and drying at elevated temperatures afterwards where the reformation probably takes place. Düvel et al. [62] investigated the phase transformation of γ-Al_2O_3 into α-Al_2O_3 by means of high-energy ball-milling. The authors followed the progress of this transformation by 27Al MAS NMR spectroscopy at high magnetic field (17.6 T) and claimed the formation of

a high fraction (20%) of unsaturated penta-coordinated Al ions that may act as anchoring sites for catalytically active materials [62]. By comparing the surface areas between fresh and spent samples, one can notice that the surface areas are not significantly altered in the spent solids compared to their corresponding fresh ones.

Additionally, the contents of V_2O_5 estimated in all the catalysts from ICP are in good agreement with those of nominal values (cf. Table 4-1). Moreover, the near-surface-region V/Al ratios obtained from XPS measurements are significantly higher than that of bulk V/Al ratios calculated from ICP results indicating a clear enrichment of VO_x species in the near-surface-region of catalysts irrespective of the type of alumina support used. The bulk V/Al ratios are more or less the same between fresh and spent catalysts within experimental errors. However, with an exception of V/Al-2-s, the near-surface-region V/Al ratios were observed to be decreased for spent catalysts compared to that of fresh catalysts, i.e. vanadium species moved downwards into the bulk. In case of V/Al-2-s, the originally present large VO_x particles on the low-surface area α-Al_2O_3 sample could be redispersed in the course of the high ODHE temperature causing a higher near-surface-vanadium concentration in the spent sample.

Table 4-1

The physical characteristics of the catalysts and different type of alumina support

Cat. Code	BET-SA / m²/g			V_2O_5 / wt%		V/Al (ICP)		V/Al (XPS)	
	fresh	spent	support[a]	nominal	ICP[b]	fresh	spent	fresh	spent
V/Al-1	18.3	17.9	5.8	10.0	10.3	0.07	0.08	0.32	0.22
V/Al-2	5.0	4.5	5.2	10.0	10.9	0.13	0.10	0.25	3.12
V/Al-3	79.1	57.5	102	10.0	9.7	0.06	0.07	0.39	0.17
V/Al-4	181.9	161.8	201	10.0	10.0	0.06	0.07	0.27	0.09
V/Al-5	258.5	191.5	294	10.0	12.3	0.08	0.09	0.13	0.12

[a] corresponding to different type of alumina support

[b] measured by ICP-OES

4.2.2 Thermo gravimetric analysis (TGA)

The TGA curves of the oven dried V/Al-x-od samples are depicted in Fig. 4-1. It is clear that the weight loss is depending upon the nature of the alumina support applied. The α-Al_2O_3 supported catalyst (V/Al-2) has shown the lowest weight loss (ca. 8%) while the V/Al-5 with the highest surface area γ-Al_2O_3 showed the highest weight loss (ca. 30%). The weight loss occurs primarily in two steps: the first one (<200 °C) corresponds to the removal of physically adsorbed water, dehydroxylation of catalyst surface and also partly to the initial decomposition of NH_4VO_3 (AMV), which starts at 175 °C. According to Tang et al. [108], the conversion of AMV into V2O5 runs in three steps such as i) AMV changes first to $(NH_4)_2V_4O_{11}$ at ca. 175 °C, ii) transformation to $(NH_4)V_3O_8$ in the second step at around 220 °C and iii) final formation of V_2O_5 in the third step at 350 °C and even higher for total transformation. The second and major weight loss occurs in the temperature range from >200-400 °C due to the decomposition of ammonium metavanadate and its further transformation into X-ray-amorphous and/or crystalline VOx species (V_2O_5 phase, probably) according to the changes described above. In the case of high surface area γ-Al_2O_3 support, this major weight loss is extended up to 450 °C, where a maximum weight loss (~30%) is recorded. However, no further weight loss is observed beyond 450 °C. This result also indicates the good thermal stability beyond 450 °C and particularly under the applied reaction conditions. Based on this observation, and also considering the reaction temperature range, the calcination temperature of these catalysts is fixed at 600 °C.
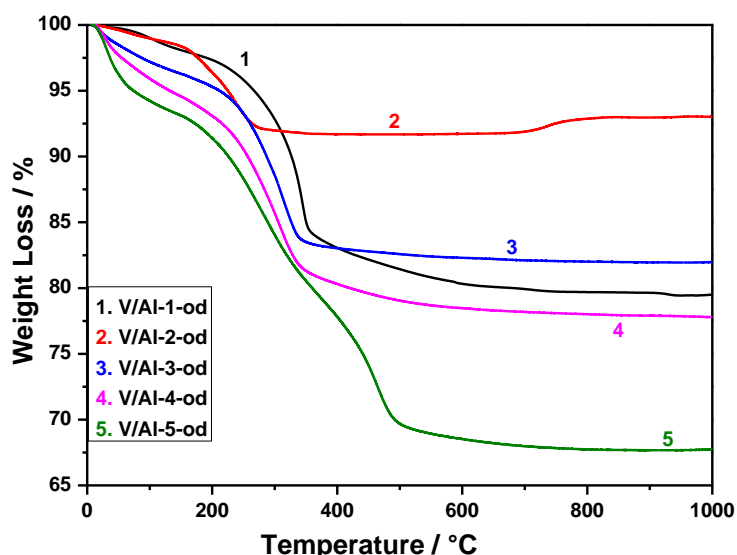
Fig. 4-1. TGA curves of the oven dried supported vanadia catalysts using different types of alumina

4.2.3 X-ray diffraction

The XRD patterns of the fresh and spent catalysts are shown in Figs. 4-2a and 4-2b. It is clear from Fig. 4-2a that no reflections corresponding to crystalline V_2O_5 phase are present in the γ-alumina supported catalysts, while clearly distinct crystalline reflections belonging to larger V_2O_5 crystallites could be seen in the case of V/Al-2-f (i.e. α-Al$_2$O$_3$ supported catalyst). This result implies that the vanadia is finely dispersed on the γ-alumina supports but V_2O_5 crystallites can be seen only in the α-alumina supported catalyst due to its lower specific surface area.
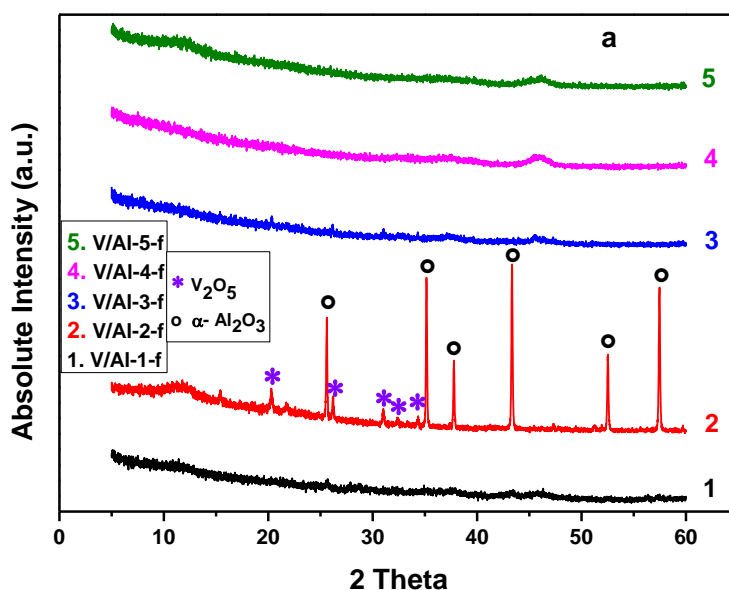

Fig. 4-2a. X-ray diffraction patterns of fresh supported vanadia catalysts using different types of alumina
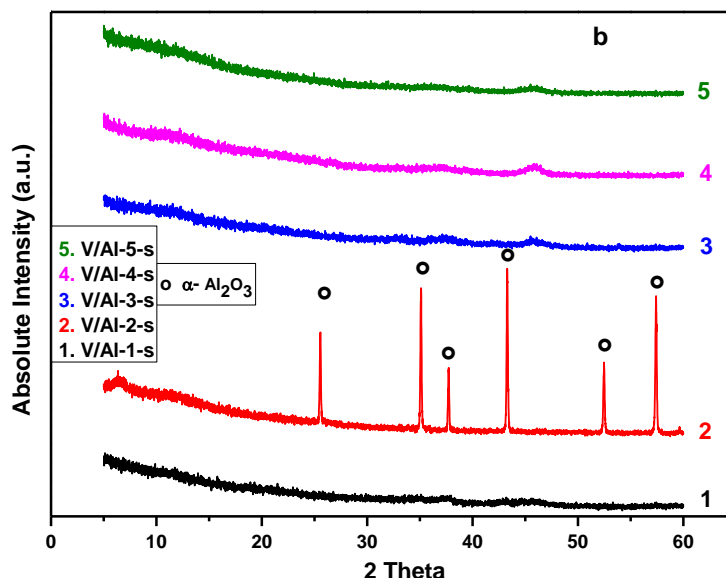
Fig. 4-2b. X-ray diffraction patterns of fresh supported vanadia catalysts using different types of alumina

Another notable observation is that the reflections corresponding to V_2O_5 disappeared in the spent catalyst (V/Al-2-s), probably due to redispersion or reduction of V^{5+} species during the course of the reaction. These results are also backed by the inspection of the near-surface region showing a dramatically increased V/Al ratio (cf. Table 4-1). Comparing the XRD patterns of the four fresh γ-alumina supported catalysts with those of spent ones, no considerable differences could be noticed in terms of phase composition and crystallinity.

4.2.4 UV-vis diffuse reflectance spectroscopy

UV-vis was used to obtain information on the nature of the VOx species formed in the present V/Al catalysts. After high temperature calcination (600 °C), the vanadium oxide species could be present in these catalysts in several VOx structures such as isolated monomeric tetrahedral VO_4 species (O=V-(O-sup)$_3$), one-dimensional polymeric surface species connected by V-O-V bonds in distorted tetrahedral coordination, two-dimensional polymeric species in octahedral coordination and bulk V_2O_5 [96].

UV-vis diffuse reflectance spectra of V/Al-x-f fresh samples plus that of pure bulk V_2O_5 for better comparison are illustrated in Fig. 4-3a. It seems that V/Al-1-f revealed a high proportion of the monomeric VOx species. Compared to the V/Al-1-f sample, a red shift was observed in case of the other four catalysts, which is more

pronounced in case of the V/Al-2-f and V/Al-3-f samples compared to the V/Al-4-f and V/Al-5-f solids. This shift in the band position (oxygen to vanadium charge-transfer bands) to lower energy (higher wavelength) indicated the increasing coordination number of the vanadia species [97, 98]. In addition, a visible shoulder appeared in the spectrum of the V/Al-2-f solid (α-Al$_2$O$_3$ supported) at 350 nm and higher wavelength 475 nm, which is due to the formation of a higher concentration of the oligomeric/polymeric VO$_x$ species as well as aggregated vanadia species in octahedral coordination. The existence of these species is due to the presence of larger crystallites as identified by XRD.
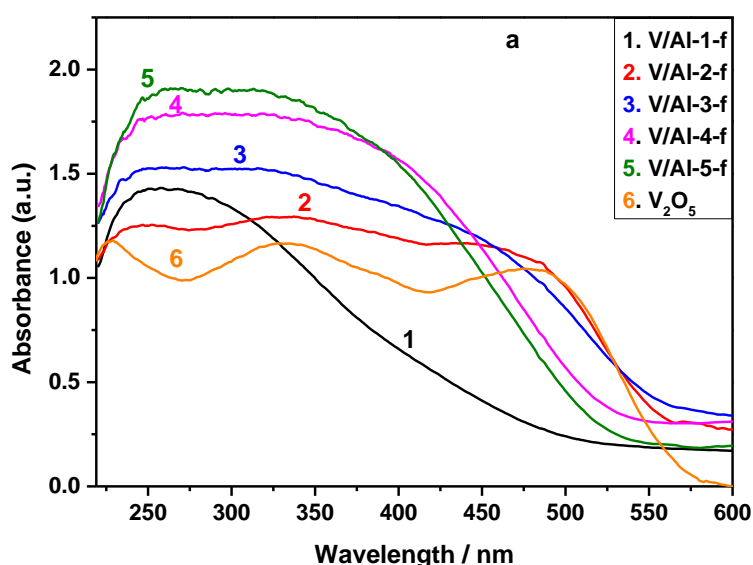

Fig. 4-3a. UV-vis spectra of the fresh supported vanadia catalysts using different types of alumina along with pure V$_2$O$_5$

The UV-vis spectra have been deconvoluted to several bands with Gaussian line shape (Fig. 4-3b) to determine the structure of the vanadia species in more detail. With the exception of V/Al-2-f, all these deconvoluted bands exclusively appeared below 400 nm irrespective of the type of alumina support. This result revealed the formation of monomeric (<300 nm) and polymeric/oligomeric VO$_x$ species (between 300-400 nm) in these solids [109]. There was one additional band which appeared at 475 nm only in case of V/Al-2-f sample, indicating the presence of bulk V$_2$O$_5$ as already stated above. The UV-vis spectrum of the V/Al-2-f sample is quite similar to that of a pure V$_2$O$_5$ sample indicating the formation of a similar type of VO$_x$ species in both the cases.

It is clear that the formation of oligomeric vanadium oxide species is decreasing in the following order V/Al-2-f > V/Al-3-f > V/Al-4-f > V/Al-5-f > V/Al-1-f. With the exception of V/Al-1-f, the decreasing tendency was found to be in opposite direction with the BET-SA value. The unique vanadia dispersion of V/Al-1-f might be attributed to the modified structure of γ-Al$_2$O$_3$ support containing unsaturated penta-coordinated Al ions, which might act as efficient anchoring sites for active species such as VO$_x$ in this study preventing the formation of larger vanadia units.
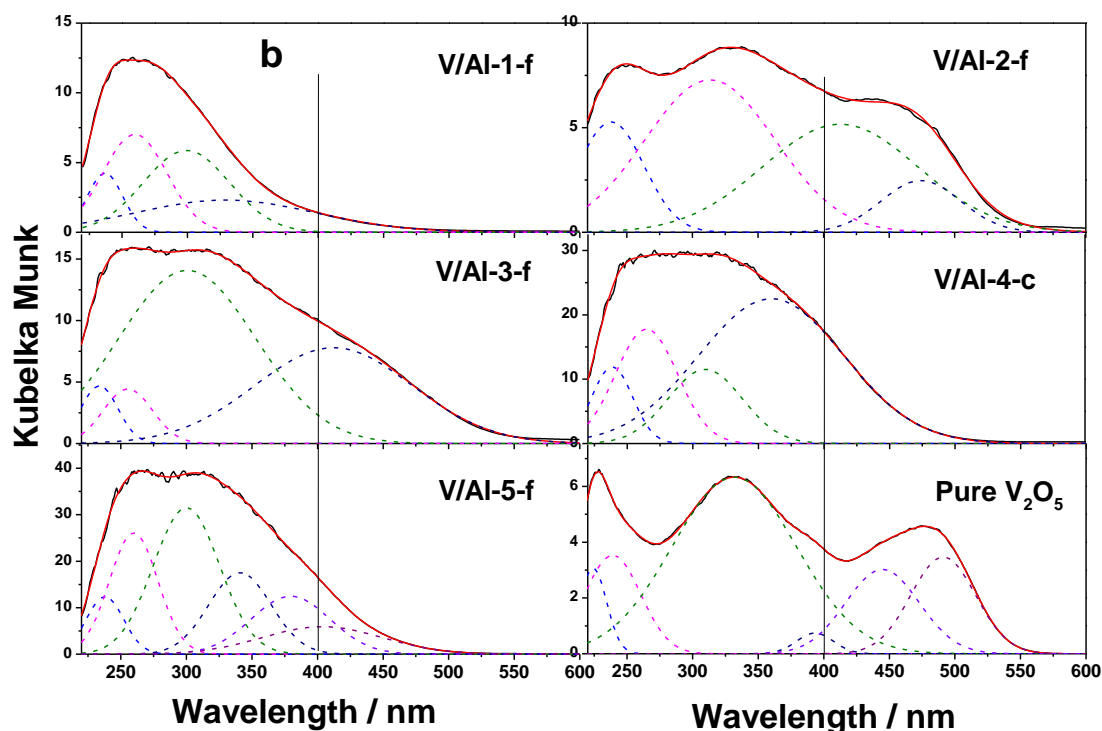

Fig. 4-3b. **Deconvoluted UV-vis spectra of the fresh V/Al-x catalysts along with pure V$_2$O$_5$ (Measured: solid lines; Deconvoluted: dashed lines; vertical line at 400 nm points to oligomeric species peak maxima region).**

4.2.5 X-ray photoelectron spectroscopy

XPS analyses were performed to gain information about the oxidation state and the chemical composition of the near-surface-region as well as their atomic ratios [105, 106]. The results of the fresh and spent alumina supported vanadia catalysts are depicted in Figs. 4-4a and b. In addition, the value of Δ (i.e. the energy difference between the binding energy of the O1s level and that of V2p$_{3/2}$) is also given. The results show the presence of vanadium in +5 oxidation state in all fresh solids with evidence of V2p$_{3/2}$ peaks located at 517.0 eV (Fig. 4-4a) [21, 107]. Moreover, the value of Δ that varies between 13.2 eV to 13.6 eV also provides further indication that

the vanadium is present in +5 oxidation state in all the fresh samples. On the other hand, the intensity of the peak corresponding to V2p$_{3/2}$ decreased particularly in the spent γ-Al$_2$O$_3$ supported solids compared to their corresponding fresh samples. In contrast, the spent α-Al$_2$O$_3$ supported catalyst (V/Al-2-s) revealed an increased intensity of the V2P$_{3/2}$ peak. This result is probably due to a redispersion of larger V$_2$O$_5$ crystallites into smaller units reflecting a higher near-surface concentration. The V/Al ratio also increased due to covering of the initially "free" alumina surface by vanadia species (cf. Table 1). Besides this, there was also a considerable increase in the value of Δ of spent V/Al-1-s and V/Al-3-s solids compared to their corresponding fresh ones (Fig. 4-4b). It was reported by Mendialdua et al. [107] that the decreased degree of oxidation could be correlated to larger values of the binding energy difference. Therefore the vanadia species might be reduced from V^{5+} in fresh catalysts to V^{+4} in spent catalysts especially on the surface of spent V/Al-1-s catalyst with a Δ value of 14.4 eV, which is typical for VO$_2$ [107, 110].
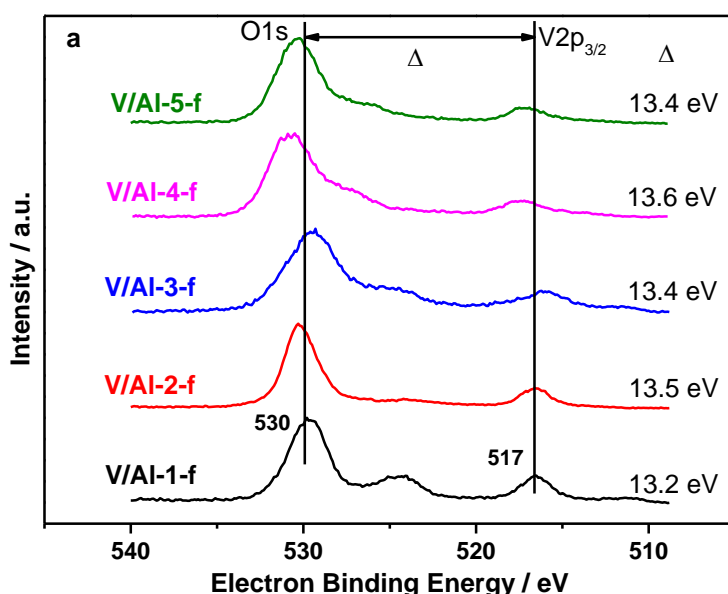

Fig. 4-4a. XP spectra of the fresh supported vanadia catalysts using different types of alumina
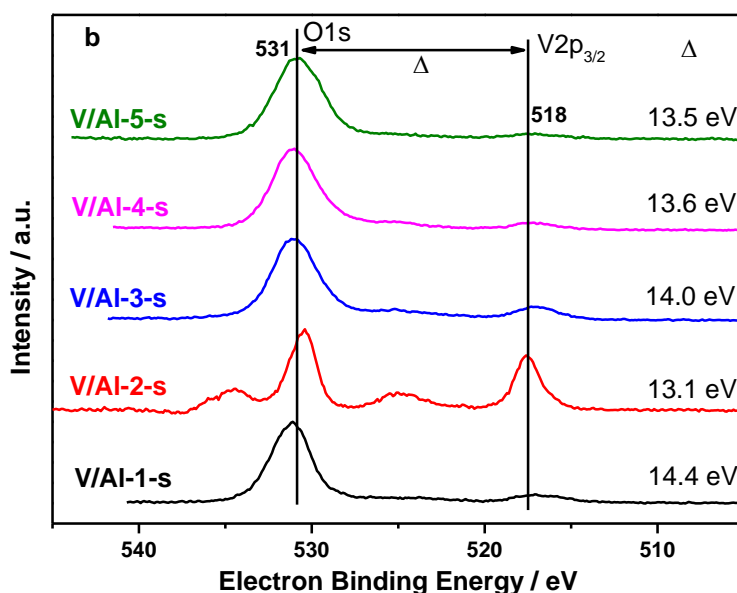
Fig. 4-4b. XP spectra of the spent supported vanadia catalysts using different types of alumina

4.2.6 Pyridine Fourier transform infrared spectroscopy (Py-FTIR)

The results of the Py-FTIR analyses are displayed in Fig. 4-5a. In general, the typical bands from pyridine adsorption related to Lewis acid sites (L-Py, LS) can be observed at around 1450 cm^{-1} and in the region 1625-1600 cm^{-1}, while the presence of Brønsted acid sites (PyH+, BS) can be seen from the appearance of a band at 1540 cm^{-1} [e.g. 111]. As expected, there was almost no adsorption of pyridine at the V/Al-2-f sample indicating the absence of both BS and LS. However, the Py-FTIR spectra of all other four γ-alumina supported catalysts revealed the presence of both LS and BS. Interestingly, the LS are dominating in all the samples irrespective of the type of support used. Among all, from the intensity of the band at 1450 cm^{-1}, it appears that the V/Al-5-f sample consists of high amount of Lewis sites, while V/Al-2-f exhibits the lowest proportion.
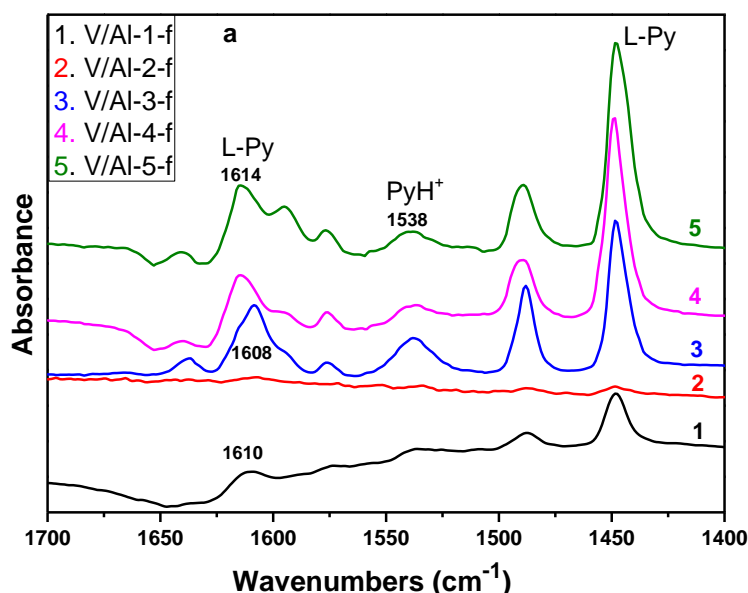
Fig. 4-5a. Py-FTIR spectra of fresh V/Al-x catalysts

Additionally, the integral intensity of BS and LS as well as the LS-to-BS ratio were depicted in Fig. 4-5b, where integral intensities of the characteristic bands at 1538 cm-1 for BS and 1448 cm^{-1} for LS are normalized to the BET surface area of the corresponding samples. Both the Brønsted and Lewis acidity of V/Al-x-f catalysts are varied with changing the nature of alumina support. The V/Al-1-f and V/Al-3-f catalysts showed comparable Brønsted acidity higher than that of V/Al-4-f and V/Al-5-f samples, which possessed the same Brønsted acidity. The Lewis acidity of all alumina supported vanadia catalysts is much higher than their Brønsted acidity. In terms of integral intensity ratio of Lewis acid to Brønsted acid, it decreased in the following order: V/Al-3-f < V/Al-1-f < V/Al-5-f < V/Al-4-f. This difference in concentration of LS and BS in turn shows clear differences on the performance of different V/Al-x catalysts in ethylene formation via ODHE reaction.
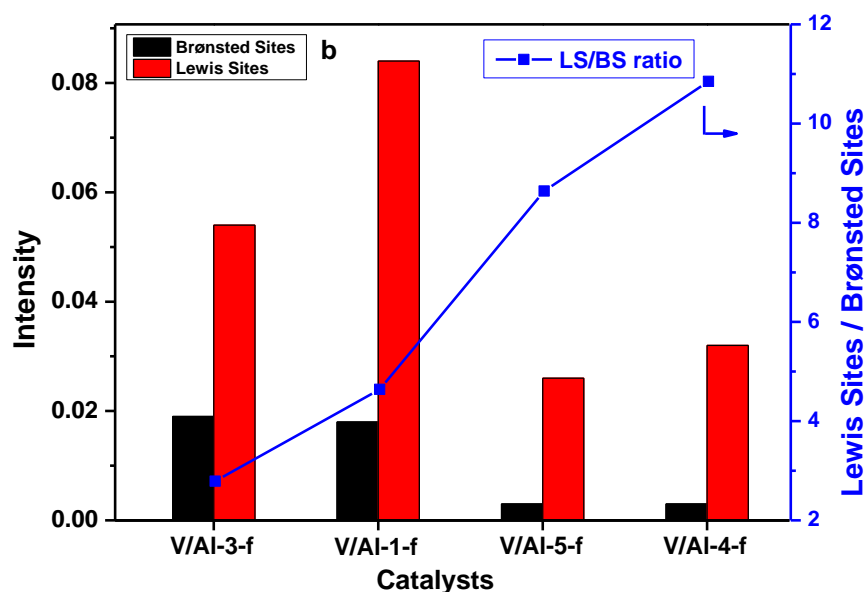
Fig. 4-5b. Comparison of the number of Brønsted and Lewis acid sites and LS/BS intensity ratio on the surface of the fresh V/Al-x catalysts.

4.2.7 Transmission electron microscopy (TEM)

Fig. 4-6 depicts some micrographs of three typical alumina supported vanadia catalysts. The TEM analyses showed that the nature of the alumina support determines the morphology, composition and size of vanadium species and their distribution over the support. The vanadium oxides formed are uniformly distributed over the surface of the support in case of V/Al-1-f sample (Fig. 4-6a). Obviously no larger particles can be seen even in 10 nm scale. Moreover, the V/Al atomic ratios are found to be mostly uniform and remain at 1: 1. Otherwise, it could be clearly seen from Fig. 4-6b (300 nm scale) that highly aggregated vanadium oxide particles were formed in case of sample V/Al-3-f. The VOx particle morphology and its composition were observed completely different from the V/Al-1-f sample. Here in this V/Al-3-f sample, we found a plate-like morphology for the VOx particles and also the composition was sometimes V-rich (i.e. V: Al = 1: 0.01) and sometimes Al-rich (i.e. V: Al = 1: 11) pointing to a not homogeneous distribution of VOx species. This result is mainly due to the small BET-SA leading to a V-rich region containing bigger vanadia particles. These seem to be responsible for the high activity in ethane conversion and low selectivity to ethylene obtained on this catalyst as discussed below. Fig. 4-6c depicts the morphology and composition of the V/Al-5-f catalyst (30 nm scale). It is obvious from the electron micrograph that the deposited vanadia is nicely distributed on the surface of the support. In most regions, the composition of V and Al are

remained unchanged and very uniform, i.e. a V/Al ratio of 1: 8-16 was found constant throughout. This highly distributed vanadia species could be related to the higher ethylene selectivity in ODHE reaction over such V/Al-5-f catalyst.
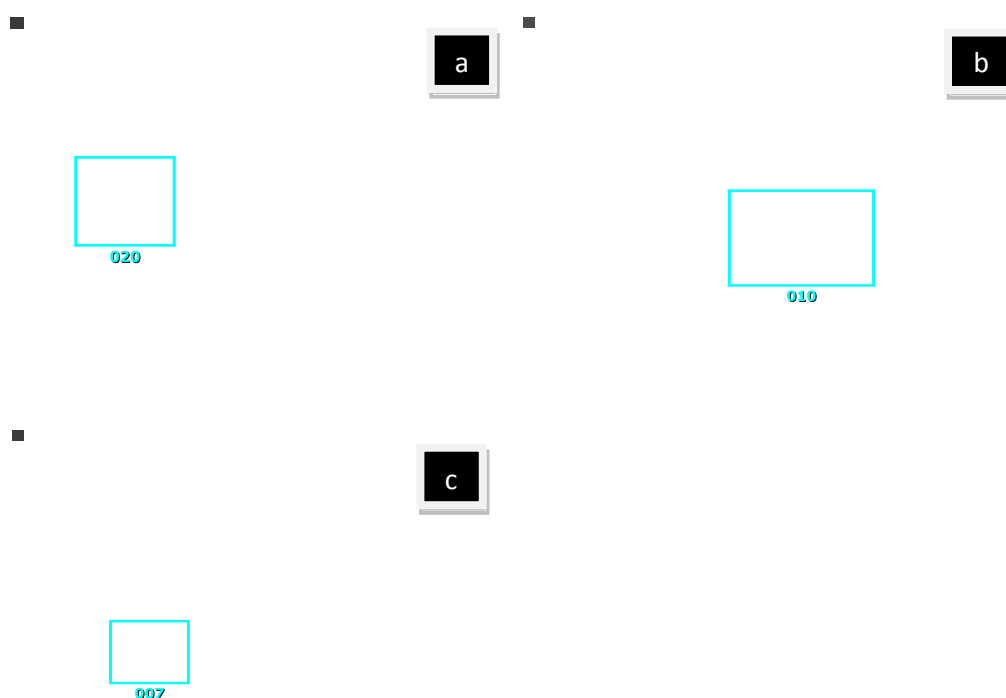

Fig. 4-6.   TEM images of fresh V/Al-1-f (a), V/Al-3-f (b) and V/Al-5-f (c) samples (the given V/Al ratios belong to the marked square areas).

The STEM-EDX mapping results provided more visible information on the morphology of V/Al-x samples. It can be seen from Fig. 4-7a that on the region I of V/Al-3-f catalyst there are less traces of Al, it is an intermixed V and O, both homogeneous in elemental distribution the whole particle area, gives hints to the formation of big size of vanadium oxide species in this V rich region (I). In the region II Al rich particles exists. Figs. 4-7b depicted the STEM-EDX mapping results of V/Al-5-f catalysts and indicated that vanadia species are well dispersed in this alumina support probably due to the high surface area.
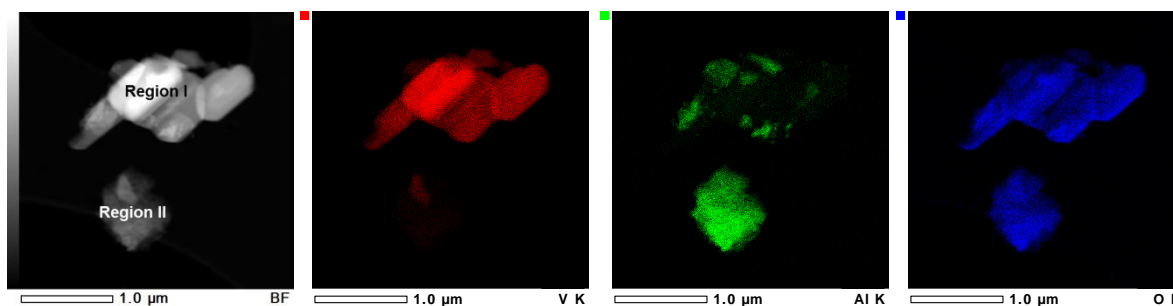
Fig. 4-7a. i)HAADF-STEM image, ii)V-K, iii)Al-K, iv)O-K EDXS elemental maps of V/Al-3 catalyst
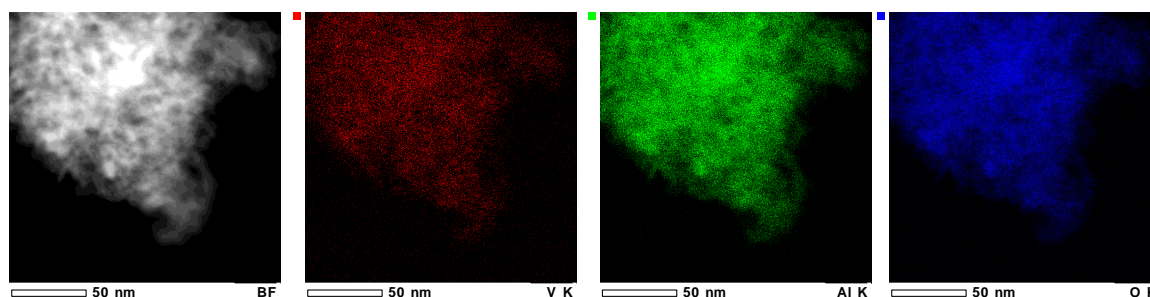

Fig. 4-7b. i)HAADF-STEM image, ii)V-K, iii) Al-K, iv)O-K EDXS elemental maps of V/Al-5 catalyst

4.3 Catalytic activity of V/Al catalysts in the ODHE reaction

Fig. 4-8a depicts an increasing ethane conversion with temperature over supported V/Al-x-f catalysts in the ODHE, as expected. The nature of alumina has shown a visible influence on the catalytic performance. Quite interestingly, V/Al-1-f solid displayed a reasonably good performance despite its low surface area. Such promotional effect of this particular alumina can be ascribed to the presence of a high amount of coordinatively unsaturated Al sites in this support. In contrast, the V/Al-2-f and V/Al-3-f catalysts showed highest ethane conversion. This higher activity was probably due to the presence of crystalline vanadium pentoxide species, which were aggregated in the V-rich regions of the V/Al-3-f catalyst as evidenced by the TEM analysis. To support this view, the XRD patterns showed the presence of reflections belonging to V_2O_5 crystallites only in case of the V/Al-2-f catalyst. Moreover, the UV-vis results also revealed the formation of bulk vanadia species in V/Al-2-f sample responding to its higher activity in ethane conversion. With respect to the other three γ-Al_2O_3 (V/Al-1-f, V/Al-4-f, V/Al-5-f) supported vanadia catalysts, on the basis of different characterization techniques, it could be concluded that monomeric with little portion of polymeric vanadium oxide spices were mainly formed and well dispersed in

these three γ-Al_2O_3 supported vanadia catalysts. These types of highly dispersed vanadia species play a crucial role on selectivity to ethylene at the expense of ethane conversion. In addition, the geometry and the structure of the Al_2O_3 support also seem to play an important role on the formation of V-oxide nanostructures and thereby catalytic properties as well. To be brief, in α-Al_2O_3, the Al-ions are octahedrally coordinated by oxygen while in the γ-Al_2O_3 phase the Al-ions are distributed among tetrahedral and octahedral sites [62]. Such differences in the structure of parent Al_2O_3 support can show considerable influence on the formation and distribution of VO_x species after impregnation of V-precursor on to the Al_2O_3 surface. Subsequently the nature of VO_x species formed certainly affect the activity and selectivity properties to a large extent.
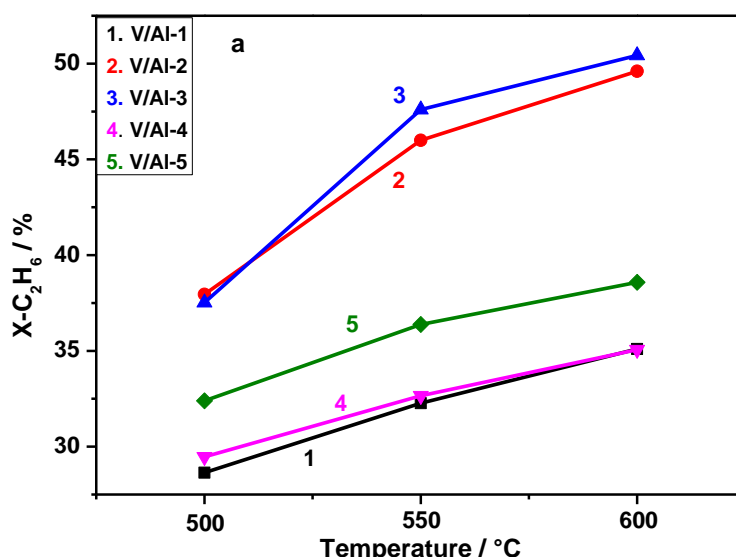

Fig. 4-8a   Ethane conversion as a function of temperature in the ODH of ethane over V/Al-x catalysts (conditions: C_2H_6: O_2: N_2=1: 0.7: 2.7; GHSV= ~3250-3270 h^{-1}; τ= 1.1 s; T= 500-600 °C)

Fig. 4-8b displays the selectivity to ethylene; V/Al-2-f and V/Al-3-f catalysts, which showed highest ethane conversion, gave the lowest ethylene selectivity compared with the other three γ-Al_2O_3 supported catalysts. The V/Al-4-f catalyst revealed the highest ethylene selectivity, which showed the highest integral intensity ratio of Lewis acid sites to Brønsted acid sites. It can be deduced from careful observation that the ethylene selectivity was increased in the order of V/Al-2-f < V/Al-3-f < V/Al-1-f < V/Al-5-f < V/Al-4-f which is in line with the integral intensity ratio values of LS to BS in V/Al-x-f catalysts (cf. Fig. 4-8c). It can be assumed that the

concentration of LS and BS of alumina supported vanadia catalysts showed a promotional effect on the selectivity of ethylene.
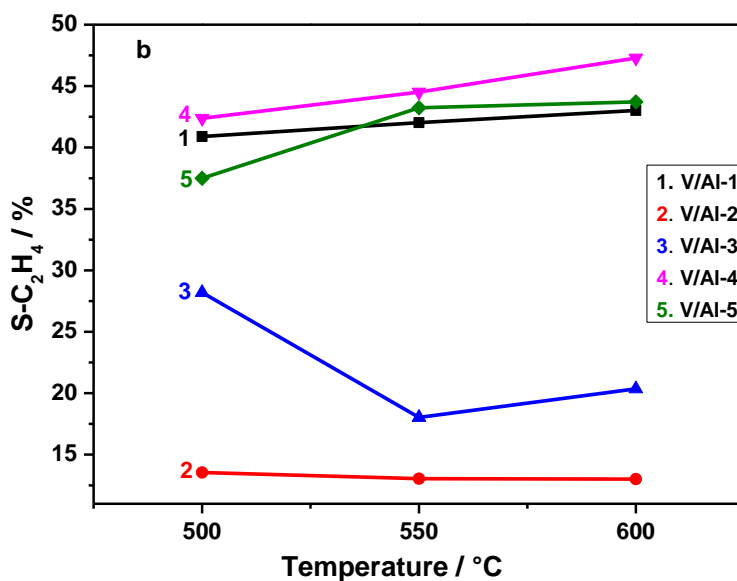

Fig. 4-8b **Ethylene selectivity as a function of temperature in the ODH of ethane over V/Al-x catalysts (conditions: C_2H_6: O_2: N_2=1: 0.7: 2.7; GHSV= ~3250-3270 h^{-1}; τ= 1.1 s; T= 500-600 °C)**
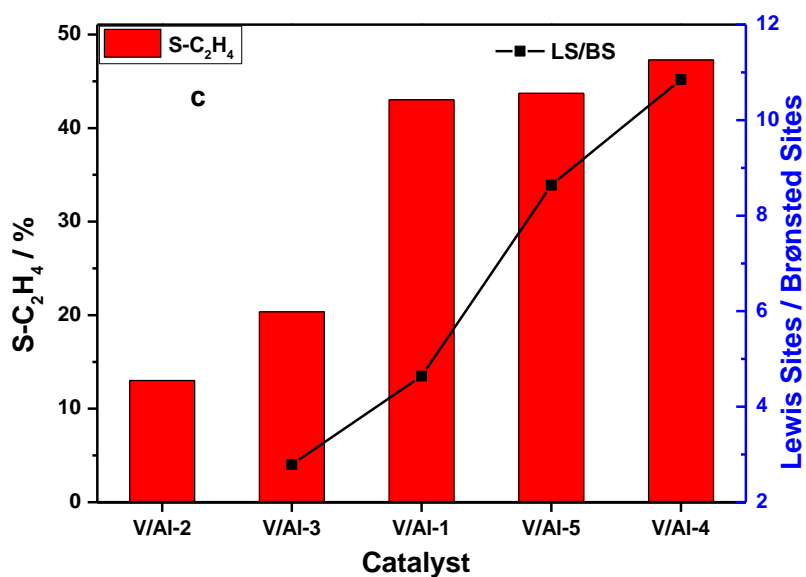

Fig. 4-8c. **Influence of LS to BS ratio on selectivity to ethylene in the ODHE reaction over V/Al-x catalysts (conditions: C_2H_6: O_2: N_2 = 1: 0.7: 2.7; GHSV= ~3250-3270 h^{-1}; τ= 1.1 s; T= 600 °C)**
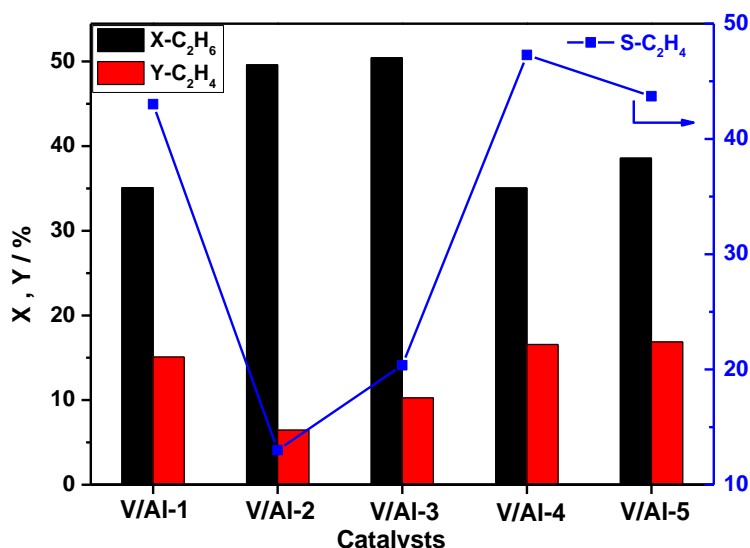
Fig. 4-9. **Comparison of catalytic performance of different V/Al-x catalysts at 600 °C (conditions: C_2H_6: O_2: N_2=1: 0.7: 2.7; GHSV= 3270 h-1; τ= 1.1 s)**

Fig. 4-9 compares the best activity performance of each V/Al-x-f catalyst at 600 °C. Among all aluminas investigated, it can be clearly seen that the γ-Al_2O_3 containing a high amount of penta-coordinated Al sites (V/Al-1-f) displayed a surprisingly enhanced performance compared to V/Al-2-f (α-Al_2O_3 support, BET-SA: 5.2 m^2/g) and V/Al-3-f (γ-Al_2O_3 support, BET-SA = 102 m^2/g), but quite comparable performance to the two other γ-Al_2O_3 supports with BET surface areas of 201 m^2/g and 294 m^2/g, respectively. The V/Al-1-f catalyst exhibited an ethane conversion of 34.1% and ethylene yield of 15.4%, respectively, being close to the values seen for V/Al-5-f. The catalytic performances of V/Al-4-f and V/Al-5-f solids are probably related to the well distributed monomeric and oligomeric vanadia species caused by the higher surface area of the parent supports.

4.4 Conclusions

The nature of the alumina support used has shown a substantial influence on the type of the VO_x species formed their dispersion, acidity characteristics, morphology as well as surface composition. The characterization results revealed that the fresh V/Al-x-f catalysts are quite stable in the reaction temperature range from 500 to 600 °C. XRD reflections corresponding to V_2O_5 could only be seen in the case of the α-alumina supported V/Al-2-f sample due to its lowest surface area and poor dispersion compared with the other samples. UV-vis deconvolution and TEM

images also gave hints on the existence of bulk V_2O_5 species in the V/Al-2-f catalyst. It can also be concluded that the loaded vanadium oxide species were well dispersed on the V/Al-1-f, V/Al-4-f and V/Al-5-f catalysts. XPS results provided clear hints on the presence of vanadium in +5 oxidation state in all fresh V/Al-x-f catalysts. Py-FTIR showed that both the Lewis and Brønsted acid sites exist in all catalysts, but the amount of Lewis sites is dominating.

The activity test results revealed that among the five aluminas, V/Al-4-f gave the best performance (X-ethane = 35% and S-ethylene = 48%) at 600 °C while the V/Al-2-f showed a poor behaviour only (X-ethane = 50% and S-ethylene = 13%). This latter result was mainly due to a very low surface area of V/Al-2-f solid and consequently poor VO_x dispersion; the opposite was seen in case of V/Al-4-f. Amazingly, the penta-coordinated aluminium-containing V_2O_5 catalyst (i.e. V/Al-1-f) gave an ethane conversion of 35% and selectivity to ethylene of 45 %, respectively.

Further work points to stabilizing the high proportion of penta-coordinated aluminium in aluminas and, probably to reach such effects with higher BET-SA materials for increasing deposition of monomeric and oligomeric VO_x species for more effective oxidation catalysts.

5. Marked effect of the support on the catalytic performance of V_2O_5 catalysts in the ODHE to ethylene

Chapter 5 compares the catalytic data obtained by different supported vanadia catalysts (V/Nb, V/Ti, V/Al-BM, V/Al-HS) with the aid of BET-SA, ICP, UV-vis, XRD, XPS, FTIP, TEM, TPR etc. in detail.
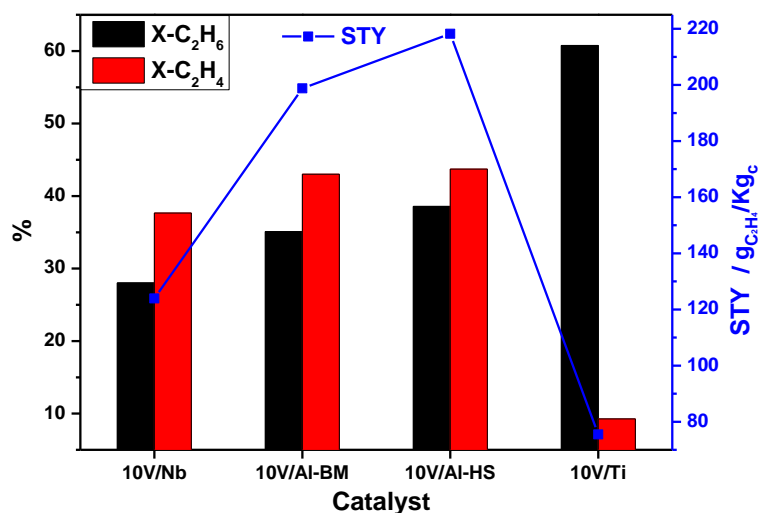
5.1 General studies on effect of the support on the catalytic performance of V_2O_5 catalysts in the ODHE to ethylene

The ODHE to ethylene was performed over a series of vanadia-based oxides with a fixed 10 wt% vanadia loading on different types of supports (V_2O_5/Nb_2O_5, V_2O_5/TiO_2 and V_2O_5/Al_2O_3). The physicochemical properties of catalysts were characterized by TGA, ICP, BET, XRD, FTIR, XPS and TEM techniques. The nature of support significantly influences the catalytic performance in the ODHE to ethylene reaction, which could be attributed the different strength of metal-oxide and support interaction. Despite constant V_2O_5 loading (10wt%) in every case, the phase composition, reducibility, acidity characteristics, nature of VO_x species formed are found to be considerably different, which however depend strongly on the type of support used. The changes in these properties have shown substantial impact on the catalytic performance. Among all, the V_2O_5 catalyst supported on Al_2O_3 (with highest surface area) yielded the highly dispersed monomeric vanadia species resulting in the superior catalytic performance in the ODHE to ethylene reaction.

Nb_2O_5, TiO_2, Al_2O_3 (high surface area 294 m^2/g) and ball-milled Al_2O_3 supported catalysts are denoted by V/Nb, V/Ti, V/Al-HS and V/Al-BM, respectively.

5.2 Characterization studies of different 10 wt% V_2O_5 catalysts supported on different carriers

5.2.1 Structure properties

The thermo gravimetric analysis curves of oven dried supported vanadia samples are illustrated in Fig 5-1. The weight loss observed in each vanadia sample is found to depend on the nature of alumina support applied. The V/Ti had the lowest weight loss (ca. 7 %) while the V/Al-HS showed the highest weight loss (~30 %). It can be observed that the weight loss occurred in two steps in case of V/Nb, V/Ti and V/Al-BM samples and three steps in that of V/Al-HS solids. The weight loss at low temperatures (<120 °C) corresponds to the liberation of physically adsorbed water. The maximum weight loss appeared between 120 to 360 °C due to the decomposition of ammonium metavanadate. It is known that the decomposition of NH_4VO_3 begins even at 175 °C and involves three stages in the process of transformation NH_4VO_3 of into V_2O_5. More details on the steps involved in the

conversion of ammonium metavanadate into vanadia can be found elsewhere [108].In case of V/Al-HS sample, the weight loss continued up to a temperature of 490 °C. However, no weight loss is occurred beyond 500 °C in all the supported vanadia samples irrespective of the type of support used. This result clearly indicates the good thermal stability of different supported vanadia catalysts. Based on this observation and also considering the reaction temperature, the calcination of all these solids is fixed at 600 °C for 6 h in air.
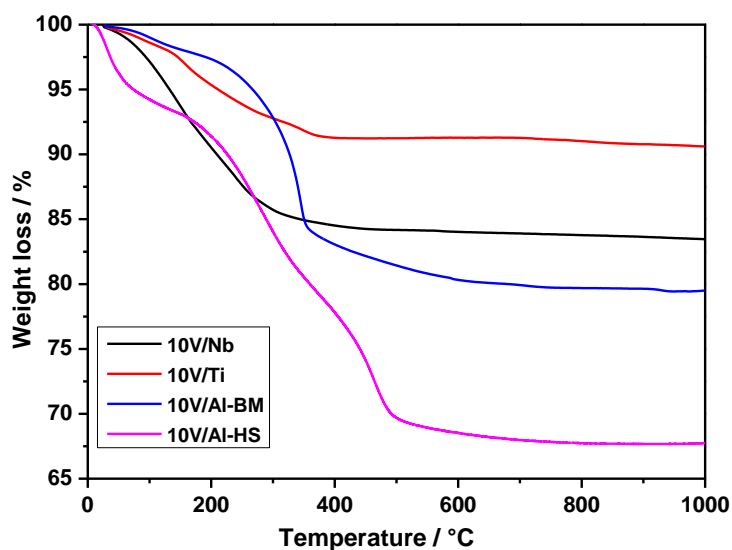

Fig. 5-1   TGA of 10 wt% V$_2$O$_5$ catalysts with varying supports

Table 5-1.

The physical characteristics of the catalysts and different type of support

cat. code	BET-SA (m^2/g)		pore volume (cm^3/g)		support	BET-SA (m^2/g)	pore volume (cm^3/g)	V$_2$O$_5$ wt% (ICP)	
	fresh	Spent	fresh	spent				fresh	spent
V$_2$O$_5$	6.3	-	0.021	-	-	-	-	-	-
10V/Ti	14.5	16.7	0.022	0.139	TiO$_2$	59.2	0.177	9.1	8.8
10V/Nb	16.8	16.7	0.053	0.086	Nb$_2$O$_5$	21.0	0.021	9.6	10.2
10V/Al-BM	18.3	17.9	0.057	0.034	γ-Al$_2$O$_3$	5.8	0.012	10.3	11.2
10V/Al-HS	258.5	191.5	0.513	0.455	γ-Al$_2$O$_3$	294	0.310	12.3	12.2

Table 5-1 presents the surface area, pore volume and bulk composition of supported vanadia catalysts on different metal oxide carriers. The results revealed that supporting vanadium pentoxide on different metal oxides used in this work significantly affects both the surface areas (14.5 – 258.5 m^2/g) and pore volumes

$(0.022 - 0.513\ cm^3/g)$ that of course strongly depend upon the parent support. As expected, the surface areas decreased considerably compared to the pure supports. However, V/Al-BM samples seem to be an exception to this generally expected phenomenon, where the surface area is increased substantially compared to its pure support (Al-BM). The reason for this deviation could be explained on the basis of its origin. In fact, the surface area of 10V/Al-BM sample is increased from 5.8 to 18.3 m^2/g, which might be due to the reformation of a part of the γ-Al_2O_3 into γ-AlO(OH) when it comes in contact with the water used during the preparation by wet impregnation (excess solvent) method. Interestingly, there were no big differences in the surface areas between fresh and spent 10V/Ti, 10V/Nb and 10V/Al-BM catalysts; however, there was a large decrease in case of 10V/Al-HS sample. In addition, the bulk vanadium pentoxide content in all the fresh catalysts was found to be around 9.6 - 10.3 wt%, which is in line with their corresponding theoretical values.
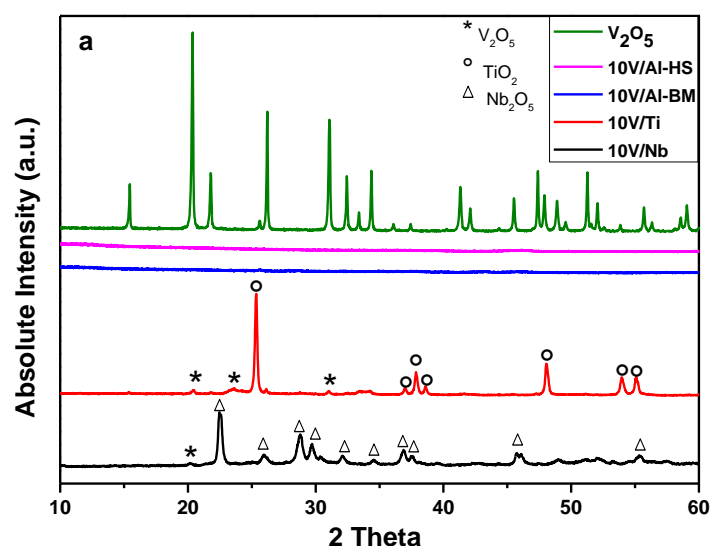

Fig. 5-2a. X-ray diffraction patterns of the fresh 10 wt% V_2O_5 catalysts with varying supports

X-ray diffraction patterns of both fresh and spent 10 wt% V_2O_5 catalysts with varying supports are depicted in Figs. 5-2a and 2b. For better comparison, the pure V_2O_5 was also included in X-ray diffraction patterns of fresh catalysts. It can be clearly seen that the minor reflections corresponding to vanadia pentoxide phase are only appeared in V/Ti and V/Nb samples. On the other hand, no such reflections corresponding to crystalline V_2O_5 could be observed in the other two alumina supported vanadia catalysts (V/Al-BM and V/Al-HS). Nonetheless, the presence of

V_2O_5 in X-ray amorphous form in these two samples cannot be excluded. These results also suggest that the VO$_x$ species are more crystalline in V/Ti and V/Nb solids, while they are finely dispersed on alumina supported samples. Quite interestingly, despite low surface area of Al-BM solid, the crystalline V_2O_5 is absent, which points to the effective active phase support interaction. That is again due to the presence of penta-coordinated Al sites in this solid. Moreover, the minor reflections of vanadia pentoxide appeared in the fresh catalysts are found to be disappeared in both the spent V/Ti and V/Nb catalysts. Further, no considerable changes could be noticed between the fresh and spent catalysts of V/Al-BM and V/Al-HS solids.
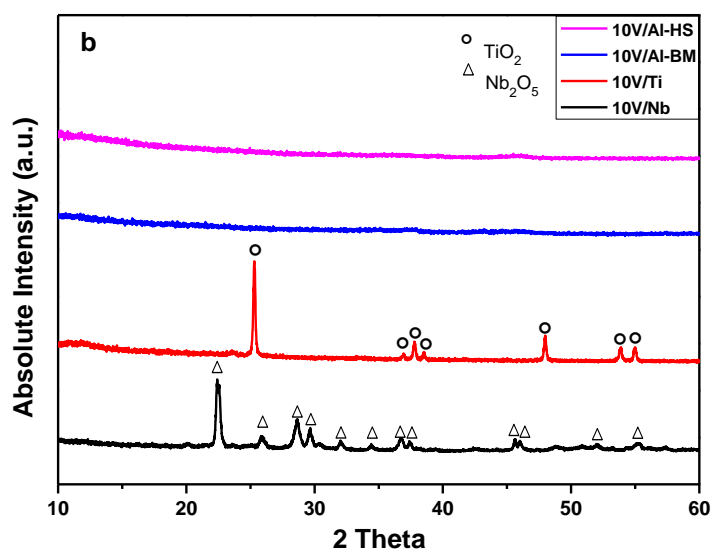

Fig. 5-2b. X-ray diffraction patterns of the spent 10 wt% V_2O_5 catalysts with varying supports

The UV-Vis raw spectra of fresh vanadia catalysts supported on different host metal oxides were illustrated in Fig. 5-3a, which provides the information about the local geometry and the nature of VO$_x$ species formed in the present supported vanadia catalysts. Additionally, the deconvoluted UV-Vis spectra of the same samples are presented in Fig. 5-3b. For comparison, the pure V_2O_5 is also shown in these figures (Figs. 5-3a and 3b). The bands appeared below 350 nm are generally ascribed to the existence of monomeric or one-dimensional VO$_x$ species with four coordination number in tetrahedral environment. With increasing the coordination number, a red shift to higher wavelength is observed. The bonds between 350 – 400 nm can be attributed to the polymeric vanadia species, which is surrounded by five oxygen ligands in square pyramid geometry. In case of crystalline vanadium

pentoxide, where the vanadium ions are located in the centre of a distorted octahedron, the UV-Vis bands are usually appeared at round 450 nm. The reflectance band at 467 nm gives rise to the typical orange-brown colour of vanadia pentoxide. According to this general information, it is evident from Fig. 5-3b that the vanadia species on the surface of all these catalysts contain both the monomeric/polymeric VO_x species in different proportions that is clearly reflected by the UV-Vis bands appeared below 400nm (Figs. 5-3a and 3b). V/Al-BM contains mainly monomeric VOx species with four coordination numbers in tetrahedral form, while there is a small portion of polymeric vanadia species in a square pyramid form were observed on the surface of Nb_2O_5 support. In case of Al-HS supported sample two band maxima appeared at 235 nm and 300 nm, respectively. However, this band is also further extended to 400 nm. The first and second bands are purely due to formation of monomeric VOx species, while the extension of this band further to 400 nm indicates the presence of small amounts of polymeric VOx species in this sample (V/Al-HS). Nevertheless, due to its high surface area, this sample exhibited high dispersion and easily reducible VOx compared to all other solids. Such high dispersion and better reducible properties will be discussed below separately in TPR discussion. As can be seen from Fig. 5-3b, the UV-Vis spectra of pure V_2O_5 is considerably different from the spectra of supported samples. It clearly showed the presence of an intense band centered around 450 nm (Fig. 5-3b) due to its highly crystalline nature, which is however completely absent in the supported samples. The different nature of supports used in this work plays a crucial role in directing the structure of the vanadia with the formation of different vanadia species dispersed on the surface of support resulting in different catalytic performance, which will be discussed separately in the following sections.
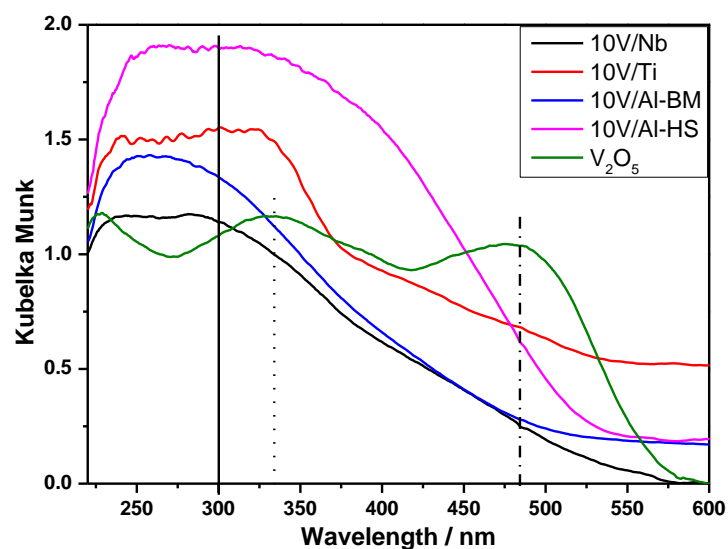
Fig. 5-3a. UV-vis-DR spectra of the fresh 10 wt% V_2O_5 catalysts with varying supports along with pure V_2O_5
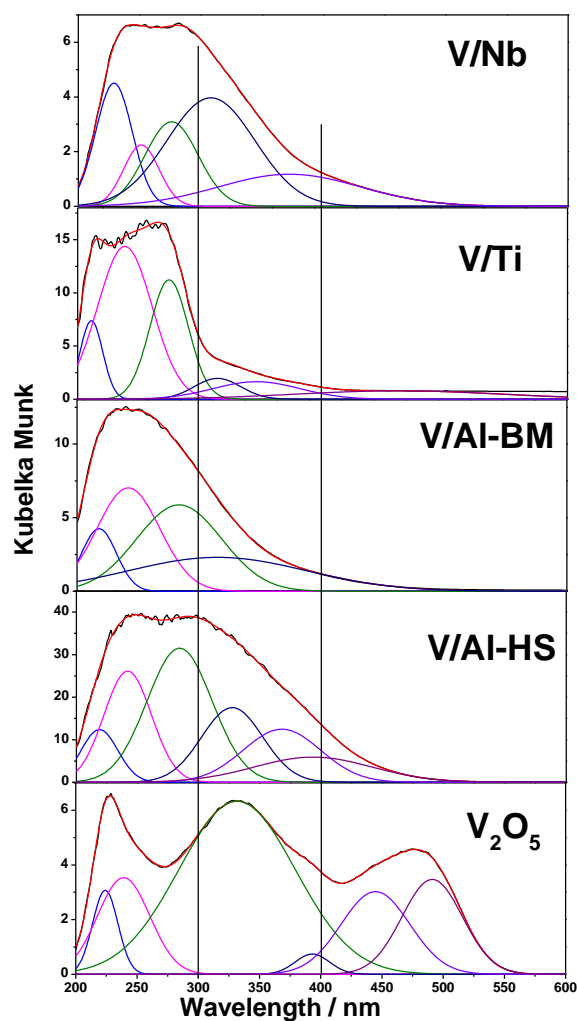

Fig. 5-3b. UV-vis-DR spectra of the fresh 10 wt% V_2O_5 catalysts with varying supports along with pure V_2O_5 (Measured: solid lines; Deconvoluted: dashed lines)

The FT-IR spectra of (fresh) supported vanadia catalysts and pure V_2O_5 are shown in Fig. 5-4a. It is clear from Fig. 5-4a that the bands appeared at 1022 cm^{-1}, 1029 cm^{-1} and 1013 cm^{-1} in case of V/Nb, V/Ti and V_2O_5 are assigned to $V^{+5}=O$ stretching vibrations. The bridge V-O-V stretching vibrations are reflected by the band at 813 cm^{-1} in the spectra of V_2O_5 solid. Surprisingly, no visible vibrations could be seen in case of V/Al-BM and V/All-HS samples. This observation can be explained on the basis of effective active phase-support interaction and enhanced dispersion of VOx over these two samples. XRD also gave good supporting evidence for this observation. Interestingly, the FT-IR spectra of spent V/Nb, V/Al-BM and V-Al-HS samples did not show any considerable changes compared that of corresponding fresh ones. Another notable difference in case of spent of V/Ti catalyst is that the bond at 1029 cm^{-1} appeared in the fresh samples seemed to be shifted to higher wavenumber (i.e. at 1066 cm^{-1}) in the spent solid (Fig. 5-4b).
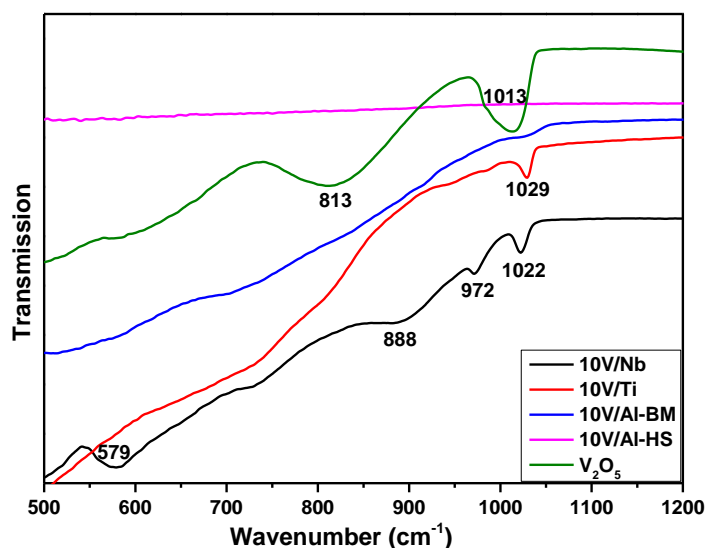

Fig.5-4a.   FTIR spectra of the fresh 10 wt% V_2O_5 catalysts with varying supports
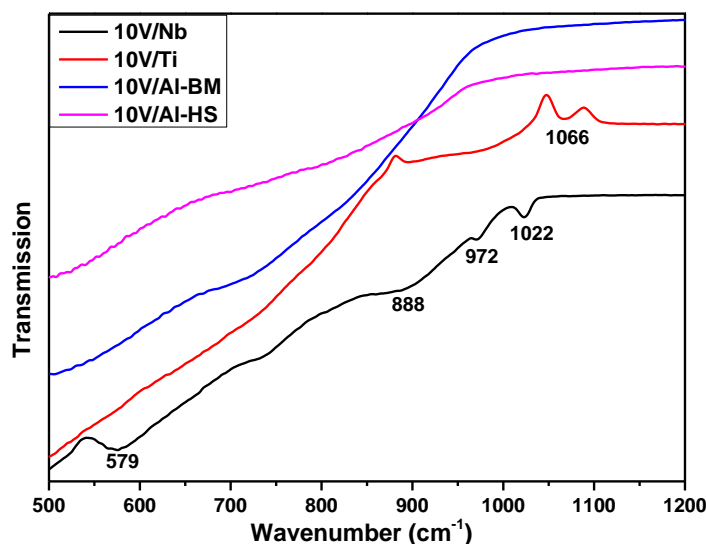
Fig.5-4b.   FTIR spectra of the spent 10 wt% V_2O_5 catalysts with varying supports

The XP-spectra of O1s and V2p3/2 region of the fresh and spent catalysts are displayed in Figs. 5-5a and 5b, respectively. For the fresh samples, XPS V2p3/2 peaks are located at around 517 eV in all the catalysts, which can be attributed to the presence of vanadium in V^{+5} oxidation state. Moreover, the values of Δ (i.e. the energy difference between O1s and V2p3/2 peaks) are also varied between 12.7 and 13.2 eV (Table 5-2), which provides further evidence that the vanadium oxide species in all these four supported vanadia catalysts are present in +5 oxidation state. Even though marginal changes in the V2p3/2 peak width and position is observed in V/Nb V/Al-BM and V/Al-HS samples, no changes in the peak shape could be observed. However, a much broader V2p3/2 peak in lower intensity for TiO_2 supported sample, compared with other three supported catalysts, was obtained. This might be due to high enrichment of V in the near-surface-region. On the other hand, the O1s peaks of samples are slightly shifted from 529 to 530 eV, respectively.
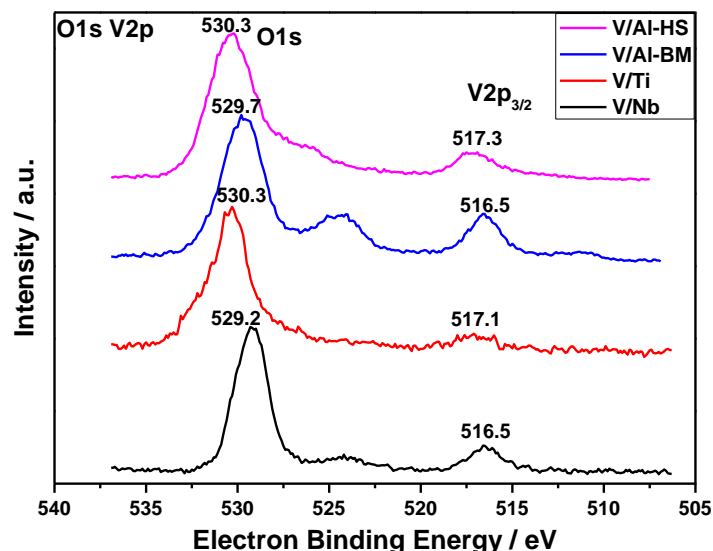
Fig. 5-5a. XP spectra of the fresh 10 wt% V_2O_5 catalysts with varying supports
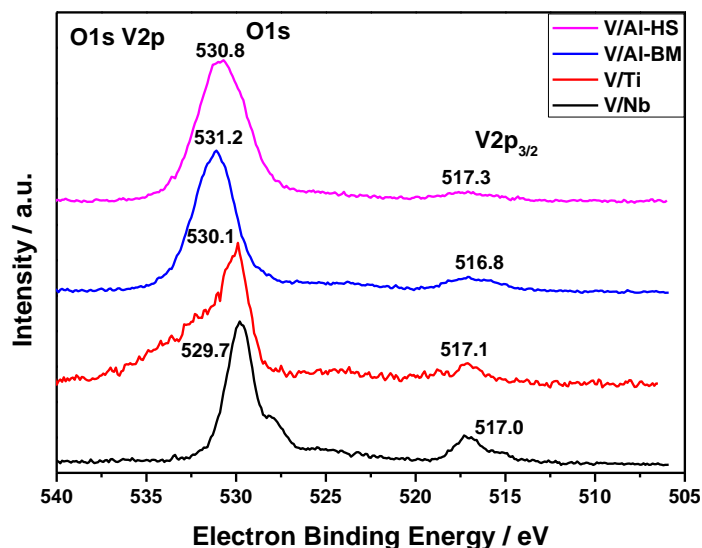
Fig. 5-5b. XP spectra of the spent 10 wt% V_2O_5 catalysts with varying supports

In case of the XP-spectra for spent catalysts (Fig. 5-5b), there are only small changes in O1s position compared to their corresponding fresh ones. However, the shape of O1s peaks for spent catalysts are similar to the relative fresh ones with the exception of TiO_2 supported spent sample which becomes much sharper. However, in all spent catalysts, the intensity of V2p$_{3/2}$ peaks decrease to certain extent especially for Al_2O_3 and TiO_2 supported catalysts but a small extent for Nb_2O_5 supported sample. Regarding to the value of Δ (Table 5-2), considerable changes only occurred in Al_2O_3 supported catalysts and the Δ value of ball-milled γ-Al_2O_3 supported catalyst increased from 13.2 to 14.4 eV showing the reduction of V^{+5} to V^{+4} species.

64

Table 5-2

Results of XPS studies and comparison of V/s ratio in bulk and surface region

Cat.	Δ^* / eV		V/s** (XPS)		V/s (ICP)	
	fresh	spent	fresh	spent	fresh	spent
V/Nb	12.7	12.7	0.29	0.25	0.16	0.17
V/Ti	13.2	13.0	0.31	0.34	0.10	0.10
V/Al-BM	13.2	14.4	0.32	0.22	0.07	0.08
V/Al-HS	13.0	13.5	0.13	0.12	0.08	0.09

*:Δ is the energy difference between O1s and V2p$_{3/2}$ peaks

**:s - support cation

Table 5-2 also represents the ratio of V/s (s: support cation) both from the bulk and surface region characterized by ICP and XP-spectra techniques, respectively. It can be seen clearly from Table 5-2 that the vanadium enriched in the near-surface-region irrespective different type of supports. The surface V/s ratios of V/Nb, V/Ti and V/Al-BM samples are more or less the same probably due to the similar surface areas of these catalysts. In contrast in case of higher surface area of Al-HS support, the surface V/s ratio is much lower. This might be due to the presence of high amount of Al atoms due to its high surface area but constant number of V atoms in every case due to constant loading. This seems to be more probable reason for the relatively low V/s ratio. On the other hand, this solid exhibits high dispersion of VO$_x$ species. If we compare the spent samples, a considerable decrease of surface V/s ratio could be observed only in case of ball-milled γ-Al$_2$O$_3$ sample, which can be attributed to the probable migration of vanadium species to sub surface layers. Moreover the difference in Δ value between fresh and spent V/Al-BM sample also provide further information about the changes of vanadia species on the surface of this ball-milled γ-Al$_2$O$_3$ support.

5.2.2 Morphological studies

Figs. 5-6a, 6b, 6c and d present the electron micrographs, HAADF-STEM images as well as energy dispersive X-ray (EDX) analysis of supported vanadia catalysts. The nature of the support has shown a significant effect on the morphology and size of vanadium species distributed on the support. The TEM and HAADF-

STEM images of V/Nb sample are illustrated in Figs. 5-6a. It could be seen from Fig. 5-6a that the distribution of VO_x is not uniform, i.e. sometimes V-enriched and in some regions Al is enriched and hence the ratio of V/Al is also not uniform. STEM-EDX mapping is a very useful technique to study the composition of the particles seen from TEM. The results from the STEM-EDX mapping showed that the enriched regions of vanadia species.
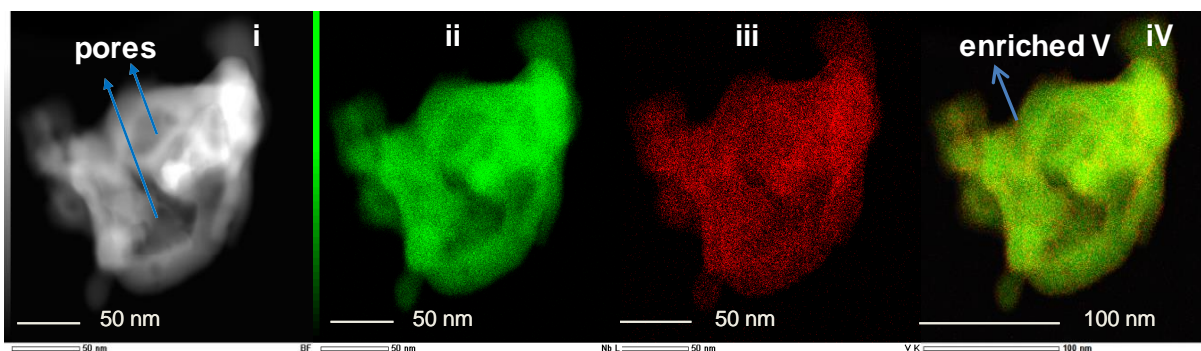
Fig. 5-6a. i) HAADF-STEM image, ii) Nb-L, iii) V-K, iv) EDXS elemental maps of V/Nb catalyst

In case of TiO_2 supported vanadia catalyst, the presence of small amount of tungsten could also be detected in TEM images, which is due to its presence in the parent TiO_2 support. And the formation of needle-like structures (i.e. typical morphology for V_2O_5) of crystalline vanadium pentoxide particles in this TiO_2 supported catalyst due to the agglomeration of vanadia species in TiO_2 support with low surface area. The observation of existence of crystalline vanadium pentoxide species found by TEM images of V/Ti catalyst is in good agreement of the XRD and UV-Vis results. Both the existence of tungsten and vanadia pentoxide species in V/Ti catalyst seems to display different catalytic performance of V/Ti catalyst.
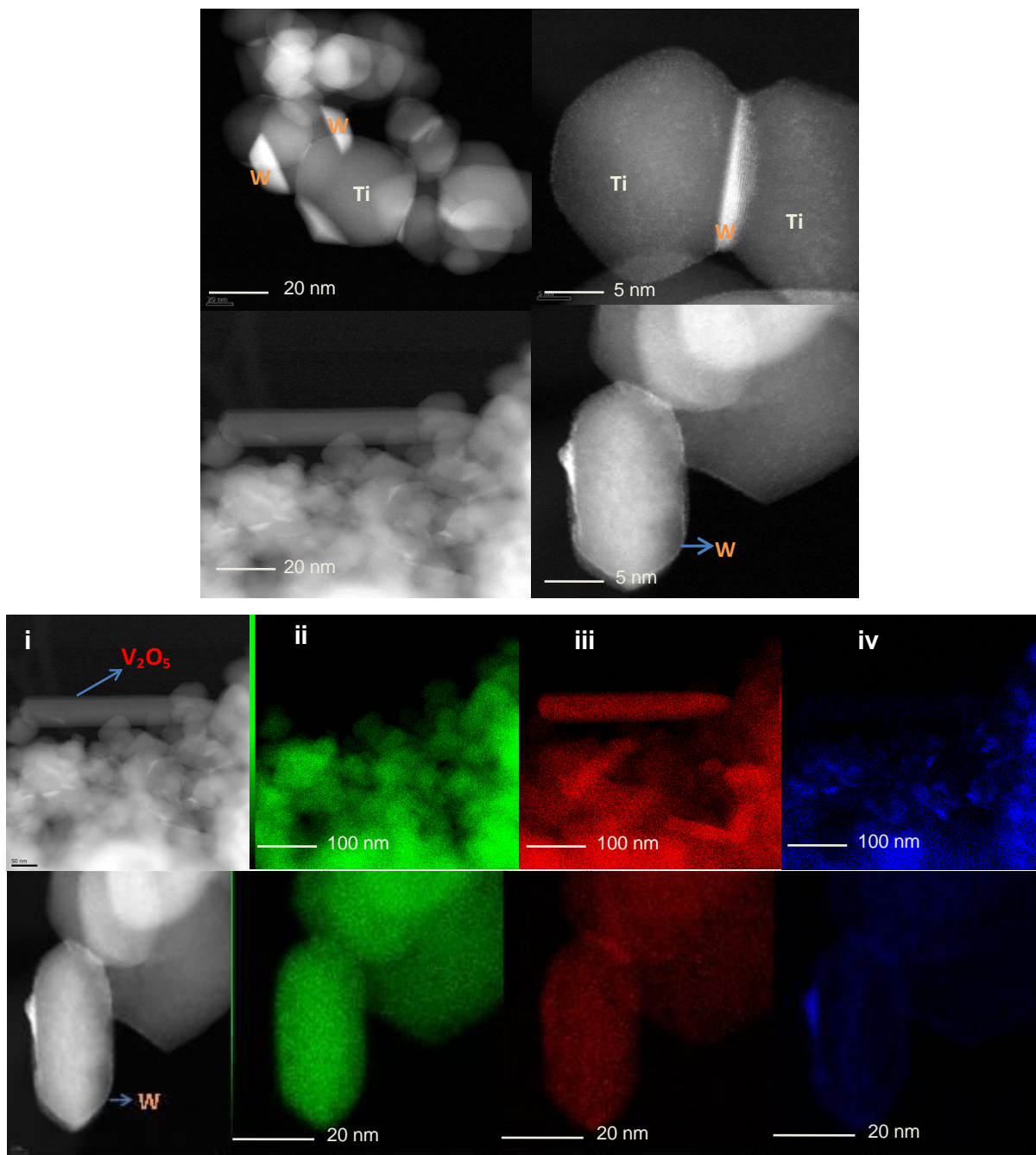
Fig. 5-6b. Transmission electron micrographs and i) HAADF-STEM image, ii) Ti-K, iii) V-K, iv) W-M, EDXS elemental maps of V/Nb catalyst fresh V/Ti sample

Fig. 5-6c shows the results for the fresh ball-milled alumina supported vanadia sample (V/Al-BM). The vanadium oxides are well dispersed and no larger vanadia particles were found. The atomic ratios of V to Al are mostly 1:1 and this ratio is frequently observed throughout the V/Al-BM sample, rarely the Al rich region also exists. Compared with V/Nb and V/Ti catalysts, the highly dispersed vanadia species can be seen in V/Al-BM catalysts that could be probably attributed to the unusual

properties of this ball-milled γ-alumina support, with which the vanadia species could be well anchored due to high amount of penta coordinated Al sites.
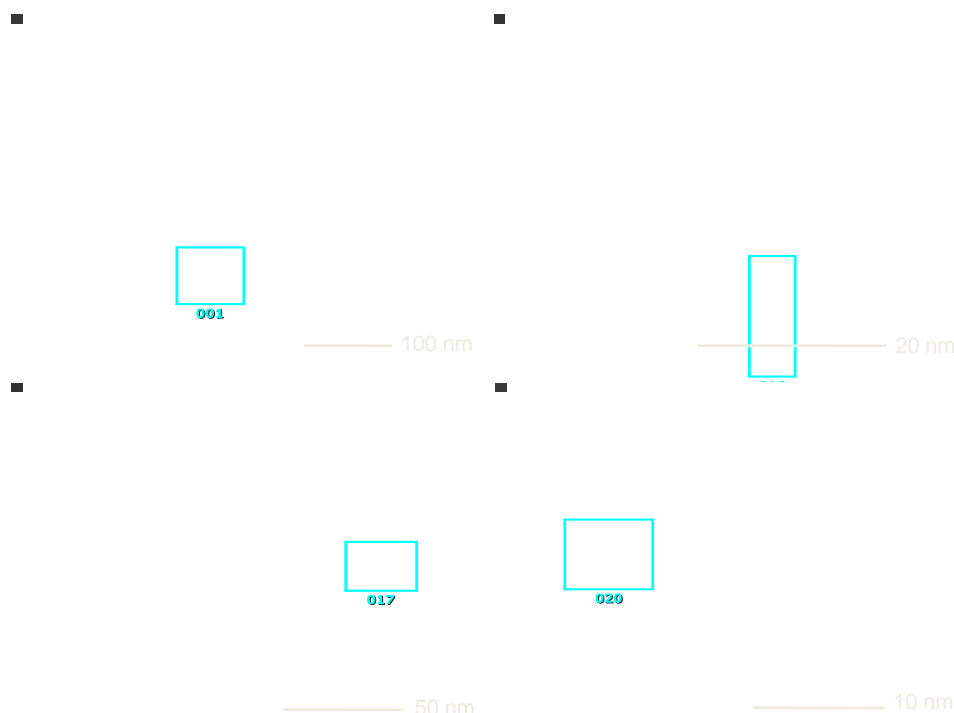
Fig. 5-6c. Transmission electron micrographs and EDX analysis of V/Nb catalyst fresh V/Al sample and the atomic ratio of V_2O_5 to Al_2O_3

Figs. 5-6d depicts the morphology and composition of the V/Al-HS catalyst with the highest surface area (294 m^2/g). The STEM-EDX mapping results indicated that vanadia species are well dispersed in this alumina support probably due to the high surface area of support. The V to Al ratios were also found to be uniform throughout. This highly distributed vanadia species could be related to the lower ethane conversion and higher ethylene selectivity in the ODHE reaction over V/Al-HS catalyst, which will be discussed in the following sections.
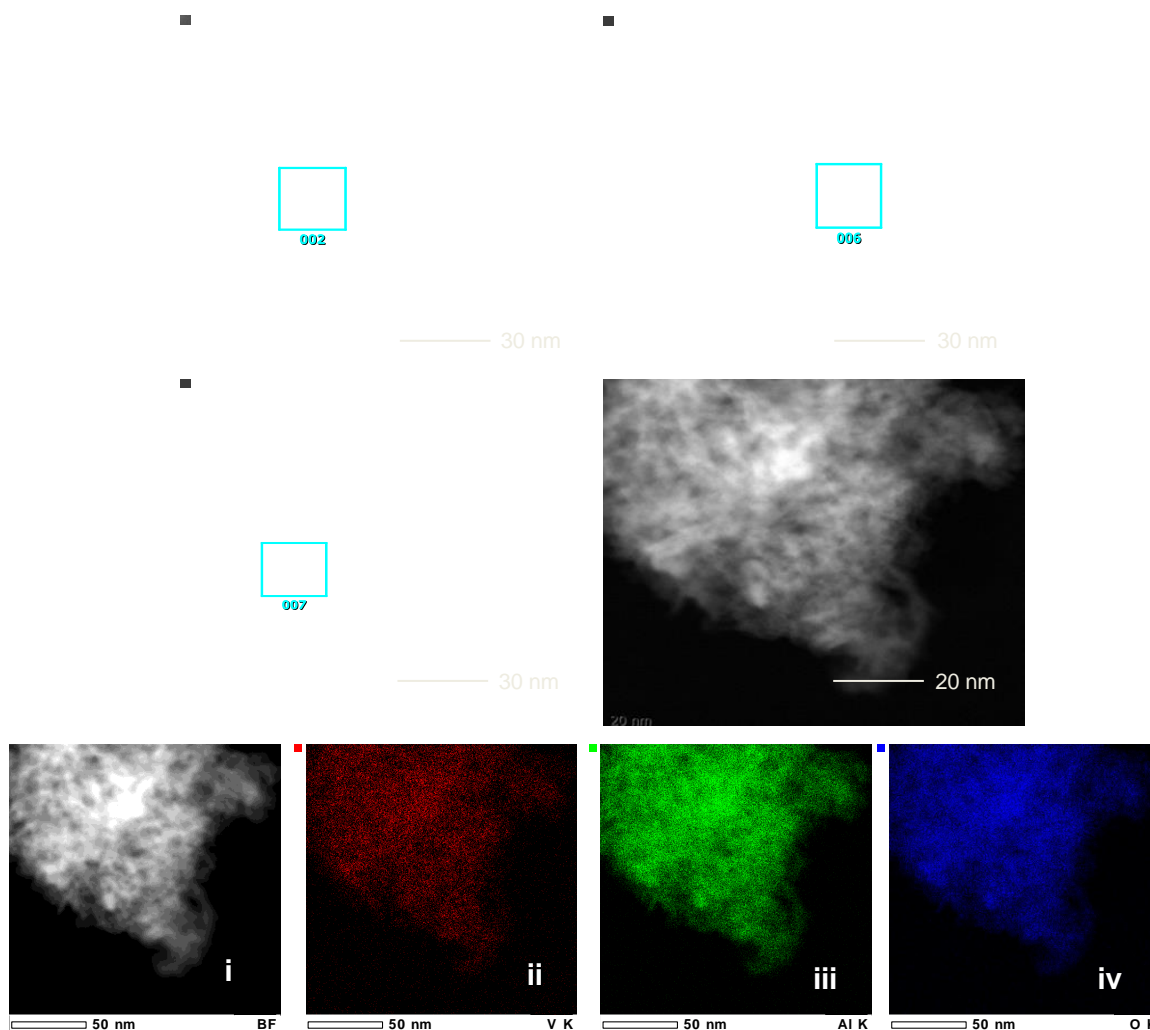
Fig. 5-6d. **Transmission electron micrographs, the atomic ratio of V$_2$O$_5$ to Al$_2$O$_3$ and i) HAADF-STEM image, ii) V-K, iii) Al-K, iv) O-K, EDXS elemental maps of V/Nb catalyst fresh V/Al-HS sample**

5.2.3 Surface acidity

In order to study the surface acidity properties of supported vanadia catalysts, Py-FTIR analysis was explored. It is known from pyridine adsorption that Lewis sites (L-Py) give characteristic bands at around 1450 cm^{-1} and in the region 1625 cm^{-1}. From the intensity of band, the concentration of Lewis acid sites can be evaluated. Besides, the typical band corresponding to Brønsted acid sites (PyH$^+$) can be found at around 1540 cm^{-1} [111].

The FTIR spectra of pyridine adsorbed at 100 °C on different supported vanadia catalysts are displayed in Fig. 5-7a and the quantitative comparison of Lewis and Brønsted acid sites are shown in Fig. 5-7b, where the integral intensity of characteristic bands at 1538 cm^{-1} (PyH$^+$) and 1448 cm^{-1} (L-Py) are given. It is evident

from Fig. 5-7a that all the catalysts contain both Lewis and Brønsted sites in different proportions, which however the distribution of LS and BS strongly depends on the type of support used. Between the two, Lewis acidity dominates in all samples. Among them, V/Al-HS solid exhibit the highest intensity of the band at 1450 cm^{-1} compared to others and hence enhanced Lewis acidity as well.
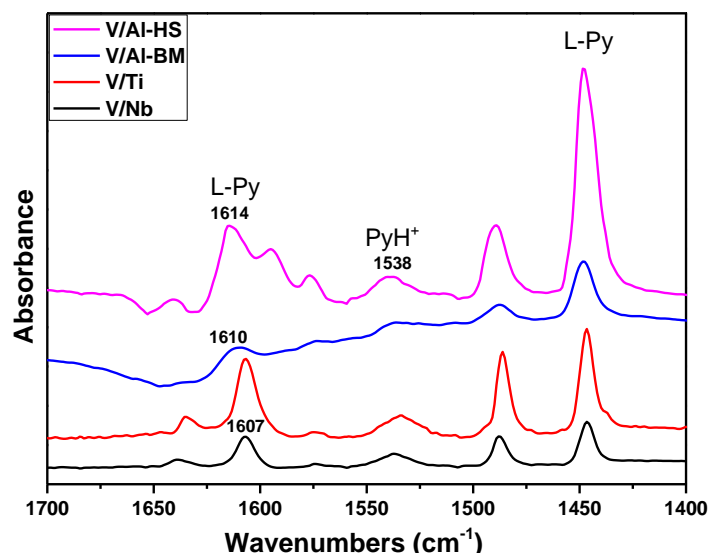
Fig. 5-7a.   Py-FTIR spectra of supported 10 wt% V$_2$O$_5$ catalysts with varying supports
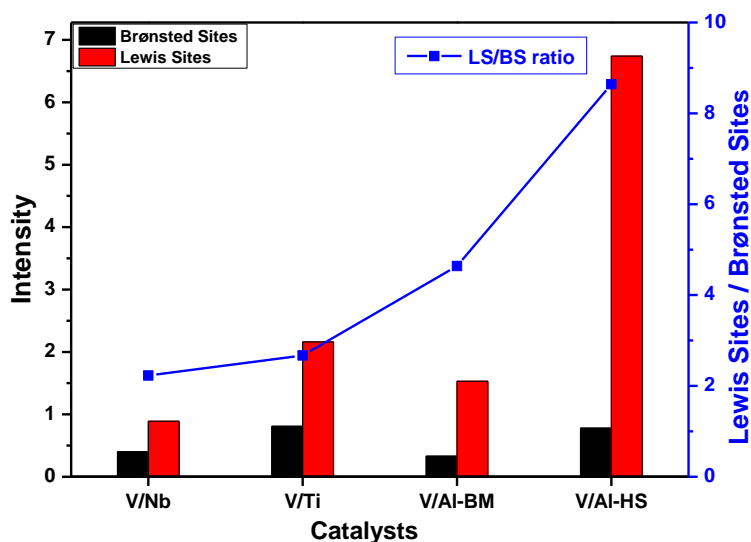
Fig. 5-7b.   Lewis to Brønsted acid sites ratio of supported 10 wt% V$_2$O$_5$ catalysts with varying supports

Fig. 5-7b illustrates the integral intensity of Brønsted and Lewis acid sites of vanadia catalysts, which are considerably varied with changing the nature of support. The γ-alumina with high surface area (i.e. V/Al-HS) showed the highest Lewis acidity, while V/Nb sample has the lowest Lewis acidity. The ratio of LS to BS is found to

increase from V/Nb to V/Al-HS sample. The increasing intensity ratio of Lewis to Brønsted acid sites is found to be in the following the order: V/Nb < V/Ti < V/AL-BM < V/Al-HS. The differences in the integral intensity ratios of different supported vanadia catalysts in turn showed different catalytic performance in the ODH of ethane to ethylene reaction. From these results, it appears that acidity characteristics in particular Lewis sites seem to play a key role on the performance.

5.2.4   Reducibility properties

The reducibility of different supported vanadia catalysts of the present study can be evaluated by examining the temperature-programmed reduction (TPR) profiles. It is well-known that low reduction temperatures correspond to a high degree of V dispersion [112, 113, 114]. Monomeric vanadyl species are more easily reducible compared to the polymeric and crystalline vanadia species. Fig. 5-8 shows the TPR profiles obtained for the present vanadia based catalysts supported on different oxides. The reduction temperatures are observed to be clearly dependent on the type of support applied. The current TPR profiles are found to be substantially different from each other despite constant V_2O_5 content in every case. Such differences can be ascribed to the differences in the nature of active phase-support interaction, type of VOx species formed and the reducibility of these species. The profile of V/Al-HS sample exhibits a main intensive reduction peak at 490 °C, which is the lowest reduction temperature compared to all other vanadia catalysts indicating the easily reducible nature of VOx species formed in this sample. In addition, this sample showed only one reduction peak, which hints to the assumption that the VOx species is highly dispersed on the surface of V/Al-HS catalyst. We assign the reduction peak appeared at 490 °C in V/Al-HS solid is due to reduction of monomeric and/or the highly dispersed vanadia species. Besselmann et al. [113] also found a peak at 487 °C in their TPR measurements and ascribed such peak to reduction of monomeric and dispersed VOx species that are obviously present as a monolayer in strong interaction with the support. Our results are in good agreement with them. The V/Al-BM sample showed the reduction peak at 543 °C together with a shoulder around 490 °C, which is indicative of presence of monomeric and polymeric vanadia species that get reduced at different temperatures. The TiO_2 and Nb_2O_5 supported vanadia catalysts displayed quite different reduction profiles compared with that of Al_2O_3 supported catalysts, both in terms of shape and peak intensity. More than one

reduction peaks at much higher reduction temperatures were observed for V/Ti and V/Nb catalysts. Although the TPR patterns are rather sensitive to the experimental conditions like apparatus, heating rate, sample weight and so on, the number of peaks and position differs in the publications. In case of V/Ti and V/Nb catalysts multiple reduction peaks appeared at varying temperatures from 539 to 781 °C. The other two reduction peaks of V/Ti catalyst at 539 and 640 °C can be attributed to the monomeric and polymeric vanadia species respectively. The reduction temperatures at 575 and 702 °C in the pattern of V/Nb catalyst are probably due to the reduction of polymeric and large three-dimensional vanadium oxide species. The peak at 702 to 781 °C can be ascribed to the reduction of crystalline vanadia pentoxide according to the reported TPR value for bulk vanadium pentoxide [112]. The existence of crystalline vanadium pentoxide in V/Ti catalyst was also proved by the UV-Vis XRD and TEM results. A shift in reduction temperature from 490 °C (on V/Al-HS) to 575 °C (on V/Nb) is certainly due to the change in the nature of VOx species formed on varying catalyst supports.
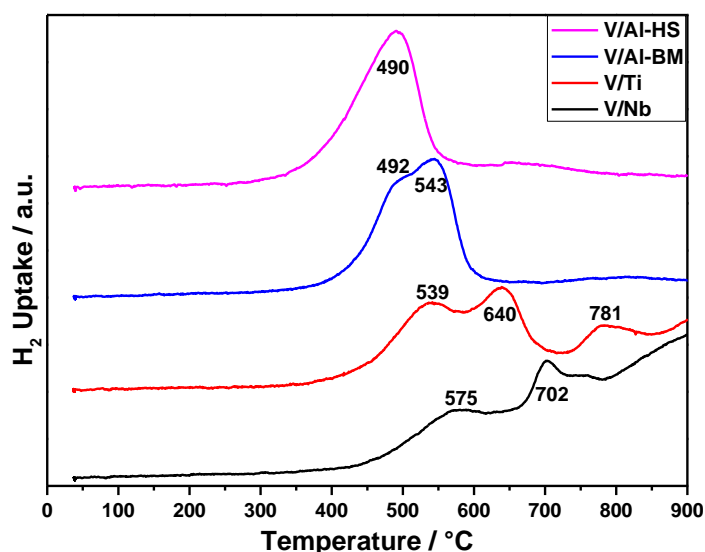
Fig. 5-8. **Temperature programmed reduction curves of fresh 10 wt% V_2O_5 catalysts with varying supports**

5.3 Catalytic results

Figs. 5-9a and 9b show the variation of ethane conversion and ethylene selectivity by varying the type of support for V_2O_5 catalysts in the reaction temperature range from 500 to 600 °C. The ethane conversion increased with rise of temperature irrespective of support as expected. It can be clearly observed that the

activity of vanadia catalysts, compared with the bulk vanadium pentoxide, was significantly enhanced by depositing vanadia on another oxide support. However, the catalytic performance of supported vanadia catalysts differs considerably due to the different nature of support applied. As mentioned before, the nature of the oxide support influences the redox and acid-base properties, as well as dispersion of the vanadia species, which in turn affect the catalyst activity. It is known that the ODH of ethane to ethylene proceeds via Mars-van Krevelen mechanism and therefore effective redox cycle needs to be maintained and the more easily reducible catalyst, the higher the activity performance should be. The TPR results revealed that the V/Al-HS catalyst is more easily reducible followed by V/Al-BM, V/Ti and V/Nb. However, among all the supports used in this work, the ethane conversion was increased in the following order: V/Nb < V/Al-BM < V/Al-HS < V/Ti. The highest ability on ethane conversion obtained by TiO_2 supported vanadia catalyst might be due to the formation of crystalline vanadium pentoxide and/or the presence of tungsten observed by the TEM images. It is known that the tungsten is also a redox component and its presence in small amounts enhances the conversion; however the acidity, dispersion and reducible properties are also crucial for selectivity. Due to lack of those properties, this V/Ti solid exhibit poor seelctivity compared to V/Al-HS and V/Al-BM solids.
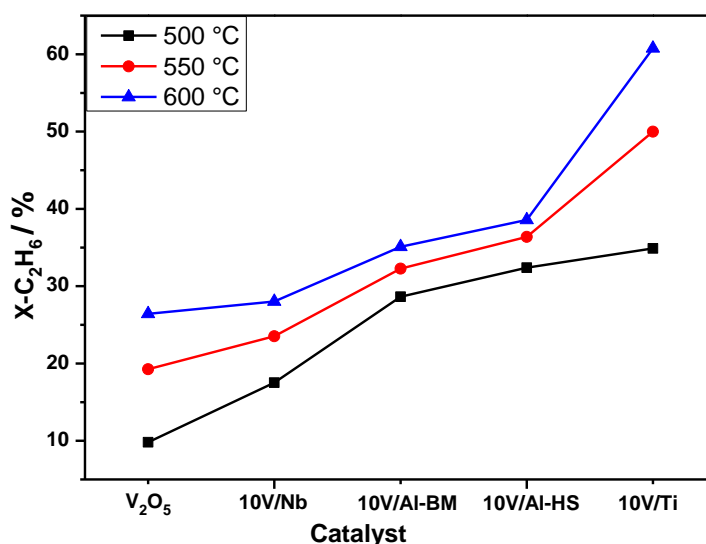

Fig. 5-9a. Ethane conversion over different supported 10 wt% V_2O_5 catalyst at different reaction temperatures

The selectivity to ethylene in the ODH of ethane reaction over different

supported vanadia catalysts is presented in Fig. 5-9b. TiO_2 supported catalyst showed the worst selectivity even lower than that of bulk V_2O_5. The selectivity of other vanadia catalysts showed the same tendency as their corresponding activity for ethane conversion. Taking into account of the acidity property of vanadia catalysts deposited on different supports, it appears that the distribution of Lewis and Brønsted acid sites is an important parameter that can significantly affect both activity and/or selectivity properties in the ODHE to ethylene reaction. Moreover, the integral intensity ratios of Lewis to Brønsted acid sites revealed further hints on the relationship between activity performance of these vanadia catalysts and the crucial effect of Lewis and Brønsted acid sites. It can be concluded that, the higher intensity ratio of Lewis acid site to Brønsted acid site provides the superior catalytic performance. The reason for the unexpected performance of V/Ti catalyst, by comparing the behaviour of V/Ti catalyst and bulk V_2O_5, can be therefore deduced to the existence of tungsten, which is enriched in the edge of V/Ti catalyst particles. The most striking result is the good catalytic behaviour of V/Al-BM sample, which is supported on a ball-milled γ-Al_2O_3. Even though this catalyst has much lower surface area but showed a comparable activity performance with that of V/Al-HS catalyst. The ball-milled γ-Al_2O_3 support contained about 20% penta coordinated Al sites, which seem to be responsible for its improved performance.
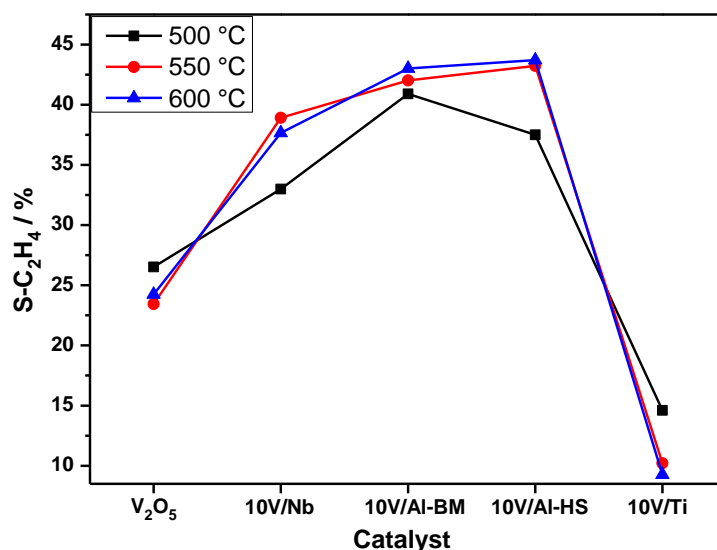

Fig. 5-9b. Ethylene selectivity over different supported 10 wt% V_2O_5 catalyst at different reaction temperature

5.4 Summary and Conclusion

The nature of the support has shown a remarkable influence on the structure, surface areas, type of VO_x species formed, redox, and acid-base properties of several vanadia catalysts. The changes in these properties in turn revealed significant impact on the catalytic performance. At 10 wt% loading of vanadia, the minor X-ray reflections of V_2O_5 are only exist in V/Ti sample indicating the high crystallinity of vanadia species in this sample compared to others. On the other hand, no crystalline V_2O_5 could be found in V/Al-BM and V/Al-HS samples. This indicates the well dispersion of vanadia species in these solids, which is however further proved by the results from TEM, HAADF-STEM and EDX. Such microscopic results depict the different degree of dispersion of vanadia species on different supports. In case of V,Al-BM, the V/Al ratio at 1:1 are frequently observed throughout the sample while Al rich region also exists sometimes. The crystalline V_2O_5 particles display the needle-like morphology in V/Ti samples UV-Vis results provide good supporting evidence for the presence of crystalline V_2O_5 and the nature of monomeric/polymeric vanadia species that are varied in different proportions. The concentration of these species is however found to depend strongly on the type support applied. Mainly monomeric species together with small amouts of oligomeric VO_x species were observed in these solids.

Among all the supported vanadia catalysts studied in this work, the vanadium oxide possesses +5 oxidation state in all the fresh catalysts independent of type of support applied. The vanadia species in two different types of Al_2O_3 supports are more easily reducible than that of TiO_2 and Nb_2O_5 supported ones, according to the TPR results. Py-FTIR spectra revealed the presence of both Lewis and Brønsted acid sites in all the samples. However, Lewis acidity dominates I all samples. The Lewis acid site intensity increases in the following order: < V/Nb < V/Al-BM ≈ V/Ti < V/Al-HS.

The nature of oxide carrier significantly influenced the activity and selectivity properties of the present vanadia based catalysts in the ODHE reaction. The yield of ethylene is followed the order: V/Ti < V/Nb < V/Al-BM ≈ V/Al-HS, which is in line with the reducibility and acidity characteristics of the catalysts. The ratio of integral integral intensity of Lewis and Brønsted acid sites seem to play a vital role on the ethylene selectivity. The higher the ratio of Lewis/ Brønsted sites, the higher selectivity of

ethylene. On the whole, it can be stated that the nature of catalyst support is an important parameter that needs to be carefully selected for obtaining enhanced performance of the catalysts.

6. Effect of the metal dopant M and CO$_2$-admixture on the ODHE to ethylene over Ni-Nb-M-O catalysts

Chapter 6 presents the catalytic data obtained over Ni-Nb-M-O mixed metal oxide catalysts with and without CO$_2$ admixture under the same reaction conditions (T, GHSV), along with the solid state characterization to show the correlation between the nature of catalysts and different catalytic performance.
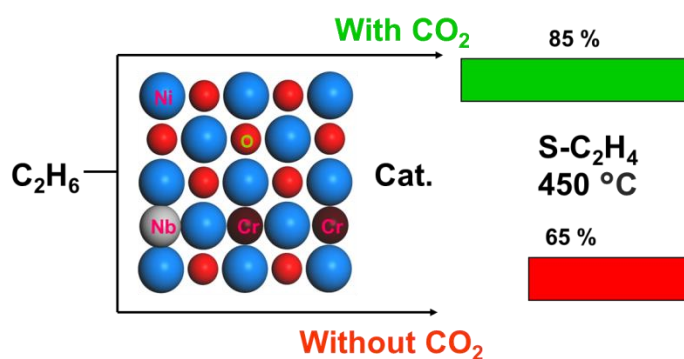
6.1 General studies on Ni-Nb-O and modified Ni-Nb-M-O (M: Cr, Mo, W) catalysts in the ODHE reaction

Ni-Nb-O based catalysts are known for high activity and selectivity towards the oxidative dehydrogenation of ethane (ODHE) to ethylene. The parent Ni-Nb-O catalyst used in this work showed an ethylene yield of 32%. This solid was further modified by three dopants, i.e. Cr, Mo, W (Ni: Nb: M atomic ratio of 1: 0.176: 0.1), that belong to the same group of elements showing different d-characters, with respect to further improve the activity and/or selectivity. However, the activity results of the doped solids revealed a clear reduced activity compared to the original Ni-Nb-O catalyst during the ODHE. Although X-ray diffraction didn't show any changes in crystalline behaviour, BET surface area data, reducibility, acidity characteristics as well as surface composition of Ni-Nb-M-O revealed significant deviations. Anyway, among the three dopants used, Cr displayed relatively superior catalytic performance compared to the other two yielding in an ethane conversion of 26% and an ethylene selectivity of ca.65% only. In addition, the introduction of CO$_2$ into the reactant feed mixture is found to improve the selectivity of ethylene in the ODHE. Ni-Nb-Cr-O solid revealed an ethylene selectivity of ca.85% at slightly less ethane conversion.

6.2 Characterization results of fresh and spent Ni-Nb-O and Ni-Nb-M-O (M: Cr, Mo, W) bulk catalyst

6.2.1 BET-surface area, pore volumes and catalyst composition

Table 6-1 lists the BET surface areas of all fresh and spent samples; for comparison, the surface area of pure NiO solid is also included. A considerable increase in the surface area upon introduction of dopant can be found. It can also be seen that the surface areas of Ni-Nb-M-O catalysts are observed to depend on the nature of dopants but varied in the range from ~55 to 75 m^2/g. The surface areas of the spent samples are somewhat decreased compared to their corresponding fresh samples. On the other hand, the pore volumes of the samples are also found to vary in the range from 0.100 to 0.250 cm^3/g, respectively. Furthermore, the metal contents estimated by ICP in all the catalysts are shown in Table 6-2. Additionally, near-surface region composition of calcined solids obtained from XP-spectra is also presented in Table 6-2 but discussed below.

6. Effect of the metal dopant M and CO$_2$ mixture over Ni-Nb-M-O catalyst

Table 6-1

BET-surface areas and pore volumes of different Ni-Nb-M-O catalysts

Cat. Code	BET-SA (m^2/g)		Pore volume (cm^3/g)	
	Fresh	Spent	Fresh	Spent
NiO	9.4	-	-	-
Ni-Nb-O	58.0	50.2	0.105	0.103
Ni-Nb-Cr-O	53.7	49.0	0.176	0.175
Ni-Nb-Mo-O	73.7	62.9	0.144	0.180
Ni-Nb-W-O	68.5	59.3	0.239	0.193

Table 6-2

Bulk and near-surface region composition of Ni-Nb-M-O (M: Cr, Mo, W) catalysts

Cat.Code	ICP measured composition (at%)			XPS measured composition (at%)		
	Ni	Nb	M	Ni	Nb	M
Ni-Nb-O	1.0	0.119	-	1.0	0.131	-
Ni-Nb-Cr-O	1.0	0.108	0.10	1.0	0.082	0.186
Ni-Nb-Mo-O	1.0	0.113	*	1.0	0.050	0.111
Ni-Nb-W-O	1.0	0.119	*	1.0	0.029	0.037

Nominal composition: Ni: Nb: M = 1: 0.176: 0.1 (atomic ratio), *:not determined

6.2.2 X-ray diffraction

Powder X-ray diffraction (XRD) was used to identify the crystalline phases formed in the calcined catalysts. Fig. 6-1a illustrates the XRD patterns of fresh Ni-Nb-M-O samples with varying dopants (Cr, Mo and W) plus that of parent Ni-Nb-O. It can be clearly seen that in all these Ni-Nb-M-O samples as well as Ni-Nb-O mixed oxides, the XRD analysis exhibits only diffraction peaks corresponding to a crystalline 'NiO-like' phase [4] in cubic structure with a lattice constant of a = 4.18 Å being in good agreement with the reported data (JCPDS 47-1049). Incorporation of an additional metal into Ni-Nb-O parent solid caused a decrease in the intensity of XRD reflections. Such decrease is however clearly depended upon the type of dopant used, i.e. the heavier the dopant, the lower the intensity. However, there were no reflections of new crystalline phase observed corresponding to these three dopants.
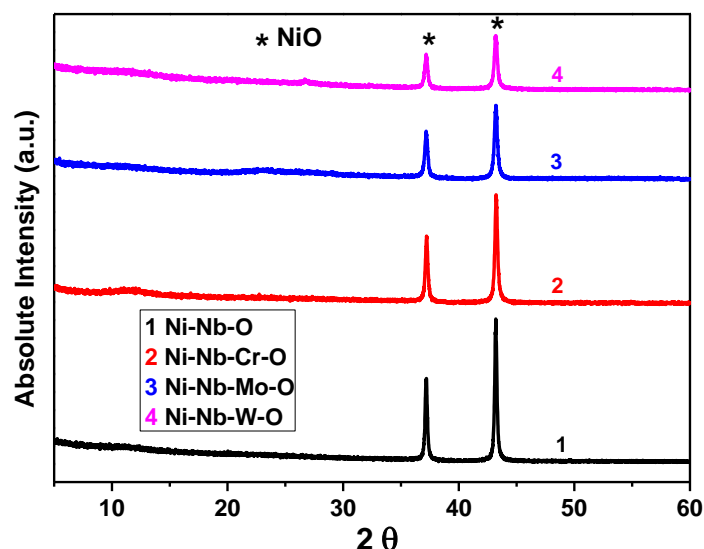
Fig. 6-1a   X-ray diffraction patterns of the fresh Ni-Nb-O and Ni-Nb-M-O catalysts with varying dopants (M: Cr, Mo, W)
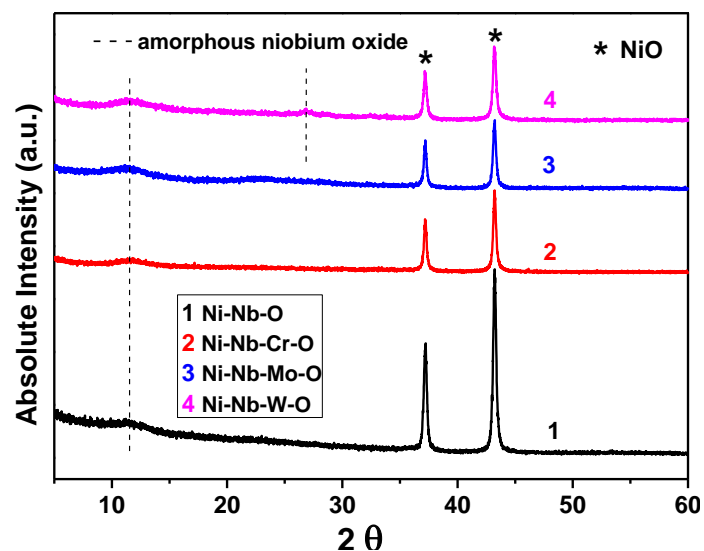
Fig. 6-1b   X-ray diffraction patterns of the spent Ni-Nb-O and Ni-Nb-M-O catalysts (M: Cr, Mo, W)

Fig. 6-1b depicts the XRD patterns of the spent Ni-Nb-M-O catalysts. It can be seen that there were changes between the fresh and the spent catalysts of both Ni-Nb-O and promoted Ni-Nb-M-O (M: Cr, Mo, W). It has been noticed that in all the solids containing dopants (Ni-Nb-Cr-O, Ni-Nb-Mo and Ni-Nb-W-O) only an additional weak broad reflection appeared at $2\theta = 12°$ and an extremely weak one at $2\theta = 27°$ in case of Ni-Nb-W-O samples. This reflection can be ascribed to an amorphous niobium oxide-rich phase [115].

6.2.3 Py-FTIR

Pyridine-FTIR spectra of Ni-Nb-M-O (M: Cr, Mo, W) calcined solids as well as parent Ni-Nb-O are depicted in Fig. 6-2. The bands appeared at 1445, 1602 and 1604 cm^{-1} can be exclusively assigned to pyridine coordinatively bound to oxygen vacancies as Lewis acidic sites (LS). Interestingly in all the samples, only LS are present while no Brønsted sites (BS) were found. Nevertheless, some differences in their band intensities could be noticed, which however depend upon the nature of dopant applied. The integral intensity of LS of Ni-Nb-O oxide is 0.11/m^2. This value is increased by introducing Cr, Mo or W into the host oxide of Ni-Nb-O. Ni-Nb-Cr-O showed the highest amount of LS with an integral intensity value of 0.23/m^2 compared to Ni-Nb-W-O (0.17/m^2) and Ni-Nb-Mo-O (0.15/m^2).
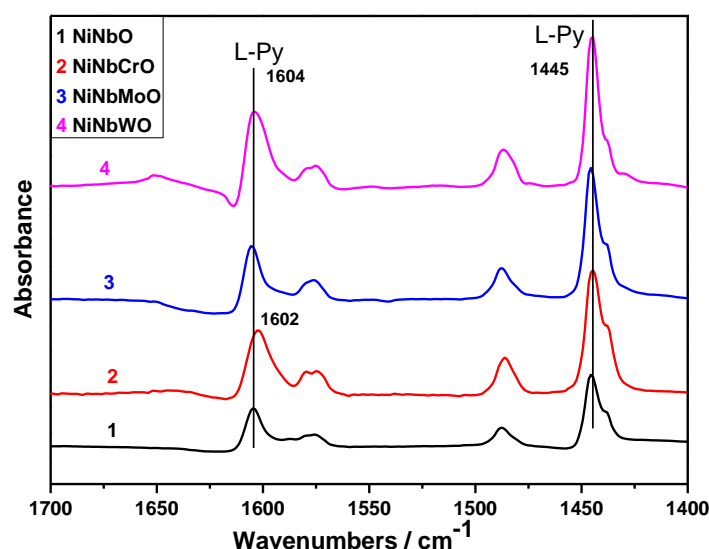
Fig. 6-2   Pyr-FTIR spectra of the fresh Ni-Nb-O and Ni-Nb-M-O catalysts with varying dopants (M: Cr, Mo, W)

6.2.4 TPR reflection

The TPR profiles of pure Ni-Nb-O and the doped Ni-Nb-M-O (M: Cr, Mo, W) samples are shown in Fig. 6-3a and the comparison of fresh and spent Ni-Nb-Cr-O sample is depicted Fig. 6-3b. Ni-Nb-O exhibits a broad reduction peak with a maximum at ~356 °C and a reduction shoulder at somewhat higher temperature (~400-450 °C). According to Heracleous and Lemonidou, the main reduction peak could be attributed to the reduction of Ni-O-Ni bonds and the broad shoulder to the removal of oxygen from Ni-O-Nb bonds [116]. The introduction of an additional metal dopant significantly modified the reduction profiles and causes a shift in the main

reduction peak to higher temperatures, which is certainly due to the interaction between the incorporated metal and the host metal. However, after reaction (i.e. in the spent Ni-Nb-Cr-O samples) the intensity of both the main peak and the weak peak is somewhat decreased (Fig. 6-3b). On the whole, it can be stated that the reducible properties of the catalysts are considerably affected by the type of dopant incorporated into the parent Ni-Nb-O solid.

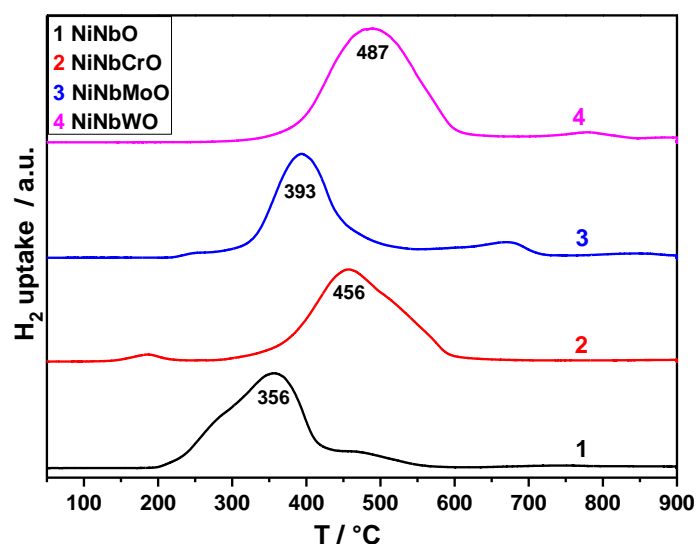**Fig. 6-3a   TPR profiles of fresh Ni-Nb-O and Ni-Nb-M-O catalysts with varying dopants (M: Cr, Mo, W)**
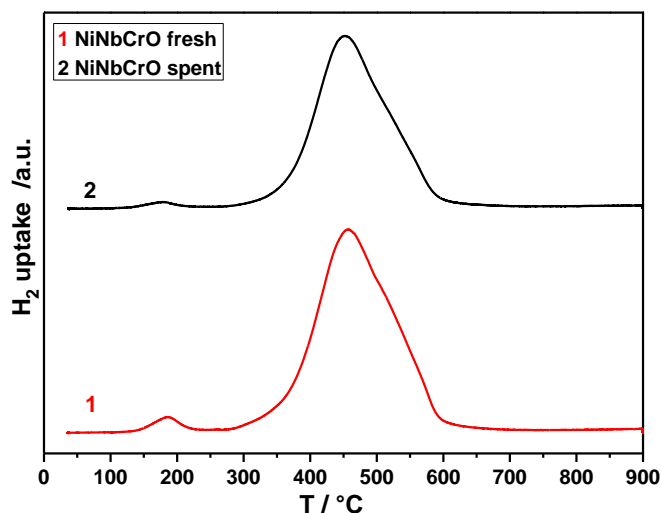

Fig. 6-3b   TPR profiles of fresh and spent Ni-Nb-Cr-O

6.2.5 XP-spectra

XPS was used to provide information about the oxidation state and the chemical environment of the elements being present in the near-surface region of the solids. The Ni 2p XP-spectra of Ni-Nb-M-O (M: Cr, Mo, W) together with Ni-Nb-O are portrayed in Fig. 6-4a. The Ni 2p$_{3/2}$ spectra of all samples (Fig. 6-4a) are typical for Ni2+ with a main peak at 854.9 eV (in case of Ni-Nb-O, it is appeared at 854.6 eV), and a broad satellite centred at around 861 eV [117]. From this, it can be deduced that the Ni-Nb-M-O samples exhibit the similar nickel species (Ni^{+2}) irrespective of type of dopant used. However, an additional shoulder appeared at 856.1 eV only in the parent Ni-Nb-O solid, which is vanished in the promoted catalysts. Some reports [e.g. 118] claimed that the appearance of a peak at a binding energy value of 856.1 eV is due to the formation of Ni^{+3} species. Nevertheless, such Ni^{+3} species are very much unstable and hence the existence of such species in our case seem to be more unlikely. The XP-spectra of Nb 3d are presented in Fig. 6-4b. A doublet peak at binding energies appeared at 207.5 and 210 eV can be assigned to Nb^{5+}, which is commonly present in both parent Ni-Nb-O and metal M (Cr, Mo, W) modified Ni-Nb-M-O samples. It can also be seen from Fig. 6-4b that the addition of dopant has some effect on the binding energy of Nb and particular the shape of the peak. The doublet peak becomes somewhat broader depending upon the dopant along with slight shift in the binding energy to higher value. Among the three, the Cr dopant influences Nb only slightly, whereas the Nb 3d spectrum of the Mo catalyst displays much broader peaks.
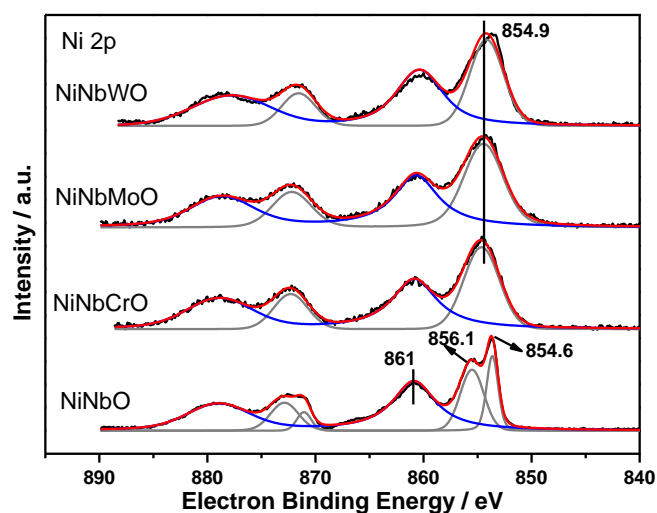
Fig. 6-4a   Ni 2p XP-spectra of the fresh Ni-Nb-O and Ni-Nb-M-O catalysts with varying dopants (M: Cr, Mo, W)
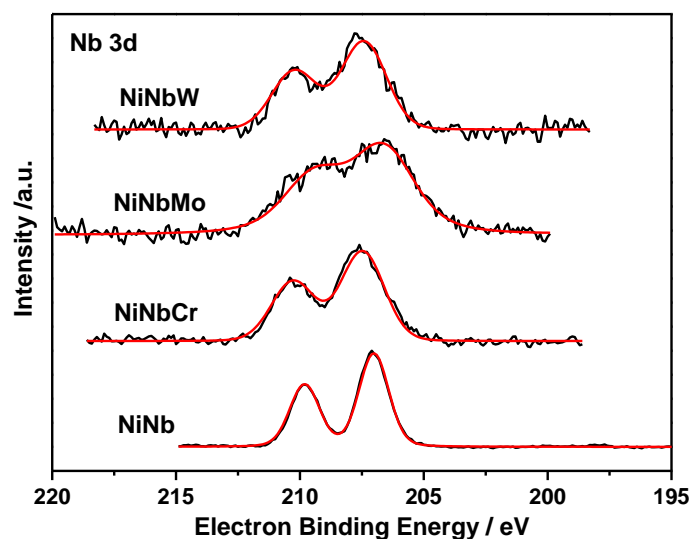
Fig. 6-4b   Nb 3d XP-spectra of the fresh Ni-Nb-O and Ni-Nb-M-O catalysts (M: Cr, Mo, W)

The XP-spectra of the dopant elements such as Cr 2p, Mo 3d and W 4f are presented in Fig. 6-4c. The spectrum of Cr 2p shows to the presence of chromium in +3 oxidation state [119]. In fact, two peaks appear in the XP-spectra at 576.9 eV and 586.0 eV corresponding to Cr $2p_{3/2}$ and Cr $2p_{1/2}$, respectively. The binding energy of the Mo $3d_{5/2}$ peak is at 232.1 eV, which is certainly due to Mo^{+6} oxidation state. This result is in good agreement with that of the literature for molybdena in the highest oxidation state [120, 121]. In the case of Ni-Nb-W-O catalyst, the peaks for W $4f_{7/2}$ at 36.0 eV and W $4f_{5/2}$ at 37.7 eV indicate the presence of tungsten in +6 oxidation state [122, 123]. However, no indication for the presence of the lower valance states of Mo

and W ions could be observed in the present promoted catalysts. Just to summarise, XP-spectra revealed the existence of Cr^{3+}, Mo^{6+} and W^{6+} in Ni-Nb-Cr-O, Ni-Nb-Mo-O and Ni-Nb-W-O, respectively.
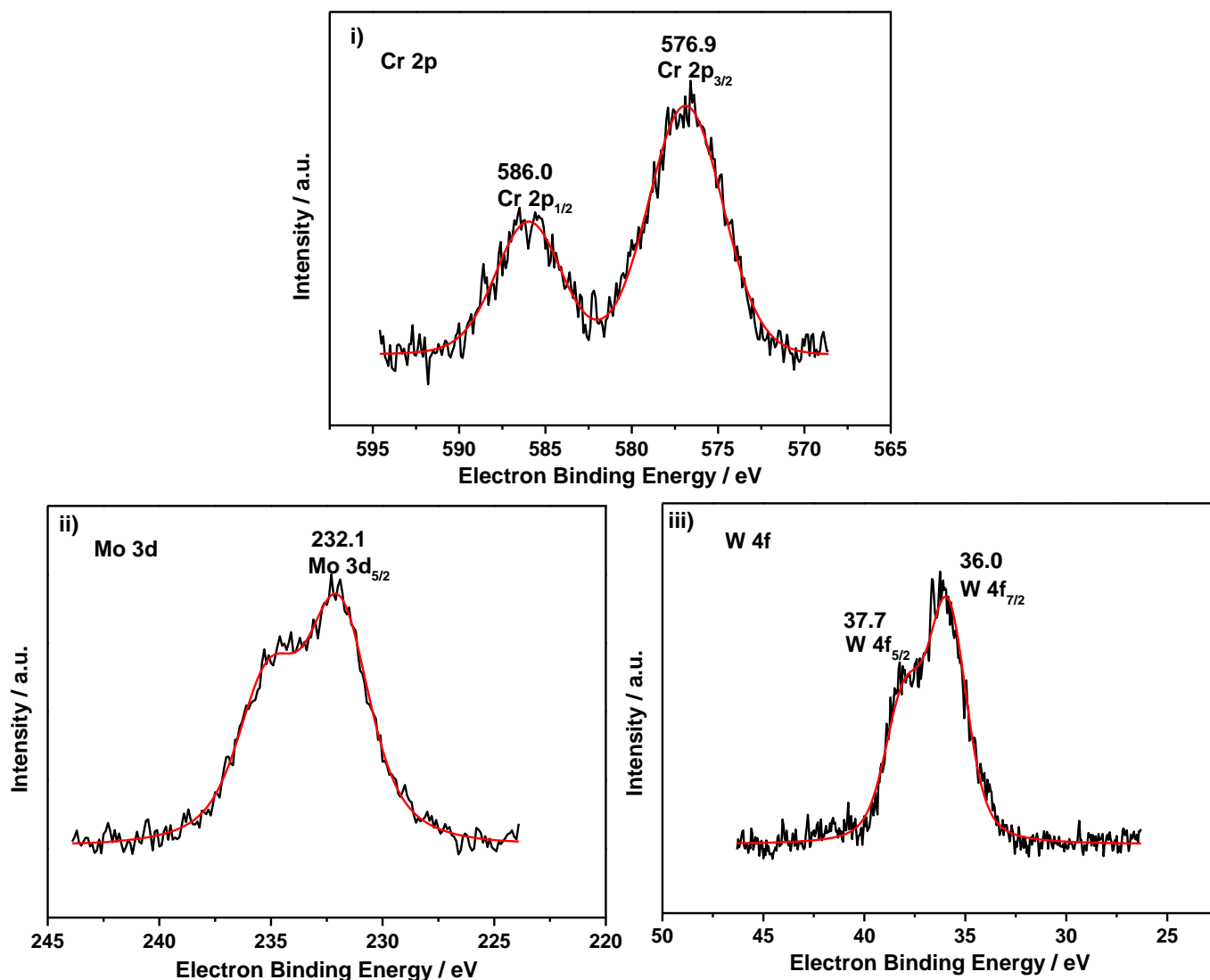
Fig. 6-4c   XP-spectra of the fresh Ni-Nb-M-O catalysts: i) Cr 2p, ii) Mo 3d and iii) W 4f

Both the near-surface region composition estimated by XPS and the bulk composition determined by ICP are compared in Table 6-2. It can be clearly seen that the near-surface metal enrichment clearly depends upon the nature of the dopant used. It is found that the Nb/Ni and the M/Ni ratios are considerably decreased in the near-surface region with changing dopant from 3d to 5d. However, the parent Ni-Nb-O solid has shown still higher value of surface Nb/Ni ratio (0.13) compared to promoted samples. Such changes in the values of surface Nb/Ni ratios

can show substantial influence on the catalytic performance, which will be discussed in the following sections.

6.3 Catalytic results

All the Ni-Nb-O and Ni-Nb-M-O (M: Cr, Mo, W) catalyst samples were tested both in absence and presence of CO_2 in the feed gas. First tests were performed in absence of CO_2 under the following reaction conditions, i.e. C_2H_6: O_2: N_2 = 1: 0.7: 2.7 under steady state conditions in a temperature window of 300-450 °C with a constant W/F (1.02 g s/cm³). Later on, the influence of CO_2 admixture in the reactant flow at a ratio of C_2H_6: O_2: CO_2: N_2 = 1: 0.5: 0.9: 2 was explored but under the same conditions as in the first case.
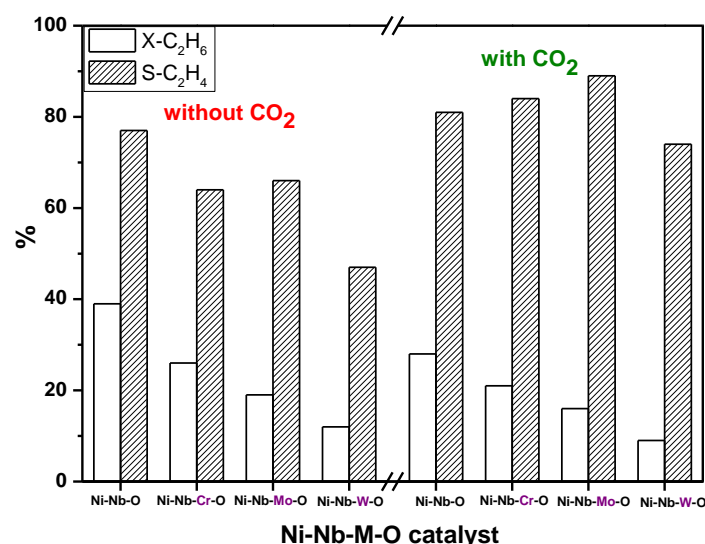
Fig. 6-5 **Effect of CO_2 admixture on the activity and selectivity of Ni-Nb-O and Ni-Nb-M-O catalysts (M: Cr, Mo, W) (reaction conditions: T = 450 °C, C_2H_6: O_2: CO_2: N_2 = 1: 0.7: 0: 2.7 (without CO_2), C_2H_6: O_2: CO_2: N_2 = 1: 0.5: 0.9: 2.0 (with CO_2), cat. wt. = 1.1 g GHSV = 3250-3545 h^{-1}, τ = 1 to 1.1 s)**

The catalytic results for parent Ni-Nb-O and promoted Ni-Nb-M-O (M: Cr, Mo, W) in absence and presence of CO_2 under the conditions mentioned above (T = 450 °C) are shown in Fig. 6-5. Surprisingly, the modified Ni-Nb-M-O (M: Cr, Mo, W) catalysts did not exhibit positive improvement on catalytic activity. Both ethane conversion and ethylene selectivity decreased to some extent. This negative effect could be attributed to the declined reduction ability of the promoted Ni-Nb-M-O samples than that of parent Ni-Nb-O oxide. On the other hand, the doping of Cr, Mo and W can tune the accommodation of Nb in the host NiO oxide, which in turn influences their

activity in the ODHE. XP-spectra also give further hints on the changes in the surface composition, particularly the decrease in Nb concentration in the near-surface-region depending on dopant used. The near-surface-region Nb/Ni ratio drops in the following order: Ni-Nb-O > Ni-Nb-Cr-O > Ni-Nb-Mo-O > Ni-Nb-W-O. Anyway, it has been clearly observed that a high concentration of Nb in the near-surface-region leads to enhanced activity. Considering the reduced activity and selectivity of promoted catalysts, it could therefore be deduced that the amount of Nb in the near-surface-region plays a crucial role on the ODH activity of ethane over Ni-Nb-oxide-based catalysts. This observation was also well supported by the investigations of Heracleous and Lemonidou and the best catalytic performance was obtained by $Ni_{0.85}Nb_{0.15}O$ in their work [116, 124].

Among these three dopants of the same group applied, Cr promoted catalyst exhibited better performance compared to other two components. This means, the increase in d-character of the dopant (from 3d to 5d) has shown an adverse effect on the conversion of ethane as well as on the selectivity of ethylene (see Fig. 6-5). According to the characterization results, the better performance of Cr promoted Ni-Nb-Cr-O samples could be related to its higher acidity and the presence of easily reduced Ni-O-Cr species. In general, it looks that the near-surface region Ni/Nb ratio (Ni/Nb near-surface ratio: Ni-Nb-O = 7.6, Ni-Nb-Cr-O = 12.2, Ni-Nb-Mo-O = 20, Ni-Nb-W-O = 35) plays a crucial role for the catalytic properties of the solids. Besides, high surface enrichment of Nb as well as Cr was observed in case of Cr promoted catalyst (i.e. Ni-Nb-Cr-O) compared to other two dopants applied.

Fig. 6-5 also compares the results in presence of CO_2 on the catalytic performance under the same reaction conditions mentioned above at 450 °C. For parent Ni-Nb-O catalyst, the introduction of CO_2 caused a drop of the ethane conversion but an increase in selectivity to ethylene to a small extent from 77% without CO_2 to 81% with CO_2. However, it is evident that the CO_2 admixture to the reactant feed commonly caused a slight decrease in the conversion of ethane but considerably improved the selectivity of ethylene in case of three metal promoted Ni-Nb-M-O catalysts. For instance, in case of the best catalyst (i.e. Ni-Nb-Cr-O) among these three promoted catalysts, the CO_2 admixture improved the selectivity to ethylene from 63% to 84% while ethane conversion is slightly reduced from 26% to 21%. Similar such tendency is also observed with the other two dopants. Addition of

6. Effect of the metal dopant M and CO_2 mixture over Ni-Nb-M-O catalyst

CO_2 to the reactant feed mixture is expected to cover some unselective electrophilic oxygen species and hereby improve the selectivity of ethylene. Moreover, CO_2 is heavier than O_2 and hence it can also limit the oxygen diffusion across the catalyst bed. Furthermore, nature of dopant also displayed considerable influence on the activity and selectivity behaviour of the catalysts. Such differences in the performance can also be ascribed to adsorption properties of dopant elements. Our results are in good agreement with those reported by Wang et al. [125] claimed that the enhanced selectivity to ethylene could be related to the poisoning effect of CO_2 in the ethane conversion by inhibiting the reactions between alkyl radicals with the active site on catalyst surface. Similar such effect of CO_2 admixture can also be expected here in the present study on improving the selectivity of ethylene. The other possible reasons could be i) CO_2 is a by-product of this reaction, and hence it is already present in the product mixture, and admixture of additional CO_2 might shift the equilibrium and as a result selectivity is improved while the activity is slightly lost and ii) addition of CO_2 might block the unselective sites (e.g. more reactive electrophilic oxygen species, probably by forming some kind of surface carbonates) and also inhibit and/or affect the formation of alkyl radicals [125] and thereby rate of $C_2H_5\cdot$ radicals and their subsequent transformations are influenced to a certain extent, resulting in reduced ethane conversion.

From the standpoint of effect of CO_2 admixture and in view of the best performance obtained on Ni-Nb-Cr-O catalyst in comparison with other solids, this particular catalyst was further used in additional catalytic tests with changing ratio of C_2H_6: O_2: CO_2: N_2. The objective was to study the influence of amount of CO_2 in reactant flow on the activity and selectivity of the catalyst. Besides, the intention was also to identify the optimum reaction conditions.

Figs. 6-6a and 6b illustrate the conversion of ethane and selectivity to ethylene obtained over Ni-Nb-Cr-O catalyst in the ODHE. As expected, in absence of O_2 in the feed, almost no conversion of ethane could be achieved in the reaction temperature region investigated. However, with increase in O_2 concentration in the feed mixture, the conversion of ethane has been increased drastically from 0.4 (in absence of O_2) to 53.8% (at C_2H_6: O_2 = 1: 1.4 mole ratio). On the other hand, ethylene selectivity is increased with rise in temperature only up to 400 °C and then decreased with further increase in temperature to 450 °C, which however strongly depends upon the O_2

concentrations in the reactant feed mixture. It should be noted that the selectivity increased progressively with temperature up to the stoichiometric oxygen concentration (C_2H_6: O_2 = 1: 0.5). However, when the oxygen concentration increased beyond the stoichiometric amount, the excess of O_2 clearly promotes the total oxidation and thereby increases consecutive oxidation of both the ethane and ethylene to carbon oxides. As a result, the selectivity to ethylene is reduced considerably. Therefore, the O_2 concentration close to stoichiometric condition is an important parameter for the better catalytic performance of Ni-Nb-Cr-O catalysts.

Fig. 6-6a   Effect of O_2/CO_2 ratios on ethane conversion at different temperatures over Ni-Nb-Cr-O catalyst (reaction conditions: T = 300-450 °C, GHSV = 3545 h^{-1}, τ = 1 s, cat. wt. = 1.1 g)

Furthermore, it can be stated that both the increase in O_2 concentration and simultaneous increase in reaction temperature caused an adverse effect on ethylene selectivity but promotional effect on the conversion of ethane. It can also be observed from Figs. 6-6a and 6b that the selectivity is relatively higher in presence of CO_2 in the reactant feed mixture. Even though the activation of ethane is difficult in absence of oxygen in the feed, but the addition of CO_2 certainly has shown a clear improvement in the selectivity of ethylene. It is further proved that the poisoning effect of CO_2 presence on ethane conversion [125], resulting in lower ethane conversion and enhanced ethylene selectivity.
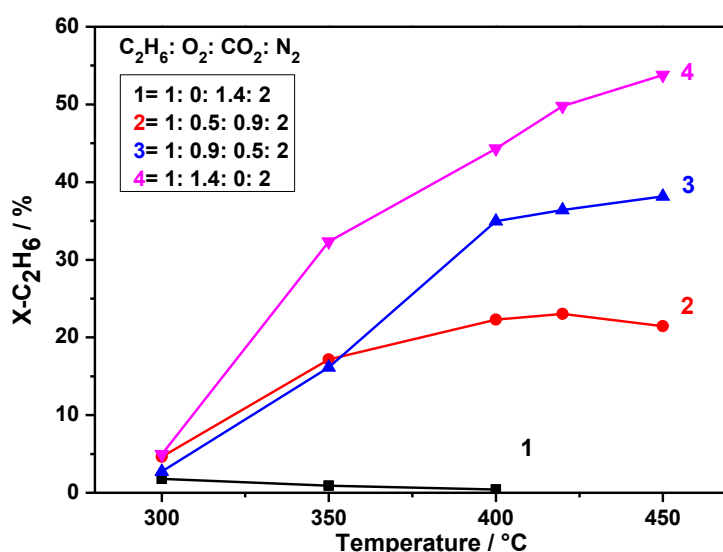
Fig. 6-6b   Effect of O_2/CO_2 ratio on ethylene selectivity at different temperatures over Ni-Nb-Cr-O catalyst (reaction conditions: T = 300-450 °C, GHSV = 3545 h-1, τ = 1 s, cat. wt. = 1.1 g)

Later on, the effect of a varying CO_2 concentration was also investigated at constant O_2 concentration (C_2H_6: O_2 = 1: 0.7) being close to stoichiometric condition. Fig. 6-7a depicts that the variations of ethane conversion as a function of temperature over Ni-Nb-Cr-O catalyst. It can be seen that at temperature below 350 °C, the CO_2-admixture does not influence the conversion to a considerable extent. However, from 350 °C onwards, a clear effect can be found. As expected, the conversion is increased with temperature to a great extent up to 400 °C and then remained more or less constant. This levelling-off appears to be due to non-availability of surplus oxygen in the reaction mixture. Actually from 400 °C, the O_2 was completely consumed. On the other hand, at the fixed O_2 concentration in the feed, increase in CO_2 ratio, a slight decrease in ethane conversion was noticed because of the poisoning effect of CO_2 on the reaction between the C_2H_5 radicals and the surface active sites as claimed elsewhere [125]. However, the selectivity to ethylene showed an inverse tendency compared to the ethane conversion as a function of temperature (*cf.* Fig. 6-7b), i.e. the selectivity to ethylene was increased considerably with increasing CO_2-admixture. In all cases, the highest selectivity to ethylene was recorded at 420 °C.
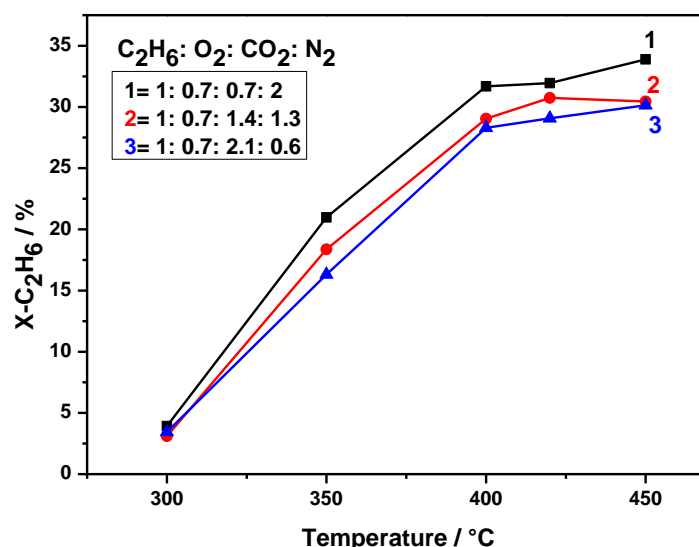
Fig. 6-7a Effect of CO$_2$ proportion on ethane conversion at different temperatures over Ni-Nb-Cr-O catalyst (reaction conditions: T = 300-450 °C, GHSV = 3545 h^{-1}, τ = 1 s, cat. wt. = 1.1 g)
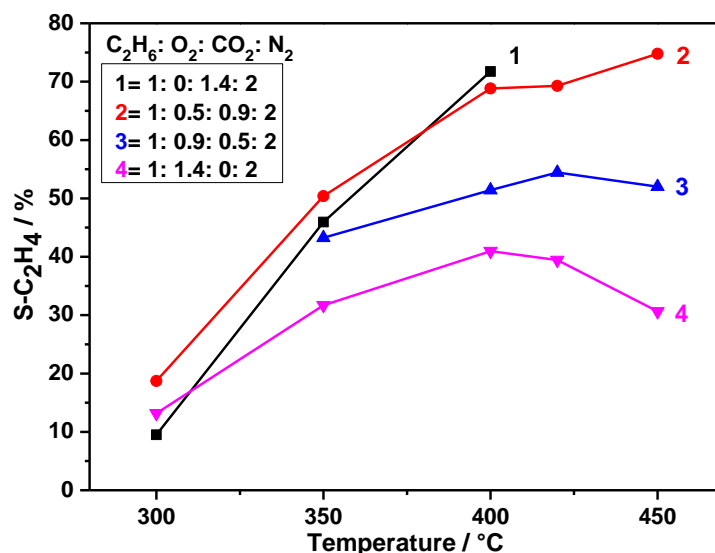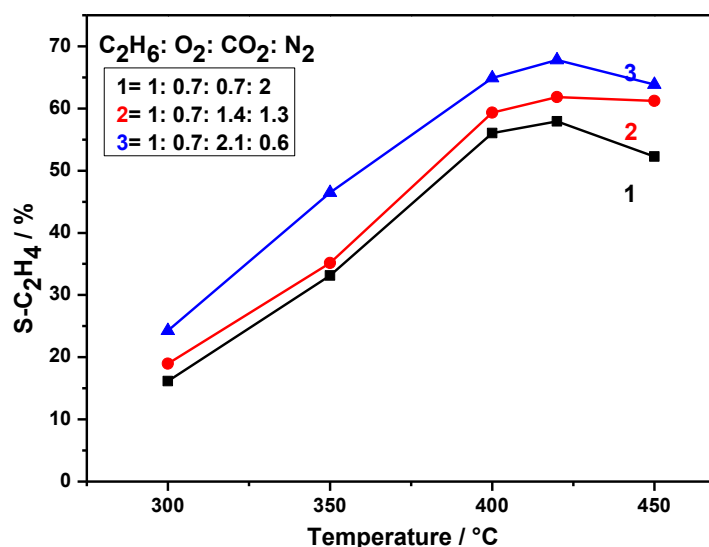

Fig. 6-7b Effect of CO$_2$ proportion on ethylene selectivity at different temperatures over Ni-Nb-Cr-O catalyst (reaction conditions: T = 300-450 °C, GHSV = 3545 h^{-1}, τ = 1 s, cat. wt. = 1.1 g)

The important parameters such as ethane conversion and ethylene selectivity at 420 °C are portrayed in Fig. 6-8 as a function of different CO$_2$/O$_2$ ratios. It is evident that the selectivity to ethylene increased with an enlarged proportion of CO$_2$ admixed from ~60% to close to 70%, i.e. with rise in CO$_2$/O$_2$ ratio from 0 to 3. However, the high conversion is obtained at a CO$_2$/O$_2$ ratio of 1. Considering these two parameters such as conversion of ethane and selectivity to ethylene it can be inferred that the

6. Effect of the metal dopant M and CO_2 mixture over Ni-Nb-M-O catalyst

CO_2-admixture has a promotional effect on the selectivity to ethylene but marginal negative effect on the conversion of ethane. These effects observed on the impact of CO_2 concentration in the feed might be due to the elimination of H_2 generated by dehydrogenation via reverse water gas shift reaction [126]. The highest ethylene selectivity was attained at 420 °C with a C_2H_6: O_2: CO_2: N_2 ratio of 1: 0.7: 2.1: 0.6, under these conditions a long-term stability test over the Ni-Nb-Cr-O catalyst was carried out. The results are presented in Fig. 6-9. This long-term test was done in two days, i.e. 11 h on the first day and 10 h on the next day, which are however labelled in the diagram accordingly. Therefore, it is obvious from Fig. 6-9 that both the conversion and selectivity were not considerably affected over a period of 21 hours-on-stream. These results clearly show the high stability of Ni-Nb-Cr-O catalyst in the ODHE under the reaction conditions applied.

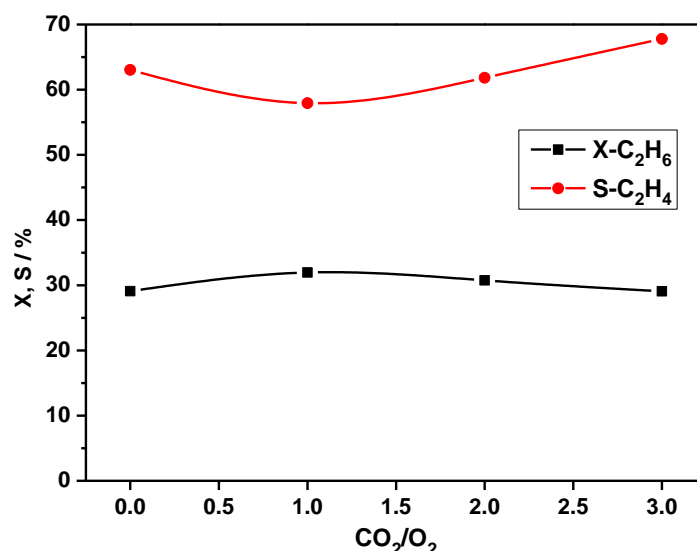**Fig. 6-8** **Comparison of ethane conversion and ethylene selectivity over Ni-Nb-Cr-O at different CO_2/O_2 ratios at 420 °C (Reaction conditions: T = 420 °C, GHSV = 3545 h^{-1}, τ = 1 s, cat. wt. 1.1 g)**
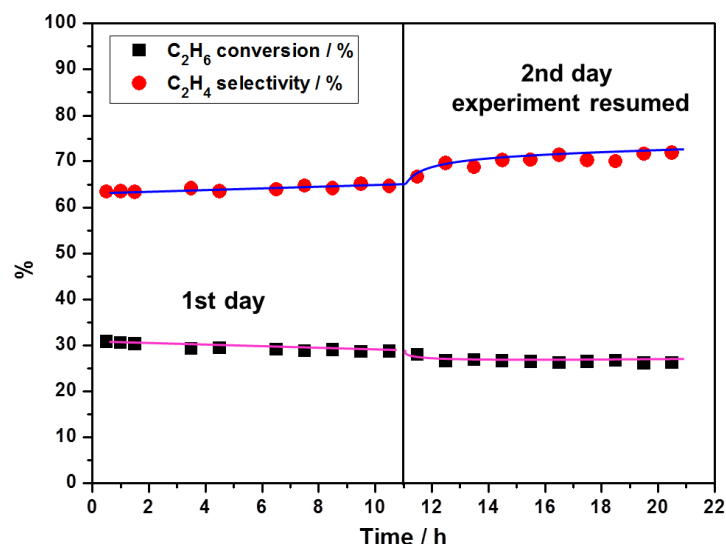
Fig. 6-9   Long term performance of Ni-Nb-Cr-O catalyst (reaction conditions: T = 420 °C, C$_2$H$_6$: O$_2$: CO$_2$: N$_2$ = 1: 0.7: 2.1: 0.6, GHSV = 3545 h^{-1}, τ = 1 s, cat. wt. 1.1 g)

6.4 Summary and Conclusion

The nature of the dopant M (Cr, Mo, W) has shown substantial influence on the surface areas, acidity characteristics, reducible properties as well as near-surface region composition of Ni-Nb-M-O catalyst. All these parameters in turn play a key role on the catalytic performance resulting in reduced ethane conversion and ethylene selectivity compared with parent Ni-Nb-O catalyst. Furthermore, among these three M (Cr, Mo, W) modified catalysts the d-character of dopant displayed a clear adverse impact on the catalytic properties. In this work, particularly Cr exhibited better performance compared to Mo and W as dopants. It could be deduced that the better performance of Cr promoted Ni-Nb-Cr-O samples could be related to its high surface enrichment of Cr and Nb and the presence of easily reducible Ni-O-Cr species besides its higher acidity. The catalytic results also revealed that the temperature of reaction, the concentration of O$_2$, presence of CO$_2$ and reactant mole ratios have shown considerable influence on the catalytic performance. Anyway, the tests have shown that a dilution of Nb sites in the near-surface region and/or a displacement downwards to the bulk reveal a negative effect on the catalytic performance.

The activation of ethane in the presence of CO$_2$ but in the absence of oxygen is difficult in the studied temperature range and hence almost no conversion of ethane could be noticed. But the addition of CO$_2$ to the reactant feed mixture exhibits appreciable effect on the catalytic performance of Ni-Nb-M-O solids with enhanced

ethylene selectivity at slight decrease of ethane conversion. It could be therefore attributed to the shifted equilibration as well as poisoning effect of present CO_2 on ethane conversion by inhibiting the reactions between radicals (e.g. $C_2H_5\cdot$) and the surface active sites.

7. Overall summary and outlook

This chapter summarizes the results of the investigations and gives some conclusions and an outlook for future research on the oxidative dehydrogenation of ethane to ethylene.

V_2O_5 based catalysts supported on different oxide carriers, i.e. Nb_2O_5, different types of Al_2O_3 and TiO_2, displayed differentiating catalytic performances in the oxidative dehydrogenation of ethane. The catalytic activity and selectivity over V_2O_5/Nb_2O_5 catalysts with varying V_2O_5 contents (5-20 wt%) were found to depend strongly on the nature of vanadium oxide species formed and the surface enrichment of vanadium in the near-surface-region. At low V_2O_5 content ($\leqslant$10 wt%), monomeric and oligomeric VO_x species were formed while more polymeric species were found (similar to bulk V_2O_5 sample) at higher loadings as shown by UV-vis-DRS studies. XPS revealed that the pronounced enrichment of vanadium occurs in the near-surface-region in the samples with low vanadia contents. Among all, 10 wt% V_2O_5/Nb_2O_5 catalyst has displayed the superior performance (X = 28%, S = 38% at 600 °C) due to the clear enrichment of vanadium in the near-surface-region and the formation of an optimum amount of monomeric and oligomeric VO_x species, respectively. Based on this result, 10 wt% V_2O_5 has been selected as an optimum loading and used in all further studies.

The nature of alumina support has shown a substantial influence on the type of VO_x species formed, their dispersion, acidity characteristics, morphology as well as surface composition. The characterization results revealed that the present V/Al-x-C catalysts are quite stable under the reaction temperature range from 500 to 600 °C. XRD reflections corresponding to V_2O_5 could only be seen in the case of the α-alumina supported V/Al-2-C sample due to its lowest surface area and poor vanadia dispersion compared with the other samples. UV-Vis spectra deconvolution and TEM images also gave hints on the existence of bulky V_2O_5 species in the V/Al-2-C catalyst. It can also be concluded that the loaded vanadium oxide species were well dispersed on the V/Al-1-C, V/Al-4-C and V/Al-5-C catalysts. XPS results provided clear hints on the presence of vanadium in +5 oxidation state in all fresh V/Al-x-C catalysts. Py-FTIR showed that both the Lewis and Brønsted acid sites exist in all catalysts, but the amount of Lewis sites is dominating. Activity results revealed that

among the five aluminas, V/Al-4-C gave the best performance (X-ethane = 35% and S-ethylene = 48%) at 600 °C while the V/Al-2-C showed poor behaviour (X-ethane = 50% and S-ethylene = 13%). This result was mainly due to a very low surface area of V/Al-2-C solid and consequently poor VOx dispersion; the opposite was seen in case of V/Al-4-C. Amazingly, the penta-coordinated aluminium-containing V_2O_5 catalyst (i.e. V/Al-1-C) gave an ethane conversion of 35% and selectivity to ethylene of 45 %, respectively.

Further work points to stabilizing the high proportion of penta-coordinated aluminum in aluminas and, probably to reach such effects using further materials but with higher surface areas for an increasing deposition of monomeric and oligomeric VO_x species for more effective oxidation catalysts.

The comparison of different oxide support material on the activity and selectivity behavior of vanadia catalysts (10 wt% V_2O_5) revealed that the nature of the support has shown a significant influence on the catalytic performance in the ODHE reaction. This phenomenon could be attributed to the dispersion of VO_x species on the support, strength of metal-oxide and support interactions, acidity characteristics, reducible properties, nature of VO_x species formed etc. The highly dispersed monomeric vanadia species on Al_2O_3 with high surface area could be responsible for the superior catalytic performance in the ODHE reaction. The yield of ethylene over different supported vanadia catalysts is followed the order: V/Ti < V/Nb < V/Al-BM $\approx$ V/Al-HS, which is in line with the reducibility and acidity characteristics of the catalysts. The ratio of integral integral intensity of Lewis and Brønsted acid sites seem to play a vital role on the ethylene selectivity. The higher the ratio of Lewis/ Brønsted sites, the higher the selectivity to ethylene.

On the whole, it can be concluded that the content of vanadia, the nature of support, the type of VO_x species formed and their dispersion on the support surface, the acidity characteristics, reducibility, surface composition etc. are some of the key parameters that need to be controlled carefully to achieve enhanced performance of the catalysts.

Additionally, Ni-Nb-O based bulk catalysts were further modified by three dopants, i.e. Cr, Mo, W (Ni: Nb: M atomic ratio of 1: 0.176: 0.1), that belong to the same group of elements but showing different d-characters. Compared with that of parent Ni-Nb-

O solid, the doped Ni-Nb-M-O (M: Cr, Mo, W) samples did not show any changes in the XRD patterns particularly in terms of crystalline behaviour and phase composition. However, considerable differences could be noticed concerning BET surface area data, reducibility, acidity characteristics as well as surface composition. Among the three auxiliaries used, Cr promoted Ni-Nb-Cr-O displayed relatively superior catalytic performance in the ODHE to ethylene, yielding in an ethane conversion of 26% and an ethylene selectivity of ca.65% at 420 °C. Ni-Nb-O and promoted Ni-Nb-M-O (M: Cr, Mo, W) catalysts were also further tested in the ODH of ethane in the presence of CO_2 with with an intention to improve activity and/or selectivity. The introduction of CO_2 into the reactant feed mixture is found to improve the selectivity of ethylene considerably but resulted in a marginal loss of activity. Among all, Ni-Nb-Cr-O solid revealed an ethylene selectivity of ca.85% at slightly less ethane conversion.

With regard to the future research attempts related to Ni-Nb-M-O catalysts, a deeper study and more attention are necessary to understand the role of different dopants M, which has changed the physicochemical properties and catalytic performance of Ni-Nb-O catalyst.

The ODHE is indeed an important reaction and highly demanding from commercial point of view. It also presents unique opportunities for fundamental research that makes a significant contribution to society. Even though a great deal has already been achieved in the field of oxidation, the productivity of alkene by the over present catalyst is still far away from commercial application. Moreover unwanted total oxidation always competes with that of selective oxidation towards desired products. Therefore new approaches and new attempts are certainly necessary to discover novel catalyst compositions capable of activating alkanes at relatively low temperatures with high alkene selectivity. Furthermore, rational approaches need to be worked out yet to sequence various functionalities in the direction of developing novel, attractive, and eco-friendly oxidation processes.

References

[1]   H. Zimmermann, R. Walzl, Ethylene, in: 6th rev. ed., Ullmann's Encyclopedia of Industrial Chemistry, vol. 12, Wiley VCH, 2003, p. 531.

[2]   A.H. Tullo, Chem. Eng. News 81 (2003) 21.

[3]   CMAI Announces Completion of Olefins World Analyses; World Light Olefins, CMAI News, 5th Dec. 2006.

[4]   E. Heracleous, A.A. Lemonidou, J. Catal. 270 (2010) 67.

[5]   K. Weissermel, H.-J. Arpe, Industrial Organic Chemistry Fourth ed., Wiley-VCH 2003.

[6]   T. Ren, M. Patel, K. Blok, Energy 31 (2006) 425.

[7]   S.M.K. Airaksinen, M.A. Banares, A.O.I. Krause, J. Catal. 230 (2005) 507.

[8]   H. Cai, A. Krzywicki, M.C. Oballa. Chem. Eng . Process 4 (2002) 199.

[9]   E.A. Mamedov, V. Cortés Corberán, Appl. Catal., A: General 127 (1995) 1.

[10] R. Grabowski, Cat. Rev. – Sci. Eng. 48 (2006) 199.

[11] S. Yang, E. Iglesia, A.T. Bell, J. Phys. Chem. B 109 (2005) 8987.

[12] B. Solsona, P. Concepción, S. Hernández, B. Demicol, J.M. López Nieto, Catal. Today 180 (2012) 51.

[13] B. Solsona, J.M. López Nieto, P. Concepción, A. Dejoz, F. Ivars, M.I. Vázquez, J. Catal. 280 (2011) 28.

[14] F. Cavani, N. Ballarini, A. Cericola, Catal. Today 127 (2007) 113.

[15] B. Savova, S. Loridant, D. Filkova, J.M.M. Millet, Appl. Catal. A: General 390 (2010) 148.

[16] X. Lin, K.R. Poeppelmeier, E. Weitz, Appl. Catal. A: General 381 (2010) 114.

[17] S.F. Håkonsen, J.C. Walmsley, A. Holmen, Appl. Catal. A: General 378 (2010) 1.

[18] M.A. Banares, Catal. Today 5 (1999) 319.

[19] H.X. Dai, C.T. Au, Curr. Top. Catal. 3 (2002) 33.

[20] E. Heracleous, M. Machli, A.A. Lemonidou, I.A. Vasalos, J. Mol. Catal. A: Chem. 232 (2005) 29.

[21] A. Qiao, V.N. Kalevaru, J. Radnik, A. Srihari Kumar, N. Lingaiah, P.S. Sai Prasad, A. Martin, Catal. Commun., 30 (2013) 45.

[22] J.M. López Nieto, P. Botella, M. I. Vázquez, A. Dejoz, Chem. Commun. (2002) 1906.

[23]   P. Botella, E. García-González, A. Dejoz, J.M. López Nieto, M.I. Vázquez, J. González-Calbet, J. Catal. 225 (2004) 428.

[24]   E. Heracleous, A.A. Lemonidou, J. Catal. 237(2006) 162.

[25]   S. Gaab, M. Machli, J. Find, R.K. Grasselli, J.A. Lercher, Top. Catal., 23 (2003) 151.

[26]   Y. Chao, E. Ruckenstein, J. Catal. 222 (2004) 17.

[27]   Jens Hagen, Handbook of Industrial Catalysis, A Practical Approach, 1999

[28]   L.J. Burcham, I.E. Wachs, Catal. Today, 49 (1999) 467.

[29]   B.M. Weckhuysen, D.E. Keller, Catal. Today, 78 (2003) 25.

[30]   J.H. Kwak, J. Hu, D. Mei, C.-W. Yi, D.H. Kim, C.H.F. Peden, L.F. Allard, J. Szanyi, Sci. 325 (2009) 1670-1673.

[31]   H. Zhao, S. Bennici, J. Cai, J. Shen, A. Auroux, J. Catal. 274 (2010) 259.

[32]   Ch. I.E. Wachs, J. Catal. 257 (2008) 181.

[33]   J.M. Lopez Nieto, P. Concepcion, A. Dejoz, H. Knozinger, F. Melo, M.I. Vazquez, J. Catal. 189 (2000) 17.

[34]   K. Wada, H. Yamada, E. Watanabe, T. Mitsudo, J. Chem. Soc., Faraday Transactions. 94 (1998) 1771.

[35]   V.V. Guliants, Catal. Today, 51 (1999) 255-268.

[36]   D.A. Bulushev, F. Rainone, L.L. Minsker, Catal. Today, 96 (2004) 195-203.

[37]   Z.P. Zhu, Z.Y. Liu, S.J. Liu, H.X. Niu, Appl. Catal. B: Envi.. 23 (1999) 229.

[38]   M.D. Amiridis, I.E. Wachs, G. Deo, J.M. Jehng, D.S. Kim, J. Catal.. 161 (1996) 247.

[39]   C.R. Dias, M.F. Portgela, M. Galan-Fereres, M.A. Banares, M.L. Granados, M.A. Pena, J.L.G. Fierro, Catal. Lett. 43 (1997) 117.

[40]   M.G. Nobbenhuis, A. Baiker, P. Barnickel, A. Wokaun, Appl. Catal.. A: General 85 (1992) 157.

[41]   G.C. Bond, S. Flamerz, R. Shukri, Faraday Discussions of the Chemical Society 87 (1989) 65.

[42]   M. Vassileva, A. Andreev, S. Dancheva, Appl. Catal. A: General 69 (1991) 221.

[43]   M. Sanati, A. Andersson, L.R. Wallenberg, B. Rebenstorf, Appl. Catal. A: General 106 (1993) 51

[44]   N.V. Kalevaru, A. Venugopal, K.S. Rama Rao, S. Khaja Mashan, V.V. Rao, P. Kanta Rao, Appl. Catal. A: General 167 (1998) 11.

References

[45] S.A. Al-Ghamdi, M.M. Hossain, H.I. de Lasa, Ind. Eng. Chem. Res. 52 (2013) 5235.

[46] S. Al-Ghamdi, M. Volpe, M.M. Hossain, H. de Lasa, Appl. Catal. A: General 450 (2013) 120.

[47] T.T. Nguyen, L. Burel, D.L. Nguyen, C. Pham-Huu, J.M.M. Millet, Appl. Catal. A: General. 433-434 (2012) 41.

[48] O.R. Evans, A.T. Bell, T.D. Tilley, J. Catal. 226 (2004) 292.

[49] M. D. Argyle, K. Chen, A.T. Bell, E. Iglesia, J. Catal. 208 (2002) 139.

[50] F. Klose, T. Wolff, H. Lorenz, A. Seidel-Morgenstern, Y. Suchorski, M. Piorkowska, H. Weiss, J. Catal. 247 (2007) 176.

[51] I.E. Wachs, Dalton Trans., 42 (2013) 11762.

[52] P. Viparelli, P. Ciambelli, L. Lisi, g. Ruoppolo, G. Russo, J.C. Volta, Appl. Catal. A: General 184 (1999) 291.

[53] Y. Liu, P. Cong, R. Doolen, H.W. Turner, W. Henry Weinberg, Catal. Today 61 (2000) 87.

[54] Ch. Zhao, I.E. Wachs, Catal. Today 118 (2006) 332.

[55] K.V.R. Chary, C.P. Kumar, A. Murali, A. Tripathi, A. Clearfield, J. Mol. Catal. A: Chem. 216 (2004) 139.

[56] P. Ciambelli, P. Galli, L. Lisi, M.A. Massucci, P. Patrono, R. Pirone, G. Ruoppolo, G. Russo, Appl. Catal. A: General 203 (2000) 133.

[57] M.E. Mahmoud, M.M. Osman, O.F. Hafez, E. Elmelegy, J. Hazard. Mater. 173 (2010) 349.

[58] J. Chen, Y. Lin, Z. Li, X. Zhang, Appl. Catal. A: General 269 (2004) 179.

[59] F. Klose, M. Joshi, C. Hamel, A. Seidel-Morgenstern, Appl. Catal. A: General 260 (2004) 101.

[60] D.S. Maciver, H.H. Tobin, R.T. Barth, J. Catal.. 2 (1963) 485.

[61] X. Zhang, J. Liu, Y. Jing, Y. Xie, Appl. Catal. A: General 240 (2003) 143.

[62] A. Düvel, E. Romanova, M. Sharifi, D. Freude, M. Wark, P. Heitjans, M. Wilkening, J. Phys. Chem. C 115 (2011) 22770.

[63] M. Vaarkamp, J.T. Miller, F.S. Modica, D.C. Koningsberger, J. Catal. 163 (1996) 294.

[64] T.T. Nguyen, M. Aouine, J.M.M. Millet, Catal. Commun. 21 (2012) 22.

[65] V. Ducarme, G.A. Martin, Catal. Lett. 23 (1994) 97.

References

[66] Y. Schuurman, V. Ducarme, T. Chen, W. Li, C. Mirodatos, G.A. Martin, Appl. Catal. A: General 163 (1997) 227.

[67] C. Mirodatos, V. Ducarme, H. Mozzanega, A. Holmen, J. Sanchez-Marcano, Q. Wu, G.A. Martin, Stu. Sur. Sci. Catal. 61 (1991) 41.

[68] X. Zhang, Y. gong, G. Yu, Y. Xie, J. Mol. Catal. A: Chem. 180 (2002) 293.

[69] X. Zhang, J. Liu, Y. Jing, Y. Xie, Appl. Catal. A, 240 (2003) 143.

[70] E. Heracleous, A.F. Lee, K. Wilson, A.A. Lemonidou, J. Catal. 231 (2005) 159.

[71] E. Heracleous, A.A. Lemonidou, J. Catal. 237 (2006) 175.

[72] Z. Skoufa, E. Heracleous, A.A. Lemonidou, Catal. Today 192 (2012) 169.

[73] E. Heracleous, A. Delimitis, L. Nalbandian, A.A. Lemonidou, Appl. Catal. A 325 (2007) 220.

[74] B. Solsona, P.Concepción, B. Demicol, S. Hernández, J.J. Delgado, J.J. Calvino, J.M. López Nieto, J. Catal. 295 (2012) 104.

[75] A.M. Gaffney, R. Song, C.Y. Yeh, P.J. Angevine, WO 2010099106 A2 (2010)

[76] Z. Yu, W. Zheng, Y. Zhang, H. Fu, H. Wu, X. Zhang, H. Li, H. Feng, W. Xu, P. Zhang, CN 102179261 A (2011)

[77] A. Martin, V.N. Kalevaru, B. Luecke, D. Van Deynse, M. Belmans, F. Boers, WO 03/101939 A2 (2003) *(Tessenderlo Chemie S.A. Belgium)*.

[78] V.N. Kalevaru, B. Lücke, A. Martin, Catal. Today 142 (2009) 158.

[79] D. Wang, M. Xu, C. Shi, J.H. Lunsford, Catal. Lett. 18 (1993) 323.

[80] K. Nakagawa, M. Okamura, N. Ikenaga, T. Suzuki, T. Kobayashi, Chem. Commun. (1998) 1025.

[81] I. Takahara, M. Saito, Chem. Lett. 973 (1996).

[82] K. Takehira, Y. Ohishi, T. Shishido, J. Catal. 224 (2004) 404.

[83] L. Liu, H. Li, Y. Zhang, Catal. Today 115 (2006) 235.

[84] N. Mimura, I. Takahara, M. Inaba, M. Okamoto, K. Murata, Catal. Commun. 3 (2002) 257.

[85] S. Deng, S. Li, H. Li, Y. Zhang, Ind. Eng. Chem. Res. 48 (2009) 7561.

[86] K.L. Fujdala, T.D. Tilley, J. Catal. 218 (2003) 123.

[87] M. Cherian, M.S. Tao, G. Deo, Catal. Today 78 (2003) 397.

[88] L. Xu, L. Lin, Q. Wang, L. Yang, D. Wang, W. Liu, Chinese J. Catal. 18 (1997) 353.

[89] G. Ertl, H. Knözinger, F. Schüth, J. Weitkamp, Handbook of Heterogeneous Catalysis, Volume 1 2008.

[90] M. Campanati, G. Fornasari, A. Vaccari, Catal. Today 77 (2003) 299.

[91] J.-F. Le Page, J. Cosyns, P. Courty, E. Freund, J.-P. Franck, Y. Jacquin, B. Juguin, C. Marcilly, G. Martino, J. Miquel, R. Montarnal, A. Sugier, H. Van Landeghem, Applied Heterogeneous Catalysis: Design, Manufacture, Use of Solide Catalysts, Technip, Paris, 1987.

[92] C. Perege, P.L. Villa, Catal. Today 34 (1997) 281.

[93] M.V. Twigg, Catalyst Handbook, 2nd ed., Wolfe, London, 1989.

[94] M. Che, O. Clause, Ch. Marcilly, in: G. Ertl, H. Knözinger, J. Weitkamp, Hand book of Heterogeneous Catalysis, New York, 1997.

[95] K.V. Narayana, A. Venugopal, K.S. Rama Rao, V. Venkat Rao, S. Khaja Masthan, P. Kanta Rao, Appl. Catal. A: General 150 (1997) 269.

[96] L. Čapek, J. Adam, T. Grygar, R. Bulánek, L. Vradman, G. Košová-Kučerová, P. Čičmanec, P. Knotek, Appl. Catal. A: General 342 (2008) 99.

[97] M. Baltes, K. Cassiers, P. Van der Voort, B.M. Weckhuysen, R.A. Schoonheydt, E.F. Vansant, J. Catal. 197 (2001) 160.

[98] H. Berndt, A. Martin, A. Brückner, E. Schreier, D. Müller, H. Kosslick, G.-U. Wolf, B. Lücke, J. Catal. 191 (2000) 384.

[99] B. Solsona, T. Blasco, J.M. López Nieto, M.L. Pena, F. Rey, A. Vidal-Moya, J. Catal. 203 (2001) 443.

[100] T. Grygar, L. Čapek, J. Adam, V. Machovic, J. Electron. Chem. 633 (2009) 127.

[101] P. Van Der Voort, M.G. White, M.B. Mitchell, A.A. Verberckmoes, E.F. Vansant, Spectrochimica Acta Part A: Molecular and Biomolecular Spectroscopy 53 (1997) 2181.

[102] C. Yan, D. Xue, Adv. Mater. 20 (2008) 1055.

[103] J. Liu, D. Xue, K. Li, Nano. Res. Lett. 6 (2011) 138.

[104] M.A. Eberhardt, A. Proctor, M. Houalla, D.M. Hercules, J. Catal. 160 (1996) 27.

[105] B.M. Reddy, B. Chowdhury, E.P. Reddy, A. Fernandez, Langmuir 17 (2001) 1132.

[106] F. Prinetto, G. Ghiotti, M. Occhiuzzi, V. Indovina, J. Phys. Chem. B 102 (1998) 10316.

References

[107] J. Mendialdua, R. Casanova, Y. Barbaux, J. Electron. Spectrosc. Relat. Phenom. 71 (1995) 249.

[108] W. Tang, Y. Liu, X. Yang, C. Wang, Ind. Eng. Chem. Res. 43 (2004) 2054.

[109] C. Pirovano, E. Schönborn, S. Wohlrab, V.N. Kalevaru, A. Martin, Catal. Today, 192 (2012) 20.

[110] G.A. Sawatzki, D. Post, Phys. Rev. B, 20 (1979) 1546.

[111] J.A. Lercher, C. Gründling, C. Eder-Mirth, Catal. Today, 27 (1996) 353.

[112] F. Klose, T. Wolff, H. Lorenz, A. Seidel-Morgenstern, Y. Suchorski, M. Piorkowska, H. Weiss, J. Catal. 247 (2007) 176.

[113] S. Besselmann, C. Freitag, O. Hinrichsen, M. Muhler, Phys. Chem. Chem. Phys, 3 (2001) 4633.

[114] A. Gervasini, P. Carniti, J. Keränen, L. Niinistö, A. Auroux, Catal. Today, 96 (2004) 187.

[115] E. Heracleous, A. Delimitis, L. Nalbandian, A.A. Lemonidou, Appl. Catal. A 325 (2007) 220.

[116] E. Heracleous, A.A. Lemonidou, J. Catal. 237 (2006) 162.

[117] M.C. Biesinger; B.P. Payne; A.P. Grosvenor; L.W.M. Lau; A.R. Gerson; R.S.C. Smart, Appl. Surf. Sci. 257 (2011) 2717.

[118] A.F. Carley, S.D. Jackson, J.N. O'Shea, M.W. Roberts, Surf. Sci. 440 (1990) L868-L874.

[119] J.F. Moulder, W.F. Stickle, P.E.Sobol, K.D. Bomben, Handbook of X-ray Photoelectron Spectroscopy, 1995.

[120] Yu.V. Plyuto, I.V. Babich, I.V. Plyuto, A.D. Van Langeveld, J.A. Moulijn, Appl. Surf. Sci. 119 (1997) 11.

[121] N.K. Nag, J. Phys. Chem. 91 (1987) 2324.

[122] R.J. Colton, A.M. Guzman, J.W. Rabalais, J. Appl. Phys. 49 (1978) 409.

[123] T.H. Fleisch, G.J. Mains, J. Chem. Phys. 76 (1982) 780.

[124] E. Heracleous, A.A. Lemonidou, J. Catal. 237 (2006) 175.

[125] D. Wang, M. Xu, C. Shi, J.H. Lunsford, Catal. Lett. 18 (1993) 323.

[126] S. Deng, S. Li, H. Li, Y. Zhang, Ind. Eng. Chem. Res. 48 (2009) 7561.

List of publications in ODHE project:

1. **Oxidative dehydrogenation of ethane to ethylene using vanadia based catalysts**

   A. Qiao, V.N. Kalevaru, A. Martin, A. Srihari, N. Lingaiah, P.S. Sai Prasad

   DGMK-Tagungsbericht 2 (2011) 189-195 (ISBN 978-3-941721-17-3).

2. **Effect of CO_2-admixture on the catalytic performance of Ni-Nb-M-O catalysts in oxidative dehydrogenation of ethane to ethylene**

   A. Qiao, V.N. Kalevaru, A. Sri Hari Kumar, N. Lingaiah, P.S. Sai Prasad, A. Martin, DGMK Tagungsbericht 3 (2012) 97 (ISBN 978-3-941721-26-5).

3. **Oxidative Dehydrogenation of Ethane to Ethylene over V_2O_5/Nb_2O_5 Catalysts**

   A. Qiao, V.N. Kalevaru, A. Srihari Kumar, N. Lingaiah, P.S. Sai Prasad, A. Martin, Catal. Commun. 30 (2013) 45.

4. **Selective oxidative dehydrogenation of ethane over MoO_3/V_2O_5-Al_2O_3 catalysts: Heteropolymolybdate as a precursor for MoO_3**

   A. Sri Hari Kumar, K. Upendar, A. Qiao, N. Lingaiah, V.N. Kalevaru, A. Martin, Ch. Sailu, P.S. Sai Prasad, Cat. Commun. 33 (2013) 76.

5. **Catalytic behavior of decomposed molybdophosphoric acid supported on alumina for oxidative dehydrogenation of ethane to ethylene**

   A. Sri Hari Kumar, V.N. Kalevaru, A. Qiao, A. Alshammari, N. Lingaiah, Ch. Sailu, P.S. Sai Prasad, A. Martin, Kinet. Catal. 54 (2013) 615.

6. **Oxidative Dehydrogenation of Ethane to Ethylene over supported V_2O_5 catalysts: Effect of nature of alumina support on the catalytic performance**

   A. Qiao, V.N. Kalevaru, J. Radnik, A. Düvel, P. Heitjans, A. Sri Hari Kumar, P.S. Sai Prasad, N. Lingaiah, A. Martin, in preparation

List of symposia contributions:

1. **Oxidative dehydrogenation of ethane to ethylene on SnO$_2$ supported molybdophosphoric acid catalysts**

B. Hari Babu, A. Sri Hari Kumar, N. Lingaiah, P. S. Sai Prasad, <u>A. Qiao</u>, V.N. Kalevaru, A. Martin

Presented at "Catsymp 21, (21st National Symposium on Catalysis "Catalysts for Sustainable Development")" held at IICT, Hyderabad, India during 10-13 Feb. 2013.

2. **Application of niobia supported vanadia/molybdena catalysts for oxidative dehydrogenation of ethane to ethylene**

<u>A. Qiao</u>, A. Sri Hari Kumar, N. Lingaiah, P.S. Sai Prasad, V.N. Kalevaru, A. Martin

Presented as poster at the "46. Jahrestreffen Deutscher Katalytiker" held at Weimar, Germany, during 13 - 15 Mar 2013.

3. **Oxidative dehydrogenation of ethane to ethylene: Effect of support on the catalytic performance of V-containing catalysts**

<u>A. Qiao</u>, V.N. Kalevaru, A. Martin, A. Sri Hari Kumar, N. Lingaiah, P.S. Sai Prasad

Oral presentation at XIth Europacat, held at Lyon, France, during 1-6 Sep 2013.

4. **The effect of Mo-V species derived from vanadium containing molybdophosporic acid for oxidative dehydrogenation of ethane to ethylene**

A. Sri Hari Kumar, V.N. Kalevaru, <u>A. Qiao</u>, P.S. Sai Prasad, N.Lingaiah, A. Alshammari, Ch. Sailu, A. Martin

Poster discussion cum presentation at XIth Europacat, held at Lyon, France, during 1-6 Sep 2013.

5. **The effect of Mo/V ratio in MPAV catalysts for oxidative dehydrogenation of ethane to ethylene**

A. Sri Hari Kumar, P.S. Sai Prasad, N. Lingaiah, <u>A. Qiao</u>, V.N. Kalevaru, A. Martin, A. Alshammari, Ch. Sailu,

Presented as poster at the "45. Jahrestreffen Deutscher Katalytiker" held at Weimar, Germany during 14 - 16 Mar 2012.

6. **Oxidative dehydrogenation of ethane to ethylene using vanadia based catalysts: influence of different alumina supports**

   A. Qiao, V.N. Kalevaru, A. Martin, A. Düvel, A. Sri Hari Kumar, P.S. Sai Prasad, N. Lingaiah

   Presented as poster at 15th int. Congr. Catal. held at Munich, Germany during 1 - 6 Jul 2012.

7. **Oxidative dehydrogenation of ethane to ethylene over V_2O_5/SnO_2 catalysts**

   A. Sri Hari Kumar, P.S. Sai Prasad, N. Lingaiah, A. Qiao, V.N. Kalevaru, A. Martin, A. Alshammari, Ch. Sailu

   Presented as poster at 15th int. Congr. Catal. held at Munich, Germany during 1 - 6 Jul 2012.

8. **Application of decomposed $H_4PMo_{11}VO_{40}$ catalysts supported on γ-Al_2O_3 for oxidative dehydrogenation of ethane to ethylene**

   A. Sri Hari Kumar, P.S. Sai Prasad, N. Lingaiah, A. Qiao, V.N. Kalevaru, A. Martin, A. Alshammari, Ch. Sailu

   Presented as poster at 15th int. Congr. Catal. held at Munich, Germany during 1 - 6 Jul 2012.

9. **Effect of CO_2-admixture on the catalytic performance of Ni-Nb-M-O catalysts in oxidative dehydrogenation of ethane to ethylene**

   A. Qiao, V.N. Kalevaru, A. Sri Hari Kumar, N. Lingaiah, P.S. Sai Prasad, A. Martin

   Presented as an oral presentation at DGMK conference held at Berlin, Germany during 8 - 12 Oct 2012.

10. **Catalytic behaviour of decomposed molybdophosphoric acid supported on alumina for oxidative dehydrogenation of ethane to ethylene**

    V.N. Kalevaru, A. Sri Hari Kumar, A. Qiao, N. Lingaiah, A. Alshammari, Ch. Sailu, P.S. Sai Prasad, A. Martin

    Presented at IX International Conference "Mechanisms of Catalytic Reactions" held at St. Petersburg, Russia, during 22 - 25 Oct 2012. (poster)

11. **Molybdophosporicacid as a precursor for molybdena in the preparation of catalysts for the oxidative dehydrogenation of ethane,**

    P. S. Sai Prasad, A. Sri Hari Kumar, N. Lingaiah, A. Qiao ˌ V.N. Kalevaru, A. Martin

Presented as an oral at "2nd International Indo-German Symposium" held at ICT, Mumbai, India during 29-31st Oct 2012.

12. **Oxidative dehydrogenation of ethane to ethylene using decomposed molybdophosphoric acid supported on zirconia**

A. Sri Hari Kumar, G. Raveendra, Ch. Sailu, A. Qiao, V.N. Kalevaru, A. Martin, N. Lingaiah, P. S. Sai Prasad

Presented as poster at 2nd Indo-German conference held at Rostock, Germany during 19 -22 Jun, 2011.

13. **Oxidative dehydrogenation of ethane to ethylene using vanadia based catalysts**

A. Qiao, V.N. Kalevaru, A. Martin, A. Srihari, N. Lingaiah, P.S. Sai Prasad,

Presented as poster at DGMK conference held at Dresden, Germany during 4 -6 Oct. 2011.

14. **Oxidative dehydrogenation of ethane using decomposed $H_4PMo_{11}O_{40}$ supported on Al_2O_3**

A. Sri Hari Kumar, B. Hari Babu, P.S. Sai Prasad, A. Qiao, V.N. Kalevaru, A. Martin, N. Lingaiah, Ch. Sailu

Presented as an oral at CHEMCON 2011 held at Bangalore, India during 27-29 Dec 2011.

Lebenslauf

Persönliche Daten

Name: Ailing Qiao

Geburtsdatum: 18.03.1982

Geburtsort: Dezhou, Shandong, China

Nationalität: Chinesisch

Geschlecht: Weiblich

Familienstand: Verheiratet

Bildung

2010.11-present, the Laboratory of Heterogeneous Catalytic Processes, Leibniz-Institute for Catalysis at Univ. Rostock, **Advisor: Dr. habil Andreas Martin**

2009.01- 2010.10, the Laboratory of Organometallic and Medicinal Chemistry, Swiss Federal Institute of Technology (EPFL), **Advisor: Prof. Paul J. Dyson**

2006.9-2008.07 Dept. of Chemical Engineering and Technology, Graduate School of Tianjin University, Major: Industry Catalysis. **Master. Advisor: Prof. Yongdan Li**

2002.9-2006.7 Dept. of Chemistry and Chemical Engineering, Hebei University of Science and Technology, Major: Pharmacy Engineering. **Bachelor.**